Curtin Medical School

Optimization of CT scanning protocol of Type B aortic dissection follow-up through 3D printed model

Chia-An Wu

This thesis is presented for the Degree of
Doctor of Philosophy of
Curtin University

December 2022

Declaration

To the best of my knowledge and belief this thesis contains no material previously published by any other person except where due acknowledgment has been made.

This thesis contains no material which has been accepted for the award of any other degree or diploma in any university.

The research presented and reported in this thesis was conducted in accordance with the National Health and Medical Research Council National Statement on Ethical Conduct in Human Research (2007) – updated March 2014. The proposed research study received human research ethics approval from the Curtin University Human Research Ethics Committee (EC00262), Approval Number HRE2018-0087.

Chia-An Wu

December 2022

Abstract

Of all cardiovascular diseases, aortic dissection (AD) is one of the most dangerous and fatal, necessitating urgent treatment. Compared to Type A AD that requires urgent open surgery, the management of Type B AD (TBAD) is more controversial and varied. Thoracic endovascular aortic repair (TEVAR) is a widely used less invasive technique for treating TBAD, compared to traditional open surgery, as it provides shorter recovery time and fewer procedure-related risks. Computed tomography (CT) is routinely used to monitor the postoperative status of AD patients. However, the radiation exposure from CT scanning raises concerns about radiation-induced malignancy. Further, postoperative follow-up of AD patients involves sequential thoracic CT scans at regular periods, therefore, low dose CT becomes an alternative way to avoid unnecessary radiation exposure to patients. Reducing the radiation dose is associated with the potential risk of decreasing image quality, therefore, it is necessary to maintain acceptable image quality while reducing radiation dose. Thus, development of an optimal CT protocol for post TEVAR AD patients has significant clinical impact and this forms the main theme of this project.

This research aims to develop and evaluate a 3D printed model used as a phantom in determining optimized scanning parameters to reduce the radiation dose for post TEVAR TBAD patients. Step one was to design a replicable segmentation method of TBAD, so that an accurate printable 3D virtual model of AD can be segmented by following the recommended optimal steps. This protocol for creating 3D model can be easily operated on open-source software to save the cost and the learning time for users. Step two was to identify a suitable 3D printing material. Four materials were selected due to their physical and radiological properties that were close to the applicable real human tissues. After testing printed samples of these materials through

a series of CT scans, Visijet CE-NT A30 was deemed the most suitable 3D printing material to represent human aorta.

After segmentation and material testing, step three involved creation of a 3D printed AD model that was used for further CT imaging studies to verify its clinical value. A commercial aortic stent-graft was deployed into the model to simulate post TEVAR procedure and the model was scanned on a 196-slice CT scanner with different parameters. In quantitative assessment, more than 20% dose reduction was achieved with the use of low tube voltage such as 80 kVp while the pitch remained constant. Thus, a low dose aortic CT is suggested for the follow-up of AD patients after TEVAR. In qualitative assessment, 6 radiologists and 10 radiographers were invited to rate the CT images acquired with the different scanning parameters. The results showed that the image quality is still acceptable for diagnosis at low tube voltage and high pitch situation. A protocol of 80 kVp with 2.5 pitch value was found to still provide adequate image quality for diagnosis. With a slightly increase of radiation dose the80 kVp with 2.0 pitch value, which had highest diagnostic value score (4.0), can provided better image quality in all scanning protocols of this study.

This study developed an optimal low dose scanning protocol for post TEVAR TBAD patients based on a patient-specific 3D printed model made of human tissue-like material. The parameters recommended in this study can reduce radiation dose by 22% compared to the traditionally recommended dual source CT protocol (120 kVp with pitch of 2.5). The radiation risk for follow-up TBAD patients can be potentially reduced. Further, the value of using 3D printed model in studying CT scanning protocols was further validated through this research with potential applications to investigate other low-dose CT protocols that involve cumulative radiation exposure.

Acknowledgements

First and foremost, I am deeply grateful to my supervisor Professor Zhonghua Sun for his invaluable guidance during the research journey and writing of this thesis. He has always been very encouraging and patient, helping me with any difficulties no matter in research or in life. Professor Sun is a pioneer in the field of Medical Radiation Science, and his extensive expertise in research and publication has been instrumental in my success.

I would like to express my gratitude to another supervisor, Dr Andrew Squelch. During my five years of study, he participated in almost every weekly meeting and can always provide valuable advice. He provided ideas from a different point of view other than medicine and gave tremendous help on technical issues.

I greatly appreciate the support from my co-supervisor, Professor Shirley Jansen. As a vascular surgeon and clinical professor and director of research institute, Prof Jansen has many roles and responsibilities. Despite her very busy schedule, she provided advice and assistance to my research which played an important role in some of my experiments.

I would like to thank Mr Tom Tiang for the computed tomography assistance. He has been very patient and selflessly sacrificed his personal time to help me on scanning my 3D printed models.

I also appreciate Dr Ashu Gupta and Dr Gregory van Schie discuss and help me with clinical cardiovascular image knowledge.

Last but not least, I owe a debt of gratitude to my parents, sister and friends for their continued encouragement and unwavering support, without which I would not have made it through this project.

List of publications included as part of the thesis

- Wu, C. A., Squelch, A., & Sun, Z. (2021). Optimal image segmentation protocol for 3D printing of aortic dissection through open-source software. Journal of 3D printing in medicine, 5(1), 37-49.
- Wu, C. A., Squelch, A., & Sun, Z. (2021). Investigation of three-dimensional printing materials for printing aorta model replicating type B aortic dissection. Current Medical Imaging, 17(7), 843-849.
- Wu, C. A., Squelch, A., Jansen, S., & Sun, Z. (2021). Optimization of computed tomography angiography protocols for follow-up type B aortic dissection patients by using 3D printed model. Applied Sciences, 11(15), 6844.
- Wu, C. A., Squelch, A., & Sun, Z. (2022). Assessment of optimization of computed tomography angiography protocols for follow-up type B aortic dissection patients by using a 3D-printed model. Journal of 3D printing in medicine, 6(3), 117-127.

Conference presentations

- Australian Society of Medical Imaging and Radiation Therapy WA rural education weekend, October 2018, Pullman Bunker Bay resort, Dunsborough, Australia (3D printing protocol for of Type B aortic dissection).
- Australian Society of Medical Imaging and Radiation Therapy WA rural education weekend, October 2019, Nelsons of Bridgetown Motel and Function Centre, Bridgetown, Australia (Development of optimal image segmentation protocol for 3D printing of Type B aortic dissection).
- Australian Society for Medical Research Virtual Scientific symposium, November 2020 (Investigation of 3D printing materials for printing aorta model replicating Type B aortic dissection).
- Australian Institute of Physics student conference, November 2021, Curtin University, Perth, Australia (Optimization of computed tomography angiography protocols for follow-up Type B aortic dissection patients by using 3D printed model).

Statements of contributions of others

Chia-An Wu input into this study and the associated papers as well as the dominant contribution to the intellectual property involved in the project. As is almost always the case in conducting research studies with assistance by collaborators, other researchers made contributions to the work that were significant enough to warrant co-authorship on the resulting journal articles. The statement of contribution of individual publications refer to the appendix I-IV.

List of Abbreviations

3D	Three dimensions / Three dimensional
3DP	Three dimensional printing
AAD	Acute aortic dissection
AD	Aortic dissection
AEC	Automatic exposure control
CECT	Contrast-enhanced computed tomography
CEUS	Contrast-enhanced ultrasound
CNR	Contrast-to-noise ratio
CT	Computed tomography
CTA	Computed tomography angiography
CTDIvol	Volume computed tomography dose index
DLP	Dose length product
DSCT	Dual-source computed tomography
EVAR	Endovascular aortic repair
FBP	Filtered back projection
FDA	Food and drug administration
FL	False lumen
HU	Hounsfield unit
IR	Iterative reconstruction
IRAD	International registry of acute aortic dissection
MRI	Magnetic resonance imaging
ROI	Region of interest
SMA	Superior mesenteric artery
SNR	Signal-to-noise ratio
STL	Stereolithography / Stereographic / Standard tessellation language / Standard triangle language
TBAD	Type B aortic dissection
TEVAR	Thoracic endovascular aortic repair
TL	True lumen
US	Ultrasound

List of Figures

List of Tables

Contents

CHAPTER 1

GENERAL OVERVIEW OF THE PROJECT

The work presented in this thesis is to explore the application of 3D printing (3DP) in aortic dissection (AD) in terms of developing 3D printed models replicating AD, identifying materials for printing the model, simulating endovascular repair of AD and testing various aortic computed tomography (CT) angiographic protocols for dose reduction. As a complex and sometimes fatal cardiovascular disease, the diagnosis and treatment of AD continue to improve. To ensure that patients receive the best possible medical care, data from real patients is necessary to improve treatments in the past. After the appearance of the phantom, such as radiation examinations can be acquired from phantoms instead of test on real patients. The emergence of 3DP technology and its application in the medical field has greatly increased the practicality of phantom experiments. A good 3D printed model can accurately represent a patient's anatomy, and materials that are close to human tissues allow the model to have many uses. This chapter will provide a complete overview of AD, purpose of developing 3DP and follow-up computed tomography angiography (CTA) dose reduction techniques.

1.1 Introduction of aortic dissection

The aorta is the largest artery in the body, originating from the left ventricle, as the ascending aorta, becoming the aortic arch and descending through the chest to the abdomen where it bifurcates into the iliac arteries. It transports oxygen-rich blood from the heart to the rest of the body. To support pressurised blood flow from the heart, the wall of the aorta is made up of three layers and is highly elastic.

AD is a complex and sometimes fatal cardiovascular disease. AD results from a breach of the aortic intima usually as the result of hypertension or connective tissue defects (1). Blood can flow into the wall, forming a "false lumen" (FL) which tracks alongside and can compress the true lumen (TL) (**Figure 1.1**). Compression of TL may cause insufficient blood supply to vital organs, such as brain, gut, kidneys, lower limbs or spinal cord (2). Due to the incomplete structure, FL is relatively fragile and can rupture, resulting in massive haemorrhage or death from cardiac tamponade. Consequently, early detection and treatment are crucial for lowering mortality (3-6).

According to statistics, if acute AD left untreated, at least 50% of patients will die within 48 hours after the occurrence, which is an increase of about 1% in 1 hour. Therefore, diagnosis and treatment are a race against time, about 71% will die within 2 months, 89% within 3 months, and 91% within 6 months. According to Australian Institute of Health and Welfare, from 2009 to 2018, about 1,000 people died each year from aortic aneurysms and dissections in Australia, with more men than women (**Table 1.1**) (4, 6).

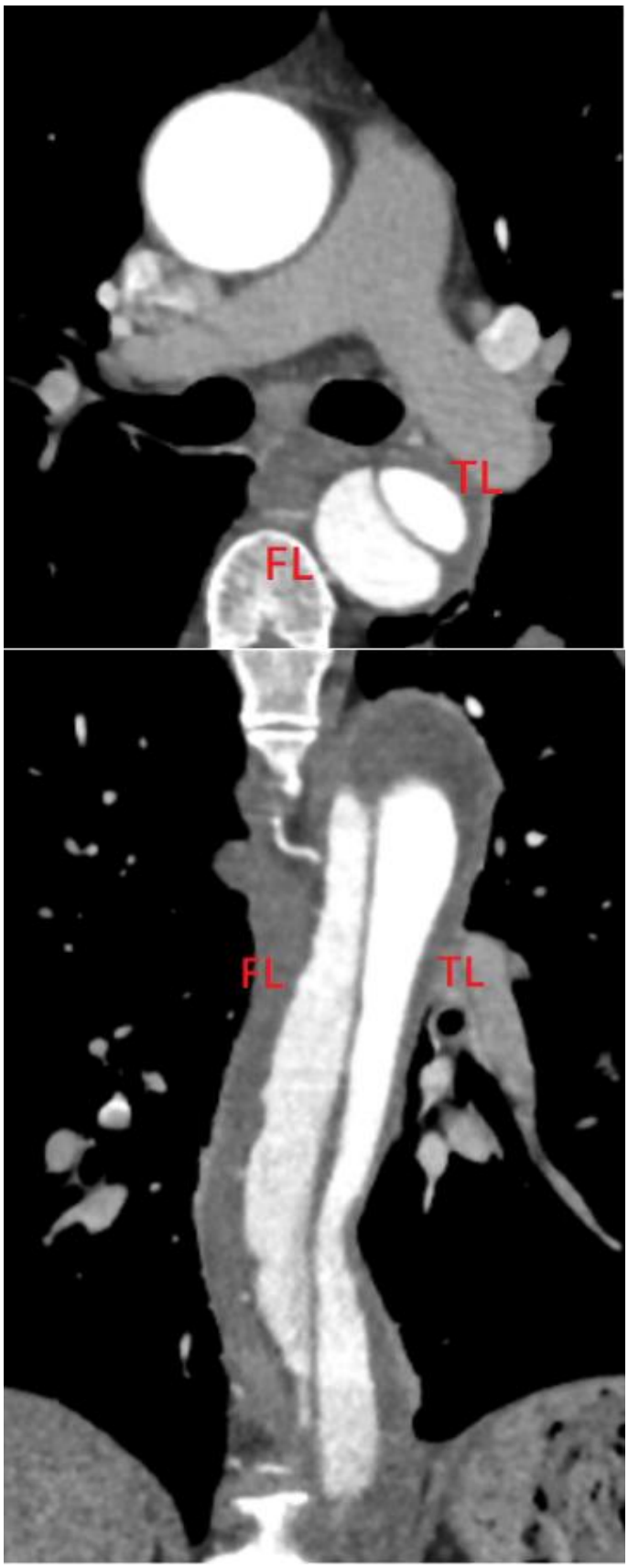

Figure 1.1 Under CT scan, aorta tear into TL and FL due to dissection. Axial view (top) and coronal view (bottom).

Table 1.1 Statistics of total deaths and deaths from cardiovascular disease in Australia from 2010 to 2020.

Year		Total deaths	Diseases of arteries, arterioles and capillaries	Aortic aneurysm and dissection	Other aneurysm and dissection
	Males	**73,484**	1,063	688	14
2010	**Females**	**69,989**	950	471	16
	Persons	**143,473**	2,013	1,159	30
	Males	**75,330**	1,068	670	31
2011	**Females**	**71,602**	905	460	15
	Persons	**146,932**	1,973	1,130	46
	Males	**74,794**	1,030	631	26
2012	**Females**	**72,304**	941	464	29
	Persons	**147,098**	1,971	1,095	55
	Males	**75,782**	976	573	23
2013	**Females**	**71,896**	846	388	17
	Persons	**147,678**	1,822	961	40
	Males	**78,341**	973	572	43
2014	**Females**	**75,239**	866	405	23
	Persons	**153,580**	1,839	977	66
	Males	**81,330**	1,013	586	41
2015	**Females**	**77,722**	896	448	15
	Persons	**159,052**	1,909	1,034	56
	Males	**81,867**	1,006	588	27
2016	**Females**	**76,637**	883	411	15
	Persons	**158,504**	1,889	999	42
	Males	**82,858**	973	553	31
2017	**Females**	**78,051**	850	386	23
	Persons	**160,909**	1,823	939	54
	Males	**82,320**	1,065	595	42
2018	**Females**	**76,173**	872	393	26
	Persons	**158,493**	1,937	988	68
	Males	**88,346**	1,133	662	51
2019	**Females**	**80,955**	972	490	40
	Persons	**169,301**	2,105	1,152	91
	Males	**84,588**	1,001	595	48
2020	**Females**	**76,712**	945	492	27
	Persons	**161,300**	1,946	1,087	75

1.2 History of aortic dissection

On 25 October 1760, George II, as always, got up at 6 a.m. and enjoyed his chocolate as usual. The German valet heard a noise that he characterised as "louder than royal wind" as the king was using the restroom, followed by a groan of anguish. When he entered, he discovered the king on the ground. Even though they called Mr Andrews, surgeon to the household immediately, the king lost his life. The king's personal doctor, Frank Nicholls, was asked to open the royal body during the autopsy the next day. He embalmed the body and left this intriguing note: "…the pericardium was found distended with a quantity of coagulated blood, nearly a pint … ; the whole heart was so compressed as to prevent any blood contained in the veins from being forced into the auricles; therefore, the ventricles were found absolutely void of blood …; and in the trunk of the aorta we found a transverse fissure on its inner side, about an inch and a half long, through which some blood had recently passed under its external coat and formed an elevated ecchymosis." Nicholls's record was the first to clearly and comprehensively describe what we now consider to be AD (7).

In 1802, Maunoir described the blood "dissecting throughout the circumference of the aorta" (8). Few years later, René Laennec became famous in Europe for inventing the stethoscope in 1819. He used the term "dissecting aneurysm" to describe AD. Despite the fact that the name has caused misunderstanding regarding the differences between AD and thoracic aortic aneurysms, it was nonetheless more widely used than AD at the time due to Dr. Laennec's fame (9).

DeBakey, Cooley, and Creech et al. successfully completed the first surgical resection of a dissecting thoracic aortic aneurysm on 7th July, 1954, about a century later. (10). After that, DeBakey and his colleagues continued to conduct research and treatment on AD patients, accumulated a lot of clinical surgical experience, and

published a surgical treatment report of 527 patients over the past 20 years in 1982 (11). Interestingly, he himself underwent surgery of his own invention at the age of 97 for type A AD and survived (12).

International Registry of Acute Aortic Dissection (IRAD) was established in 1996. This is undoubtedly a major milestone for the development of AD treatment in modern times. It integrates up to 20 international centres and provides a large amount of valuable and reliable clinical information with the assistance of researchers from different countries.

In 1999, Nienaber et al. and Dake et al. each published a paper on world leading journal *New England Journal of Medicine*, which describe the earliest clinical experience of endovascular stent-graft intervention for acute type B AD (TBAD) (13, 14). In the descriptions of the two papers, they implied that endovascular repair might become mainstream and replace traditional open surgery. Since endovascular repair has obvious advantages over traditional surgery, centred around reduced mortality and morbidity, it has become commonest means of intervention for aortic aneurysms and TBAD.

1.3 Anatomy and classification

AD is mainly caused by tearing of the intima of the aorta, through which blood enters the medial layer of the aorta and separates the intima from its surrounding medial and outer layers, forming a so-called false lumen. Alternatively, and less commonly, intramural haematoma or penetrating aortic ulcer can precede dissection (3, 15-18).

1.3.1 Classification system for aortic dissection

The classification of AD includes the more commonly used Stanford system (types A and B) and the earlier DeBakey system (types I, II, and III). Stanford's definition is relatively simple, as long as the dissection involves the ascending aorta, it is called type A, and the rest is called type B (19, 20). The DeBakey system is mainly defined according to the origin of the dissection, the type I is that the dissection originates from the ascending aorta and extends at least to the aortic arch, the type II is from and limited to the ascending aorta, and the type III is from the descending aorta, and can extend down or up (20, 21). Therefore, Stanford type A is equal to the general term for the DeBakey type I and the type II (**Figure 1.2**).

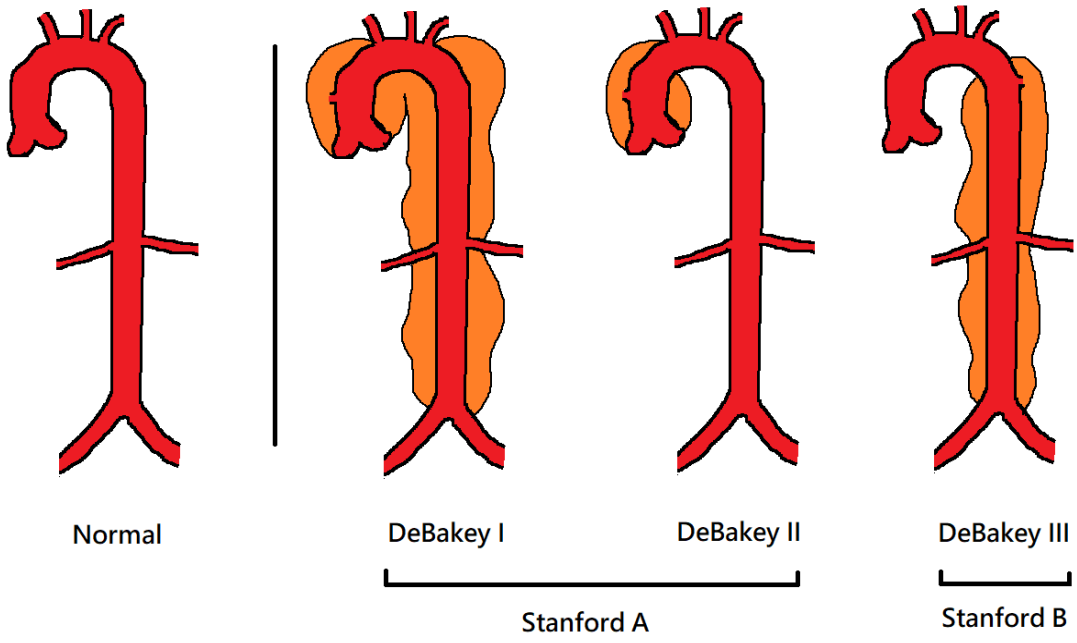

Figure 1.2 Depending on the AD onset location, classification can be performed using the DeBakey or Stanford systems. Adapted from: www.saem.org.

1.3.2 Clinical classification

AD can be classified as acute or chronic. In general, acute AD is defined as within 14 days from the onset of symptoms. If exceeding more than 14 days, then defined as

chronic. According to different clinical classifications, prognosis and treatment direction will also be different (22). Clinical classification is particularly important when choosing optimal treatment, especially for endovascular aortic repair (EVAR). The aim of treatment therefore, is to re-expand the TL to the original outer wall while the initial flap is still elastic and free to move, thereby compressing the septum (or flap) which will become rigid over time, losing its elasticity and mobility as well as becoming constrained by FL thrombosis (23, 24).

1.3.3 Complicated and uncomplicated type B aortic dissection

Clinically, acute TBAD is often divided into two types: complicated and uncomplicated. Complicated TBAD refers to manifestations of aortic rupture, shock, hypotension, recurrent or refractory pain, resistant hypertension and ischemia of vital organs. About 30% of patients with acute TBAD have complicated TBAD. There are differences in the treatment modalities advocated for complicated and uncomplicated TBAD (25). Treatment of uncomplicated TBAD is controversial, as uncomplicated TBAD generally has fewer early complications however carries a significant risk of long term aneurysmal dilatation and late aortic mortality (26, 27).

1.4 Treatment of aortic dissection

For type A AD, although the risks of surgery increase with age, surgical management is mandatory and the only option to save life (28, 29). Since there are many differences in the clinical treatment of TBAD (**Table 1.2**), the treatment complicated and uncomplicated TBAD will be explained in the following paragraph.

Table 1.2 Treatment options for aortic dissection.

Open surgery	● First choice for type A acute aortic dissection ● Type B acute aortic dissection with one of the following symptoms: 1. Ruptured or impending rupture of the aorta 2. Critical organ blood flow is compromised 3. Dissection continues to expand 4. Dissection retrogradely extends to the ascending aorta
Medical treatment	● First choice for uncomplicated Type B acute aortic dissection ● Subacute or chronic Type B Acute Aortic Dissection ● Dissection location remains stable
TEVAR interventional therapy	● First choice for complicated Type B acute aortic dissection ● Hypoperfusion ● Combined with medical treatment for uncomplicated type B dissection.

1.4.1 Treatment of complicated type B aortic dissection

Compared with type A AD, there are more treatment options for TBAD but still remain many controversies. For acute complicated TBAD, most of the current treatment methods are combined medical therapy in the form of blood pressure lowering with thoracic endovascular aortic repair (TEVAR) to seal the origin tear as soon as possible. According to the IRAD study, patients who undergo TEVAR have a 20% incidence of in-hospital complications, while on the other hand, open surgery is

as high as 40%. Furthermore, open surgery also has a higher mortality rate than TEVAR (30, 31).

According to a study by Zeeshan et al. of 77 patients with acute complicated TBAD, in-hospital mortality was 4% for those having TEVAR surgery and 40% for those having open surgery. Those who had TEVAR surgery had considerably greater 1, 3, and 5-year survival rates than patients who underwent open surgery (32). According to Moulakakis et al., patients who received TEVAR surgery for acute TBAD had a 30-day mortality rate of 7.3% overall, compared to 1276 patients who underwent open surgery, who had a 30-day mortality rate of 19.0%. The 30-day survival rate of patients who had TEVAR was higher than patients who had open surgery. (33). Hanna et al. followed up 50 patients with acute complicated TBAD who underwent TEVAR for five years, and their postoperative in-hospital 30-day mortality were 0% in 5 and 7 years. The overall survival rate was 84%, and no deaths were attributed to aortic disease (34). In conclusion, TEVAR has been widely accepted as the treatment of acute complicated TBAD, and it can effectively improve the survival rate of patients and reduce complications compared with traditional open surgery (35-39).

1.4.2 Treatment of uncomplicated type B aortic dissection

TEVAR has been regarded as an effective treatment modality in complicated TBAD. However, there is currently insufficient evidence to prove that TEVAR has absolute advantages in the treatment of uncomplicated TBAD. Therefore, the treatment options are more controversial in uncomplicated TBAD. Performing TEVAR at this time is likely to aggravate the inflammation, also may lead to the extension of the dissection and make the condition more dangerous (4, 40, 41). Some studies had pointed out that TEVAR is not suitable for patients with uncomplicated acute TBAD because of edema and decreased support of the arterial wall. The expansion force of the stent is easy to

damage the fragile aortic wall and extend the tear or even form a retrograde type A AD (42-44).

VIRTUE registry investigators conducted a study of the mid-term prognosis of TBAD patients after TEVAR. They classified patients into acute (<15 days), subacute (15–92 days), and chronic (>92 days). Results of 3-year follow-up showed that TEVAR effectively reduces aortic-related death but with a high rate of aortic re-intervention (20%, 22%, and 39%). Patients with acute AD have higher chance due to dissection (12%, 4%, and 9%), this may be related to unstable and brittle intima of acute AD (45). In a study of 132 patients with TBAD treated with TEVAR, Desai et al. found that TEVAR surgery in the early (<2 d) and late (2-14 d) acute stages carries an increased risks of retrograde type A AD which is often fatal (46).

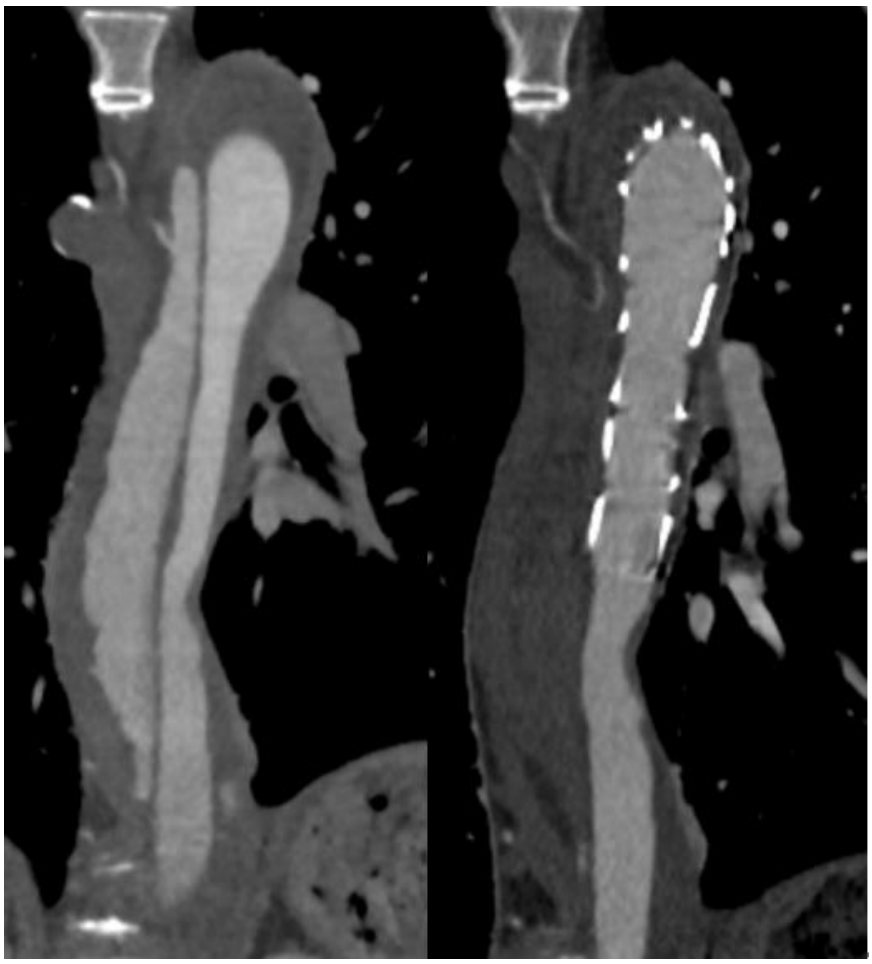

Figure 1.3 Coronal View of patient's CTA image before (left) and after (right) TEVAR treatment of AD..

On the contrary, there are some research supporting TEVAR being suitable for uncomplicated acute TBAD. Shimono et al. studied 37 patients with TBAD after transluminal stent-graft replacement and found the incidence of graft-related complications in patients with complicated acute, complicated chronic, and uncomplicated acute TBAD were 20%, 12.5%, and 0%, respectively. The incidence of false lumen thrombosis in uncomplicated TBAD was 87.5%, hence, they claimed that TEVAR is a reasonable treatment option for TBAD. However, stent graft-induced new entry is a problem that requires further investigation (47). Brunkwall et al. divided 61 uncomplicated TBAD patients into two groups based on their treatment plan, best medical treatment or best medical treatment combined with TEVAR. Their results

show that best medical treatment combined with TEVAR can effectively compress the false lumen, compared to best medical treatment alone, where the TL also extended. They believe that the time of surgery for acute uncomplicated TBAD is not necessarily after 2 weeks, TEVAR in the acute phase can induce false lumen thrombosis and aortic remodelling. However, they still expressed reservations, long-term observations would be needed to verify (26).

Most of the long-term deaths from AD are caused by rupture of the false lumen. If the false lumen does not completely thrombose, the aortic aneurysm may continue to expand. To encourage false lumen thrombosis and aortic remodelling, stop the development of aneurysms, and enhance long-term prognosis, early TEVAR intervention to cover as many tears as feasible must be performed. (23, 48). Song et al. analysed 117 patients with uncomplicated TBAD who received medical therapy alone and 135 who received TEVAR. The results showed that the 5-year survival rate of patients who underwent TEVAR was 92.3%, which was higher than that of patients treated with drugs alone (67.6%). With advances in aortic remodelling techniques, TEVAR can improve long-term survival in patients with acute uncomplicated TBAD (49). Early TEVAR is possible to prevent continuous aortic dilatation because Schwartz et al. reported that approximately 40% of patients with uncomplicated TBAD later need TEVAR intervention (50).

1.4.3 Development of future type B AD treatments

Whether complicated or uncomplicated TBAD, TEVAR has become a reasonable modality currently. For acute and complicated TBAD, TEVAR has been shown to be effective and becomes a common and preferred treatment modality. The use of TEVAR in uncomplicated TBAD patients has been controversial in the past. With the continuous advancement of surgical techniques and equipment in recent years, more

and more clinical evidence has shown that TEVAR surgery as early as possible combined with medical therapy is effective. It can raise both the long-term survival rate and the long-term prognosis of patients. To determine whether TEVAR surgery is the optimum course of treatment for acute uncomplicated TBAD, additional extensive, prospective clinical studies are required.

The key of TEVAR lies in the adequate preoperative evaluation of the TL and FL of dissection, the formulation of individualized plans, and the accuracy of intraoperative operations. In order to develop a specific treatment plan for individual patient, a suitable auxiliary model can increase the accuracy of the surgical procedure. However, producing patient-specific model for each patient is hard to achieve through traditional manufacturing. On the other hand, a new manufacturing technology, three dimensional printing (3DP) is able to solve this problem. In **Chapter 2**, Introduction of 3DP and its application in medical area, especially for TBAD, will be introduced. **Chapter 3** will introduce the difficulties on creating a 3D printed TBAD model and our solutions.

1.5 Follow-up of aortic dissection after endovascular aortic repair

The risks of TEVAR for TBAD depend on many factors including the patient age and comorbidities, anatomy of dissection, length to be covered, pre-existing end organ ischemia, spinal cord variability in blood supply, etc. As discussed in section **1.4**, compared to open surgery, TEVAR reduces mortality and morbidity in thoracic aortic aneurysm. Short and mid-term prognosis of TEVAR has been reported to be better than open surgery (51-55). However, some studies show that long-term survival rate of TEVAR is about equal to open surgery, plus, the high re-intervention rate of TEVAR patients is also a serious issue (56-59). Bicknell et al. summarized the mortality of TBAD non-acute patients after TEVAR in 30-day, 1-year and 5-year. 30-day death rate

was reported between 2.5 and 3.2%, 1-year and 5-year mortality from 10.5 to 11.5% and 9.2 to 30% respectively. The re-intervention rate of TEVAR was between 15.9 and 29% (60). Due to the high re-intervention rate of TEVAR and to prevent complications, lifelong surveillance is required (61).

1.5.1 Current imaging modalities for follow-up of aortic dissection and intervention

1.5.1.1 Ultrasound and contrast enhanced ultrasound

Conventional ultrasonography (US), a simple and affordable technology, has replaced other imaging modalities as the primary option for quick diagnosis in daily practise. Contrast-enhanced ultrasound (CEUS), a new method for vascular pathology detection, has gained popularity in recent years (62-64). The main benefit of CEUS is that it enables safer, more precise diagnosis without the use of radiation. The formation of endoleaks is one of the main complications following EVAR. Endoleaks happen when arterial blood escapes out of the stent graft lumen and into the aneurysm sac (64). Because of high sensitivity for detecting endoleaks, CEUS is one of the recommended tools for EVAR follow-up (65-67). For TBAD patients, endoleaks could be one of the concerns when left untreated or treated in late stage. Therefore, for TBAD patients who have proper treatment in early stage, CEUS is still not a widely accepted modality for post-TEVAR surveillance (68). However, colour duplex US is an adjunct modality which can be applied with computed tomography angiography (CTA) for in post-EVAR surveillance (69).

1.5.1.2 Magnetic resonance imaging

There are two main significant advantages of using magnetic resonance imaging (MRI) for AD follow-up. First, compared to CT, the contrast does not affect renal function. Second, it is a radiation free imaging examination. Several studies have

reported that MRI has been evaluated in the follow-up of EVAR. When Guo et al. combined four investigations about the detection of endoleaks using MRI and CT, MRI revealed 42 extra endoleaks during the paired scans that CTA missed, while CTA discovered 2 endoleaks that MRI missed (70). Due to greater soft tissue contrast and thus improved contrast sensitivity for small and slow-flow endoleaks, Habet et al. indicated that MRI detects a considerably higher proportion of new endoleaks (71). In addition to the two obvious advantages mentioned above, similar to US, MRI is not recommended for image tracking most TBAD patients who accept proper treatment in early stage (70). Also, compared to the speed and convenience of US, MRI is considered time-consuming and expensive.

1.5.1.3 Computed tomography angiography

Compared to US and MRI, CTA can enable accurately evaluation of aneurysm morphology changes, sac diameter, graft anchorage and integrity (68). There are graft-related complications after invasive treatment, so regular imaging monitoring is considered mandatory. CTA is recognised as a standard imaging technique for EVAR follow-up due to its excellent sensitivity in detecting endoleaks (71, 72). Following the procedure, CTA follow-up examinations are advised to be made at 1, 6, and 12 months, then once a year (73). Although CTA is already the standard modality for post-TEVAR, routine use of CTA surveillance still has some concerns, and this includes exposure to patients with high radiation doses and use of nephrotoxic contrast (74-76). Another strategy is imaging monitoring with CTA to track the change in dissection at 1, 3, and 6 months following TEVAR, and subsequently CEUS may be used to quantify the maximum aneurysm diameter at 12 months and yearly thereafter to avoid radiation exposure to patients (77). However, continuous use of CTA for long-term tracking is still the most robust and relatively convenient option. CTA can monitor stent graft

migration and aortic re-modelling in the long term as well as assess patient recovery, access-related problems, and reliably excluding dissection in the short term (78-82). Therefore, in order to balance accuracy of imaging follow-up and patient safety, further research of reducing radiation dose associated with CTA is necessary.

1.5.2 Radiation exposure associated with computed tomography angiography

Although radiation-induced cancer is commonly known to be hazardous, the real carcinogenic dangers of radiation from diagnostic CT are difficult to quantify. According to the results estimated by González et al., 29000 cancer occurrences in the USA occurred in 2007 as a result of 72 million CT scans, with chest CT angiography and CT of the chest being among the major causes (2700and 4100, respectively) (83). Due to the tiny and unreliable radiation dangers amplified by the high volume of CT scans performed, the study was found to have overstated the situation incorrectly. Levels of radiation from diagnostic CT are too low for existing epidemiological research to reliably predict cancer risk (84). Although there is uncertainty about the risk of diagnostic CT radiation, due to the gradual increase in the number of radiological examinations, the radiology community still generally believes that caution should be exercised and follow the long-standing principle of ALARA (As Low as Reasonably Achievable) (85-87).

The best strategy to limit the dose is to avoid using CT when it is clinically unnecessary. However, in many instances, the additional benefit of CT overcomes the possible radiation hazards. In general, chest CT dose reduction can be achieved in the following ways: Acquisition scan parameter optimization, automatic exposure control (AEC), technical adaptations, breast shields and reconstruction algorithms (88). Common scan parameters adjustment includes tube voltage, current–time product, pitch and scan length. AEC maintains continuous image quality at the lowest dose

achievable at each sector by varying the tube current according to patient thickness. (89). Technical adaptation refers to scanners that use different technologies such as adaptive collimation, dual energy and detector (90-93). Reconstruction algorithms means to using different algorithms to transfer data collected from detector to 2D image (94-97). Due to technical and equipment limitations, we only perform the scan parameters optimization in subsequent studies (Chapters 5 and 6) to verify the value of 3D printed models. Therefore, the scan parameter optimization will be focused in this paragraph instead of other methods.

1.5.2.1 Tube voltage

Radiation exposure is proportional to the kVp (peak kilovoltage) if all other factors remain the same. In some circumstances, it can be a potential technique for lowering the radiation exposure from thoracic CT scans. Shen et al. studied 100 patients, half of them underwent thoracoabdominal CTA with low- concentration contrast medium and low tube voltage (100 kVp), the other half were scanned with high-concentration contrast medium and conventional tube voltage (120 kVp). They claimed the low kVp is able to significantly reduce the radiation dose without compromising image quality (98). Sharara et al. compared 84 patients who underwent coronary CTA and aortic CTA. Seventy of them were scanned by low tube voltage (100 kVp), the other 14 patients were scanned by standard acquisition protocol (120 to 140 kVp). The results showed that the image quality was not significantly changed by lowering tube voltage (99). Lowering kVp reduces photon flux, which in turn produces increased noise and lowering the image quality. Patients with larger bodies can exacerbate the problem (100, 101).

1.5.2.2 Tube current time product

Current-time product is obtained by multiplying tube current (mA) and exposure time (s). The radiation dose is proportional to the current time product if all other factors remain constant. Reducing mAs could cause beam hardening and streak artefacts, which affect image quality. However, some studies have shown that mAs can be greatly reduced without being noticeable by the human eye (102, 103). Compared with kVp, adjusting mAs does not significantly affect image quality, so it is the first choice for manual adjustment of parameters in clinical practice.

1.5.2.3 Pitch

The pitch is calculated using the distance that table travels during one gantry rotation divided by the slice thickness or beam collimation. Increasing the pitch means the table to move faster and reduce the radiation dose received by the patient. However, increasing the pitch reduces the spatial resolution of the images in the Z-axis, thus increasing the pitch to reduce the radiation dose is limited in terms of feasibility (104-106). High pitch will negatively affect the image quality, therefore, increasing the pitch value was not a commonradiation dose reduction strategy until the advent of dual-source CT. Apfaltrer et al. provided a new aortic CTA dose reduction idea by using high pitch value in dual-source CT. In their study, radiation dose dropped 45% in high pitch value mode but the image quality was still acceptable (107). Through the comparison of a low dose protocol and conventional protocol patients, Shen et al. also proved high pitch is available with the use of dual-source CT (98). By using dual-source CT technique, increasing pitch becomes a new strategy to reduce radiation.

1.5.2.4 Scan length

Changing the scan length by focussing on key area can intuitively reduce radiation exposure. This method is suitable for use in the follow-up, as the scanning area can be limited to the lesions that need to be observed.

1.5.2.5 Iterative reconstruction (IR)

Mathematical methods for reconstructing images after scanning can directly affect radiation dose and image quality. Filtered back projection (FBP) is the most common image reconstruction method with the longest development history. This technique can reconstruct images by backprojecting the filtered projection data in order to calculate the inverse x-ray transformation using an analytical formula (108). Due to its high accuracy and computational efficiency, FBP is still widely used today. IR is another image reconstruction algorithm that has gradually emerged in the past decade. The initial step of an IR calculation compares an image assumption to actual measured values while making continuous corrections until they are in agreement. Since commercial implementations of IR algorithms have been available for more than ten years and numerous CT scanner manufacturers have created their own IR algorithms, the advantages of IR algorithms in terms of image quality improvement and artefact correction have long been understood (109). In the early days, due to insufficient computer performance, using the IR algorithm would take a lot of time, resulting in low image reconstruction efficiency. However, with the continuous development of computers, the problem of time-consuming has been solved. The IR technique has a number of advantages, including the ability to lower radiation exposure and raise reconstruction precision. Higher weights can be given to more accurate projections using photon statistics, potentially lowering artefacts and increasing dose efficiency (110, 111). Therefore, with the development of more

powerful computers, IR is a promising way to achieve low-dose CT with high image quality.

1.5.3 Conclusion of aortic dissection imaging follow-up

EVAR is increasingly used to treat AD, in contrast to open surgery, EVAR relies on insertion of a stent-graft without disrupting the physical integrity of the aneurysm wall. As a result, one of the key markers of an effective EVAR is aneurysm diameter. Therefore, one of the primary objectives of EVAR is characterised as preventing aneurysmal sac expansion (112). After EVAR, imaging follow-up often assesses not only the aneurysm size but also the endoleak status, stent graft integrity, and stent-graft migration (113).

Compared to open surgery, EVAR has a clear short-term survival benefit (114-116). However, there is a high incidence of re-intervention (117, 118). The current prevailing approach is to monitor frequently during the first year and then at least once a year thereafter (73). However, surveillance plans and methods are inconsistent across institutions in terms of frequent use of imaging modalities (119). CTA is the most popular follow-up method, but at the expense of increased costs and resource usage, besides, radiation, contrast exposure and repeated follow-up negatively affect patient health (85, 120, 121).

In order to reduce patient radiation doses, some studies have also begun to point out that the frequency of follow-up can be reduced compared to recommended frequent CTA scan in the past. Dias et al. believe that the postoperative CTA scan can be abandoned after one year and US is used instead. In their study, regular CT scans after EVAR had a benefit rate of less than 10% (122). Some limitations still occur in their research, they only used one exclusive stent-graft. Whether 10% is a low enough number to forgo a CTA scan is also something to ponder. Baderkhan et al. provide

another way to reduce CTA surveillance. They proposed that the follow-up after EVAR can be classified according to the first postoperative imaging. Two-thirds of patients in in this research demonstrated adequate seal and no endoleak on the first postoperative CTA, also they had a low risk of related adverse events five years after surgery (123).

Reducing the frequency of CTA surveillance is contrary to clinician decisions which are bespoke to each patient. In this study, we hope to reduce the dose received by patients while maintaining CTA surveillance frequency. In **Chapters 5 and 6**, we use patient-specific 3D models to study how to reduce the tracking scan dose and support the value of 3DP in the medical area.

1.5.4 Thesis overview

In **Chapter 2**, 3D printing technique will be introduced, including the development of 3D printing and its application in the medical area. Limitations of the 3D printing will also be explained. To create a 3D printed TBAD model with suitable material is important in this study, however, due to the complex anatomy structure of TBAD, to achieve an accurate TBAD model is challenging. **Chapters 3 to 6** are formatted as research papers, which have been published in peer review journals. **Chapter 3** introduces a segmentation protocol which is able to segment a TBAD model efficiently by open source software. This could potentially benefit for future 3D printing AD research. Following the third chapter, **Chapter 4** investigates commercial 3D printing materials which are readily available. The selected materials had physical property close to real human aorta. To verify their performance under CT scan, these materials were scanned with same parameters as real follow up TBAD patients. After an accurate TBAD model with proper material created, we use it as a scan phantom for lower scanning parameters investigation in **Chapter 5**. A commercial stent-graft was

deployed in the model to simulate TBAD patient after surgery. Quantitative assessment was conducted by comparing signal-to-noise ratio of different scanning parameters. This study showed that radiation dose can be reduced without sacrificing image quality by lowering tube voltage. However, diagnostic value of the images can not only be judged by quantitative assessment, whether it can be used by doctors for diagnosis is the standard for judging image quality in clinical practice. Therefore, in **Chapter 6**, several radiologists and radiographers were invited to qualitatively assess image quality. Although adjusting the pitch value will result in significant decrease in image quality, qualitative assessment showed that the image is still acceptable in high pitch scan. As a conclusion, **Chapter 7** organizes all studies in this project and proves that radiation dose from routine CT scan still has potential to continue to be reduced for follow up of TBAD patients and further validation of the value of 3D printing technique in medical applications deserves to be investigated.

References

1. DeSanctis RW, Doroghazi RM, Austen WG, Buckley MJ. Aortic dissection. New England Journal of Medicine. 1987;317(17):1060-7.
2. Khan IA, Nair CK. Clinical, diagnostic, and management perspectives of aortic dissection. Chest. 2002;122(1):311-28.
3. Hagan PG, Nienaber CA, Isselbacher EM, Bruckman D, Karavite DJ, Russman PL, et al. The International Registry of Acute Aortic Dissection (IRAD): new insights into an old disease. Jama. 2000;283(7):897-903.
4. Tran TP, Khoynezhad A. Current management of type B aortic dissection. Vascular Health and Risk Management. 2009;5:53-63.
5. Fukui T. Management of acute aortic dissection and thoracic aortic rupture. Journal of Intensive Care. 2018;6(1):1-8.
6. Apostolakis E, Baikoussis NG, Georgiopoulos M. Acute type-B aortic dissection: the treatment strategy. Hellenic Journal of Cardiology. 2010;51(4):338-47.
7. Nicholls F, Parker G. LI. Observations concerning the body of his late Majesty, October 26, 1760. Philosophical Transactions of the Royal Society of London. 1761(52):265-75.
8. Maunoir JP. Mémoires physiologiques et pratiques sur l'anévrisme et la ligature des artères: Paschoud; 1802.
9. Leonard J. Thomas Bevill Peacock and the early history of dissecting aneurysm. British Medical Journal. 1979;2(6184):260-262.
10. De Bakey ME, Cooley DA, Creech Jr O. Surgical considerations of dissecting aneurysm of the aorta. Annals of Surgery. 1955;142(4):586-610.
11. DeBakey ME. Dissection and dissecting aneurysms of the aorta. Surgery. 1982;92:1118-34.
12. Altman LK, late afternoon last Dec I, DeBakey ME. The Man on the table was 97, but he devised the surgery. New York Times. 2006:12-25.
13. Dake MD, Kato N, Mitchell RS, Semba CP, Razavi MK, Shimono T, et al. Endovascular stent–graft placement for the treatment of acute aortic dissection. New England Journal of Medicine. 1999;340(20):1546-52.
14. Nienaber CA, Fattori R, Lund G, Dieckmann C, Wolf W, von Kodolitsch Y, et al. Nonsurgical reconstruction of thoracic aortic dissection by stent–graft placement. New England Journal of Medicine. 1999;340(20):1539-45.
15. Yu H-Y, Chen Y-S, Huang S-C, Wang S-S, Lin F-Y. Late outcome of patients with aortic dissection: study of a national database. European Journal of Cardio-thoracic Surgery. 2004;25(5):683-90.

16. Spittell PC, Spittell Jr JA, Joyce JW, Tajik AJ, Edwards WD, Schaff HV, et al., editors. Clinical features and differential diagnosis of aortic dissection: experience with 236 cases (1980 through 1990). Mayo Clinic Proceedings. 1993;68(7):642-51.

17. Tsai TT, Evangelista A, Nienaber CA, Trimarchi S, Sechtem U, Fattori R, et al. Long-term survival in patients presenting with type A acute aortic dissection: insights from the International Registry of Acute Aortic Dissection (IRAD). Circulation. 2006;114(1_supplement):I-350-I-6.

18. Tsai TT, Fattori R, Trimarchi S, Isselbacher E, Myrmel T, Evangelista A, et al. Long-term survival in patients presenting with type B acute aortic dissection: insights from the International Registry of Acute Aortic Dissection. Circulation. 2006;114(21):2226-31.

19. Daily PO. Management of acute aortic dissections. Annals Thoracic Surgery. 1970;10:237-47.

20. Lansman SL, McCullough JN, Nguyen KH, Spielvogel D, Klein JJ, Galla JD, et al. Subtypes of acute aortic dissection. The Annals of Thoracic Surgery. 1999;67(6):1975-8.

21. De Bakey ME, Henly WS, Cooley DA, Morris Jr GC, Crawford ES, Beall Jr AC. Surgical management of dissecting aneurysms of the aorta. The Journal of Thoracic and Cardiovascular Surgery. 1965;49(1):130-49.

22. Nordon IM, Hinchliffe RJ, Loftus IM, Morgan RA, Thompson MM. Management of acute aortic syndrome and chronic aortic dissection. Cardiovascular and Interventional Radiology. 2011;34(5):890-902.

23. Nienaber CA, Clough RE. Management of acute aortic dissection. The Lancet. 2015;385(9970):800-11.

24. Haverich A, Miller D, Scott W, Mitchell R, Oyer P, Stinson E, et al. Acute and chronic aortic dissections--determinants of long-term outcome for operative survivors. Circulation. 1985;72(3 Pt 2):II22-34.

25. Criado FJ. Aortic dissection: a 250-year perspective. Texas Heart Institute Journal. 2011;38(6):694.

26. Brunkwall J, Kasprzak P, Verhoeven E, Heijmen R, Taylor P, Trialists A, et al. Endovascular repair of acute uncomplicated aortic type B dissection promotes aortic remodelling: 1 year results of the ADSORB trial. European Journal of Vascular and Endovascular Surgery. 2014;48(3):285-91.

27. Qin Y-L, Wang F, Li T-X, Ding W, Deng G, Xie B, et al. Endovascular repair compared with medical management of patients with uncomplicated type B acute aortic dissection. Journal of the American College of Cardiology. 2016;67(24):2835-42.

28. Trimarchi S, Eagle KA, Nienaber CA, Rampoldi V, Jonker FH, De Vincentiis C, et al. Role of

age in acute type A aortic dissection outcome: report from the International Registry of Acute Aortic Dissection (IRAD). The Journal of Thoracic and Cardiovascular Surgery. 2010;140(4):784-9.

29. Mehta RH, O'Gara PT, Bossone E, Nienaber CA, Myrmel T, Cooper JV, et al. Acute type A aortic dissection in the elderly: clinical characteristics, management, and outcomes in the current era. Journal of the American College of Cardiology. 2002;40(4):685-92.

30. Fattori R, Tsai TT, Myrmel T, Evangelista A, Cooper JV, Trimarchi S, et al. Complicated acute type B dissection: is surgery still the best option? A report from the International Registry of Acute Aortic Dissection. JACC: Cardiovascular Interventions. 2008;1(4):395-402.

31. Tsai TT, Trimarchi S, Nienaber C. Acute aortic dissection: perspectives from the International Registry of Acute Aortic Dissection (IRAD). European Journal of Vascular and Endovascular Surgery. 2009;37(2):149-59.

32. Zeeshan A, Woo EY, Bavaria JE, Fairman RM, Desai ND, Pochettino A, et al. Thoracic endovascular aortic repair for acute complicated type B aortic dissection: superiority relative to conventional open surgical and medical therapy. Elsevier; 2010. p. S109-S15.

33. Moulakakis KG, Mylonas SN, Dalainas I, Kakisis J, Kotsis T, Liapis CD. Management of complicated and uncomplicated acute type B dissection. A systematic review and meta-analysis. Annals of Cardiothoracic Surgery. 2014;3(3):234.

34. Hanna JM, Andersen ND, Ganapathi AM, McCann RL, Hughes GC. Five-year results for endovascular repair of acute complicated type B aortic dissection. Journal of Vascular Surgery. 2014;59(1):96-106.

35. Lou X, Chen EP, Duwayri YM, Veeraswamy RK, Jordan Jr WD, Zehner CA, et al. The impact of thoracic endovascular aortic repair on long-term survival in type B aortic dissection. The Annals of Thoracic Surgery. 2018;105(1):31-8.

36. Hao Z, Zhi-Wei W, Zhen Z, Xiao-Ping H, Hong-Bing W, Yi G. Endovascular stent-graft placement or open surgery for the treatment of acute type B aortic dissection: a meta-analysis. Annals of Vascular Surgery. 2012;26(4):454-61.

37. Miyairi T, Miyata H, Chiba K, Nishimaki H, Ogawa Y, Motomura N, et al. Influence of timing after thoracic endovascular aortic repair for acute type B aortic dissection. The Annals of Thoracic Surgery. 2018;105(5):1392-6.

38. Parsa CJ, Schroder JN, Daneshmand MA, McCann RL, Hughes GC. Midterm results for endovascular repair of complicated acute and chronic type B aortic dissection. The Annals of Thoracic Surgery. 2010;89(1):97-104.

39. Bavaria JE, Brinkman WT, Hughes GC, Khoynezhad A, Szeto WY, Azizzadeh A, et al. Outcomes of thoracic endovascular aortic repair in acute type B aortic dissection: results from the Valiant United States investigational device exemption study. The Annals of

Thoracic Surgery. 2015;100(3):802-9.

40. Fattori R, Montgomery D, Lovato L, Kische S, Di Eusanio M, Ince H, et al. Survival after endovascular therapy in patients with type B aortic dissection: a report from the International Registry of Acute Aortic Dissection (IRAD). JACC: Cardiovascular Interventions. 2013;6(8):876-82.

41. Jia X, Guo W, Li TX, Guan S, Yang RM, Liu XP, et al. The results of stent graft versus medication therapy for chronic type B dissection. Journal of Vascular Surgery. 2013;57(2):406-14.

42. Kato N, Shimono T, Hirano T, Suzuki T, Ishida M, Sakuma H, et al. Midterm results of stent-graft repair of acute and chronic aortic dissection with descending tear: the complication-specific approach. The Journal of Thoracic and Cardiovascular Surgery. 2002;124(2):306-12.

43. Kahn SL, Dake MD. Stent graft management of stable, uncomplicated type B aortic dissection. Perspectives in Vascular Surgery and Endovascular Therapy. 2007;19(2):162-9.

44. Dong Z, Fu W, Wang Y, Wang C, Yan Z, Guo D, et al. Stent graft-induced new entry after endovascular repair for Stanford type B aortic dissection. Journal of Vascular Surgery. 2010;52(6):1450-7.

45. Investigators VR. Mid-term outcomes and aortic remodelling after thoracic endovascular repair for acute, subacute, and chronic aortic dissection: the VIRTUE Registry. European Journal of Vascular and Endovascular Surgery. 2014;48(4):363-71.

46. Desai ND, Gottret J-P, Szeto WY, McCarthy F, Moeller P, Menon R, et al. Impact of timing on major complications after thoracic endovascular aortic repair for acute type B aortic dissection. The Journal of Thoracic and Cardiovascular Surgery. 2015;149(2):S151-S6.

47. Shimono T, Kato N, Yasuda F, Suzuki T, Yuasa U, Onoda K, et al. Transluminal stent-graft placements for the treatments of acute onset and chronic aortic dissections. Circulation. 2002;106(12_suppl_1):I-241-I-7.

48. Durham CA, Aranson NJ, Ergul EA, Wang LJ, Patel VI, Cambria RP, et al. Aneurysmal degeneration of the thoracoabdominal aorta after medical management of type B aortic dissections. Journal of Vascular Surgery. 2015;62(4):900-6.

49. Song C, Lu Q, Zhou J, Yu G, Feng X, Zhao Z, et al. The new indication of TEVAR for uncomplicated type B aortic dissection. Medicine. 2016;95(25):e3919.

50. Schwartz SI, Durham C, Clouse WD, Patel VI, Lancaster RT, Cambria RP, et al. Predictors of late aortic intervention in patients with medically treated type B aortic dissection. Journal of Vascular Surgery. 2018;67(1):78-84.

51. Makaroun MS, Dillavou ED, Kee ST, Sicard G, Chaikof E, Bavaria J, et al. Endovascular treatment of thoracic aortic aneurysms: results of the phase II multicenter trial of the GORE

TAG thoracic endoprosthesis. Journal of Vascular Surgery. 2005;41(1):1-9.

52. Makaroun MS, Dillavou ED, Wheatley GH, Cambria RP, Investigators GT. Five-year results of endovascular treatment with the Gore TAG device compared with open repair of thoracic aortic aneurysms. Journal of Vascular Surgery. 2008;47(5):912-8.

53. Gopaldas RR, Huh J, Dao TK, LeMaire SA, Chu D, Bakaeen FG, et al. Superior nationwide outcomes of endovascular versus open repair for isolated descending thoracic aortic aneurysm in 11,669 patients. The Journal of Thoracic and Cardiovascular Surgery. 2010;140(5):1001-10.

54. Leurs LJ, Bell R, Degrieck Y, Thomas S, Hobo R, Lundbom J. Endovascular treatment of thoracic aortic diseases: combined experience from the EUROSTAR and United Kingdom Thoracic Endograft registries. Journal of Vascular Surgery. 2004;40(4):670-9.

55. Afifi RO, Azizzadeh A, Estrera AL. Complications of TEVAR. Surgical Management of Aortic Pathology. Springer. 2019; 1211-23.

56. Hughes K, Guerrier J, Obirieze A, Ngwang D, Rose D, Tran D, et al. Open versus endovascular repair of thoracic aortic aneurysms: a nationwide inpatient sample study. Vascular and Endovascular Surgery. 2014;48(5-6):383-7.

57. Desai ND, Burtch K, Moser W, Moeller P, Szeto WY, Pochettino A, et al. Long-term comparison of thoracic endovascular aortic repair (TEVAR) to open surgery for the treatment of thoracic aortic aneurysms. The Journal of Thoracic and Cardiovascular Surgery. 2012;144(3):604-11.

58. Von Allmen R, Anjum A, Powell J. Outcomes after endovascular or open repair for degenerative descending thoracic aortic aneurysm using linked hospital data. Journal of British Surgery. 2014;101(10):1244-51.

59. Arnaoutakis DJ, Arnaoutakis GJ, Abularrage CJ, Beaulieu RJ, Shah AS, Cameron DE, et al. Cohort comparison of thoracic endovascular aortic repair with open thoracic aortic repair using modern end-organ preservation strategies. Annals of Vascular Surgery. 2015;29(5):882-90.

60. Bicknell C, Powell JT. Aortic disease: thoracic endovascular aortic repair. Heart. 2015;101(8):586-91.

61. Ilyas S, Shaida N, Thakor A, Winterbottom A, Cousins C. Endovascular aneurysm repair (EVAR) follow-up imaging: the assessment and treatment of common postoperative complications. Clinical Radiology. 2015;70(2):183-96.

62. Zimmermann H, Rübenthaler J, Paprottka P, Paprottka K, Reiser M, Clevert D. Feasability of contrast-enhanced ultrasound with image fusion of CEUS and MS-CT for endovascular grafting in infrarenal abdominal aortic aneurysm in a single patient. Clinical Hemorheology and Microcirculation. 2016;64(4):711-9.

63. Rübenthaler J, Reiser M, Cantisani V, Rjosk-Dendorfer D, Clevert D. The value of contrast-enhanced ultrasound (CEUS) using a high-end ultrasound system in the characterization of endoleaks after endovascular aortic repair (EVAR). Clinical Hemorheology and Microcirculation. 2017;66(4):283-92.

64. Ruebenthaler J, Zimmermann H, Armbruster M, Müller-Peltzer K, Bogner F, Reiser M, et al. Contrast-enhanced ultrasound in the follow-up of endoleaks after endovascular aortic repair (EVAR). Ultraschall in der Medizin-European Journal of Ultrasound. 2017;38(03):244-64.

65. Clevert D-A, Minaifar N, Kopp R, Stickel M, Meimarakis G, Sommer W, et al. Imaging of endoleaks after endovascular aneurysm repair (EVAR) with contrast-enhanced ultrasound (CEUS). A pictorial comparison with CTA. Clinical Hemorheology and Microcirculation. 2009;41(3):151-68.

66. Clevert D, Horng A, Reiser M. Ultrasound imaging of the abdominal aorta. Der Radiologe. 2009;49(11):1024-32.

67. de Figueiredo GN, Müller-Peltzer K, Schwarze V, Rübenthaler J, Clevert D-A. Ultrasound and contrast enhanced ultrasound imaging in the diagnosis of acute aortic pathologies. Vasa. 2019;48(1):17-22.

68. Carrafiello G, Recaldini C, Laganà D, Piffaretti G, Fugazzola C. Endoleak detection and classification after endovascular treatment of abdominal aortic aneurysm: value of CEUS over CTA. Abdominal Imaging. 2008;33(3):357-62.

69. Chung J, Kordzadeh A, Prionidis I, Panayiotopoulos Y, Browne T. Contrast-enhanced ultrasound (CEUS) versus computed tomography angiography (CTA) in detection of endoleaks in post-EVAR patients. Are delayed type II endoleaks being missed? A systematic review and meta-analysis. Journal of Ultrasound. 2015;18(2):91-9.

70. Guo Q, Zhao J, Huang B, Yuan D, Yang Y, Zeng G, et al. A systematic review of ultrasound or magnetic resonance imaging compared with computed tomography for endoleak detection and aneurysm diameter measurement after endovascular aneurysm repair. Journal of Endovascular Therapy. 2016;23(6):936-43.

71. Habets J, Zandvoort HJ, Reitsma JB, Bartels L, Moll F, Leiner T, et al. Magnetic resonance imaging is more sensitive than computed tomography angiography for the detection of endoleaks after endovascular abdominal aortic aneurysm repair: a systematic review. European Journal of Vascular and Endovascular Surgery. 2013;45(4):340-50.

72. Görich J, Rilinger N, Sokiranski R, Orend K-H, Ermis C, Krämer SC, et al. Leakages after endovascular repair of aortic aneurysms: classification based on findings at CT, angiography, and radiography. Radiology. 1999;213(3):767-72.

73. Foundation ACoC, Guidelines AHATFoP, Surgery AAfT, Radiology ACo, Association AS,

Anesthesiologists SoC, et al. 2010 ACCF/AHA/AATS/ACR/ASA/SCA/SCAI/SIR/STS/SVM guidelines for the diagnosis and management of patients with thoracic aortic disease. Journal of the American College of Cardiology. 2010;55(14):27-129.

74. Walsh SR, Tang TY, Boyle JR. Renal consequences of endovascular abdominal aortic aneurysm repair. Journal of Endovascular Therapy. 2008;15(1):73-82.

75. Howells P, Eaton R, Patel A, Taylor P, Modarai B. Risk of radiation exposure during endovascular aortic repair. European Journal of Vascular and Endovascular Surgery. 2012;43(4):393-7.

76. Hertault A, Maurel B, Pontana F, Martin-Gonzalez T, Spear R, Sobocinski J, et al. Benefits of completion 3D angiography associated with contrast enhanced ultrasound to assess technical success after EVAR. European Journal of Vascular and Endovascular Surgery. 2015;49(5):541-8.

77. Liu Y, Han M, Zhao J, Kang L, Ma Y, Huang B, et al. Systematic review and meta-analysis of current literature on isolated abdominal aortic dissection. European Journal of Vascular and Endovascular Surgery. 2020;59(4):545-56.

78. Pape LA, Awais M, Woznicki EM, Suzuki T, Trimarchi S, Evangelista A, et al. Presentation, diagnosis, and outcomes of acute aortic dissection: 17-year trends from the International Registry of Acute Aortic Dissection. Journal of the American College of Cardiology. 2015;66(4):350-8.

79. Clough RE, Barillà D, Delsart P, Ledieu G, Spear R, Crichton S, et al. Editor's Choice–long-term survival and risk analysis in 136 consecutive patients with type B Aortic dissection presenting to a single centre over an 11 year period. European Journal of Vascular and Endovascular Surgery. 2019;57(5):633-8.

80. Evangelista A, Isselbacher EM, Bossone E, Gleason TG, Eusanio MD, Sechtem U, et al. Insights from the international registry of acute aortic dissection: a 20-year experience of collaborative clinical research. Circulation. 2018;137(17):1846-60.

81. Wang D, Ma T, Guo D, Xu X, Chen B, Jiang J, et al. Endovascular treatment of acute and chronic isolated abdominal aortic dissection. Vascular. 2018;26(4):418-24.

82. Wang G, Zhai S, Zhang Z, Shi S, Zhang D, Liang K, et al. Clinical experience in treatment of the isolated abdominal aortic dissection. Chinese Journal of Radiology. 2017:607-11.

83. De González AB, Mahesh M, Kim K-P, Bhargavan M, Lewis R, Mettler F, et al. Projected cancer risks from computed tomographic scans performed in the United States in 2007. Archives of Internal Medicine. 2009;169(22):2071-7.

84. McCollough CH, Bushberg JT, Fletcher JG, Eckel LJ, editors. Answers to common questions about the use and safety of CT scans. Mayo Clinic Proceedings; 2015: Elsevier.

85. Brenner DJ, Hall EJ. Computed tomography—an increasing source of radiation exposure. New England Journal of Medicine. 2007;357(22):2277-84.

86. Bevelacqua JJ. Practical and effective ALARA. Health Physics. 2010;98(2):S39-S47.

87. Radiologists RCo. Information Submitted to Health Education England Workforce Planning and Education Commissioning Round–2015/16. The British Institute of Radiology. United Kingdom; 2016.

88. Moser J, Sheard S, Edyvean S, Vlahos I. Radiation dose-reduction strategies in thoracic CT. Clinical Radiology. 2017;72(5):407-20.

89. GuÐjónsdóttir J, Ween B, Olsen DR. Optimal use of AEC in CT: a literature review. Radiologic Technology. 2010;81(4):309-17.

90. Ohana M, Jeung M, Labani A, El Ghannudi S, Roy C. Thoracic dual energy CT: acquisition protocols, current applications and future developments. Diagnostic and Interventional Imaging. 2014;95(11):1017-26.

91. Siegel MJ, Curtis WA, Ramirez-Giraldo JC. Effects of dual-energy technique on radiation exposure and image quality in pediatric body CT. American Journal of Roentgenology. 2016;207(4):826-35.

92. Newell Jr JD, Fuld MK, Allmendinger T, Sieren JP, Chan K-S, Guo J, et al. Very low-dose (0.15 mGy) chest CT protocols using the COPDGene 2 test object and a third-generation dual-source CT scanner with corresponding third-generation iterative reconstruction software. Investigative Radiology. 2015;50(1):40-5.

93. Maldjian PD, Goldman AR. Reducing radiation dose in body CT: a primer on dose metrics and key CT technical parameters. American Journal of Roentgenology. 2013;200(4):741-7.

94. Kanal KM, Stewart BK, Kolokythas O, Shuman WP. Impact of operator-selected image noise index and reconstruction slice thickness on patient radiation dose in 64-MDCT. American Journal of Roentgenology. 2007;189(1):219-25.

95. Willemink MJ, de Jong PA, Leiner T, de Heer LM, Nievelstein RA, Budde RP, et al. Iterative reconstruction techniques for computed tomography Part 1: technical principles. European Radiology. 2013;23(6):1623-31.

96. den Harder AM, Willemink MJ, de Ruiter QM, Schilham AM, Krestin GP, Leiner T, et al. Achievable dose reduction using iterative reconstruction for chest computed tomography: a systematic review. European Journal of Radiology. 2015;84(11):2307-13.

97. Laqmani A, Regier M, Veldhoen S, Backhaus A, Wassenberg F, Sehner S, et al. Improved image quality and low radiation dose with hybrid iterative reconstruction with 80 kV CT pulmonary angiography. European Journal of Radiology. 2014;83(10):1962-9.

98. Shen Y, Fan Z, Sun Z, Xu L, Li Y, Zhang N, et al. High pitch dual-source whole aorta CT

angiography in the detection of coronary arteries: a feasibility study of using iodixanol 270 and 100 kVp with iterative reconstruction. Journal of Medical Imaging and Health Informatics. 2015;5(1):117-25.

99. Sharara SM, Monnin SR, Rubio M, Khouzam RN, Ragheb SR. Can radiation dose burden of CT angiography be reduced while still accurately diagnosing etiology of acute chest pain? Current Problems in Cardiology. 2021;46(4):100766.

100. Barrett JF, Keat N. Artifacts in CT: recognition and avoidance. Radiographics. 2004;24(6):1679-91.

101. Modica MJ, Kanal KM, Gunn ML. The obese emergency patient: imaging challenges and solutions. Radiographics. 2011;31(3):811-23.

102. Mayo J, Hartman TE, Lee KS, Primack SL, Vedal S, Müller N. CT of the chest: minimal tube current required for good image quality with the least radiation dose. AJR American Journal of Roentgenology. 1995;164(3):603-7.

103. Ravenel JG, Scalzetti EM, Huda W, Garrisi W. Radiation exposure and image quality in chest CT examinations. American Journal of Roentgenology. 2001;177(2):279-84.

104. Christner JA, Zavaletta VA, Eusemann CD, Walz-Flannigan AI, McCollough CH. Dose reduction in helical CT: dynamically adjustable z-axis X-ray beam collimation. American Journal of Roentgenology. 2010;194(1):W49-W55.

105. Lell MM, May M, Deak P, Alibek S, Kuefner M, Kuettner A, et al. High-pitch spiral computed tomography: effect on image quality and radiation dose in pediatric chest computed tomography. Investigative Radiology. 2011;46(2):116-23.

106. Gunn ML, Kohr JR. State of the art: technologies for computed tomography dose reduction. Emergency Radiology. 2010;17(3):209-18.

107. Apfaltrer P, Hanna EL, Schoepf UJ, Spears JR, Schoenberg SO, Fink C, et al. Radiation dose and image quality at high-pitch CT angiography of the aorta: intraindividual and interindividual comparisons with conventional CT angiography. American Journal of Roentgenology. 2012;199(6):1402-9.

108. Stiller W. Basics of iterative reconstruction methods in computed tomography: a vendor-independent overview. European Journal of Radiology. 2018;109:147-54.

109. Mileto A, Guimaraes LS, McCollough CH, Fletcher JG, Yu L. State of the art in abdominal CT: the limits of iterative reconstruction algorithms. Radiology. 2019;293(3):491-503.

110. Mohammadinejad P, Mileto A, Yu L, Leng S, Guimaraes LS, Missert AD, et al. CT noise-reduction methods for lower-dose scanning: strengths and weaknesses of iterative reconstruction algorithms and new techniques. RadioGraphics. 2021;41(5):1493-508.

111. Singh R, Digumarthy SR, Muse VV, Kambadakone AR, Blake MA, Tabari A, et al. Image

quality and lesion detection on deep learning reconstruction and iterative reconstruction of submillisievert chest and abdominal CT. American Journal of Roentgenology. 2020;214(3):566-73.

112. Chaikof EL, Blankensteijn JD, Harris PL, White GH, Zarins CK, Bernhard VM, et al. Reporting standards for endovascular aortic aneurysm repair. Journal of Vascular Surgery. 2002;35(5):1048-60.

113. Oderich GS, Forbes TL, Chaer R, Davies MG, Lindsay TF, Mastracci T, et al. Reporting standards for endovascular aortic repair of aneurysms involving the renal-mesenteric arteries. Journal of Vascular Surgery. 2021;73(1):4S-52S.

114. De Bruin JL, Baas AF, Buth J, Prinssen M, Verhoeven EL, Cuypers PW, et al. Long-term outcome of open or endovascular repair of abdominal aortic aneurysm. New England Journal of Medicine. 2010;362(20):1881-9.

115. Reimerink JJ, Hoornweg LL, Vahl AC. Endovascular repair versus open repair of ruptured abdominal aortic aneurysms: a multicenter randomized controlled trial. Journal of Vascular Surgery. 2013;58(5):1424-5.

116. Patel R, Sweeting MJ, Powell JT, Greenhalgh RM, Investigators ET. Endovascular versus open repair of abdominal aortic aneurysm in 15-years' follow-up of the UK endovascular aneurysm repair trial 1 (EVAR trial 1): a randomised controlled trial. The Lancet. 2016;388(10058):2366-74.

117. Becquemin J-P, Kelley L, Zubilewicz T, Desgranges P, Lapeyre M, Kobeiter H. Outcomes of secondary interventions after abdominal aortic aneurysm endovascular repair. Journal of Vascular Surgery. 2004;39(2):298-305.

118. Lederle FA, Freischlag JA, Kyriakides TC, Matsumura JS, Padberg Jr FT, Kohler TR, et al. Long-term comparison of endovascular and open repair of abdominal aortic aneurysm. The New England Journal of Medicine. 2012;367:1988-97.

119. Karthikesalingam A, Page A, Pettengell C, Hinchliffe R, Loftus I, Thompson M, et al. Heterogeneity in surveillance after endovascular aneurysm repair in the UK. European Journal of Vascular and Endovascular Surgery. 2011;42(5):585-90.

120. Brody AS, Frush DP, Huda W, Brent RL, Radiology So. Radiation risk to children from computed tomography. Pediatrics. 2007;120(3):677-82.

121. De Bruin J, Groenwold R, Baas A, Brownrigg J, Prinssen M, Grobbee D, et al. Quality of life from a randomized trial of open and endovascular repair for abdominal aortic aneurysm. Journal of British Surgery. 2016;103(8):995-1002.

122. Dias NV, Riva L, Ivancev K, Resch T, Sonesson B, Malina M. Is there a benefit of frequent CT follow-up after EVAR? European Journal of Vascular and Endovascular Surgery. 2009;37(4):425-30.

123. Baderkhan H, Haller O, Wanhainen A, Björck M, Mani K. Follow-up after endovascular aortic aneurysm repair can be stratified based on first postoperative imaging. Journal of British Surgery. 2018;105(6):709-18.

CHAPTER 2

3D PRINTING TECHNOLOGIES AND ITS MEDICAL APPLICATIONS

In order to be able to study diseases associated with aortic dissection (AD) and to simulate endovascular surgery, patient-specific blood vessel models were constructed using 3D printing (3DP) technology to reproduce arterial anatomy in this thesis. In order to be able to produce patient-specific models quickly and accurately, the primary work in this thesis is to develop an efficient and reproducible protocol. To ensure that the 3D-printed model represents the real patient vessel, the materials must have the same radiological and physical properties as the real aorta. Finally, after creating a patient-specific model that closely resembles real blood vessels, the model was validated as an experimental phantom.

2.1 Introduction of 3D printing technologies

Three-dimensional printing (3DP) is a popular manufacturing technology that has inspired creative minds in recent years. The 3D printing process initially divides the 3D computer model of the object into 2D layered slices, and then stacks the printing material to form the model according to the layered slices and repeats the stacking action until the model is formed. Prior to 3DP technology, the traditional manufacturing processing method for creating 3D models was a subtractive method of slowly cutting and carving large pieces of material, which often resulted in waste of materials (**Figure 2.1**). 3DP technology adopts the additive method of stacked layers, which avoids unnecessary material waste. This revolutionary manufacturing method is potential to build physical models with complex structure that is difficult to achieve in traditional subtraction way. This innovation technology can be traced back to the 1980s, in 1981 Dr Hideo Kodama proposed a rapid prototyping technique for fabricating a 3D plastic model with photopolymers which was the first piece of literature to describe layer-by-layer manufacturing approach (1). This method which known as Stereolithography (SLA) was the first 3DP process invented. Unfortunately, Dr Kodama failed to file the patent for rapid prototyping technology because he missed the deadline for the application. A few years later, in 1987 the very first 3D printer, SLA-1 was released by 3D Systems Corporation. 3DP was born.

Rapid prototyping technology has been in practice for many years. The most common method of 3DP is to create a digital computer model file, heat the metal powder or plastic material to make it in a molten plastic state, and then print it layer by layer to produce a model, this method is also known as fuse deposition modelling or material extrusion. Some of other 3DP methods such as SLA, powder bed fusion and material jetting are also widely using in different applications (2). Over the years, its

manufacturing process has continued to make breakthroughs and innovations. In this wave of development, more and more commercial printers and open-source software tools are playing an important role as a promoter. Since the software and hardware of 3DP were opened up, outstanding engineers from all over the world have been able to participate in collective creation and work together. It is an ideal to popularize 3DP technology in general households. Such an environment drives a variety of models to introduce new models one after another. It also allows the general public to evaluate the print quality, print speed, printable item size, output stability, and price to choose a printer that meets their personal needs.

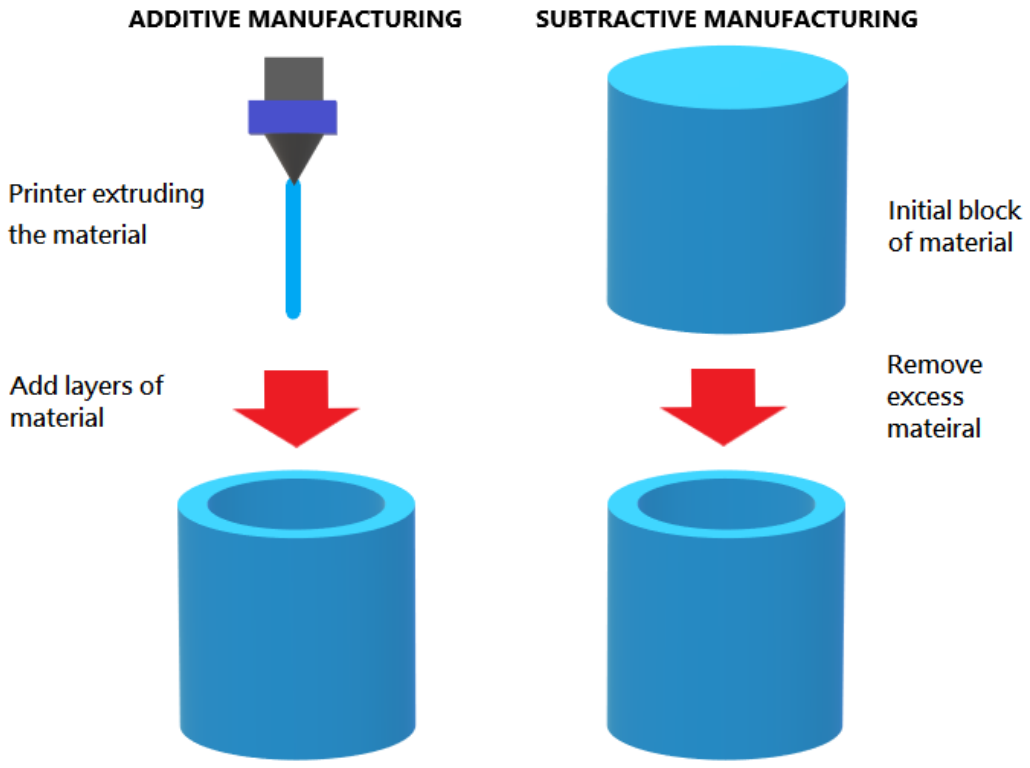

Figure 2.1 Compared to traditional subtractive manufacturing (Right), additive 3DP (Left) stacks material layer-by-layer to produce the product, which is able to avoid waste of material.

2.2 Medical applications of 3D printing

Despite the concept of 3DP was proposed since early 1980s, however, due to fancy price and immature technique, it was not popular in public domain. With the development of technique, the cost of 3DP has plummeted and the accuracy has improved, it is already a powerful manufacturing technology well known by the public. The 3D printers nowadays have affordable price, user-friendly interface and there are many open-source software which are easy to design customize models, therefore, it gets more and more exposure in front of the public. With Innovators keep to push the envelope, the potential of 3DP begins to reveal. Plenty of applications are discovered and developed, 3DP with biomaterials is potentially the solution to organ shortage (3), 3DP of buildings could possibly solve the housing crisis (4).

In early 2000s, research of medical applications were initially reported (5-8). The early medical applications reports focused on custom prostheses, few years later, patient-specific 3D printed models began to be used for preoperative guiding and surgeons training (9-12). Today, with the development of materials that are both biocompatible and printable, 3DP is becoming increasingly useful (13, 14). Personalized 3D printed models are able to accurately replicate anatomy and pathology and provide a tactile and visible way for diagnosis and treatment planning. Evolving 3D printer with faster printing speed save more time at printing process and the friendly software interface lower the threshold of software learning and practicing. Multiple material printers allow operators use different materials and colours to distinguish different organs or tissue on the models, which make the models visually easier to understand (15).

Four main applications are fulfilled and used in medical area nowadays, including 3D printed research phantom, implantable and assistive devices, training and

education, preoperative planning and guiding.

2.2.1 3D printed models for research

3DP is able to customize complex patient-specific anatomical model which is difficult to achieve through traditional subtractive manufacturing. This amazing characteristic brings new approaches into academia and clinical practice. A 3D printed model with high quality and accuracy with mechanical property close to real human organ or tissue is helpful in various applications. With use of 3D printed models, experimental research can be conducted on these models instead of real human organs, thus avoiding unnecessary exposure of risks such as radiation exposure to patients (16).

A patient-specific vascular model, due to its complex and hollow anatomical structure, could be easier produced by 3DP than subtractive manufacturing. Ionita et al. successfully created several vascular phantoms through a PolyJet 3D printer, including a complex neurovascular phantom (17). Their results showed that despite the pre- and post-print phases are challenging due to the limitation of process workflow, the accurate phantoms generated could be used to test new endovascular device performance and study physiological aspects of the vascular disease. Hazelaar et al. thought the commercially available phantoms are commonly manufactured in simple, generic forms and sizes and therefore do not resemble the clinical situation for many patients, therefore, they made an anthropomorphic thorax phantom based on a patient data with lung cancer (18). They used different materials to represent bone, soft tissue, lung structure and tumour which gave this model life-like feature and radiological property under CT scan. Despite the results CT image look like similar enough for their requirements, the mechanical and radiological properties are still different from the patient.

Within the last several years, some studies investigated the printing materials with different properties for human body phantom (19-22). Although there are various printing materials in the market, some of them have mechanical property similar to real human tissue, however, there are still no printing material that can represent real human tissue mechanically or radiologically. To improve the 3D printed phantom, identifying the materials which are able to represent each human body part is the main challenge now.

2.2.2 Implantable and assistive devices

Use 3DP to create implantable devices or prosthesis is one of the fantastic applications in medical area. Due to the characteristic that 3DP is able to customize and personalize devices for each patient, with the right materials, development of this technology could potentially solve the organ shortage crisis and save lives from incurable disease by switching a personalized organ for them. However, this promising technique is still in its early stage.

2.2.2.1 3D Bioprinting

3D Bioprinting is an additive layer-by-layer manufacturing process that similar to traditional 3DP except the materials. Bioprinting use cells and biomaterials as materials to replicate living tissue, bone, blood vessels and can potentially create whole organ for use in medical procedures and researches. Since 1988 the concept of bioprinting was first introduced by Klebe (23), the bioprinting technique has been developed more slowly than mainstream 3DP because of the cellular complexity of the living body. Till 2002, the first extrusion-based bioprinting technology was reported by Landers et al (24). The following years saw the introduction of many bioprinting methods and printer improvement (25-28). Recently in 2019, Noor et al. successfully manufactured a perfusable scale-down heart (29). Despite bioprinting having

prospective future for engineering whole organs, it still has a long way to go. In recent years, 3D bioprinting technology has gradually been adopted in the medical and health industry and has become a high-potential technology for the manufacture of artificial tissues and organs. Experts and scholars hope that it can change the dilemma of various medical clinical diagnosis and treatment, especially the development of medicine. In the past, compound drugs gradually turned to the diagnosis and treatment of cells and various active factors. This has drawn high attention in bioprinting. How to effectively mix, design and assemble bio-ink, cells and active factors together are the key development directions of future regenerative medicine.

2.2.2.2 Implantable devices

Contrary to 3D bioprinting, 3D printed Implantable devices were successively passed the United States Food and Drug Administration (FDA) approvals since 2010 (30) and become widely used in medical procedures. Implants are commonly used medical devices today, such as pedicle screws, dental nails or artificial hip joints, etc. Depending on the patient's condition, its function can be used as an auxiliary corrective treatment or directly replace the original tissue of the human body. Compared to soft tissue bioprinting, development of hard tissue application is relatively mature. Hard tissue 3DP had been used in modern medical area such as orthopaedics and dentistry (31-33). The certification and commercial sales of these customized metal implant medical devices demonstrate that future medical treatment plans will gradually be patient-centric, and the quality of medical care will be greatly improved from precise planning, precise surgery to precise treatment.

2.2.2.3 Assistive devices

The main function of the assistive device is to make it easier for the user to move around, thereby achieving the purpose of independence. Generally, assistive devices

are obtained through purchase or tailor-made. The former often cannot meet the user's size, and the latter often requires a long time to wait and has the disadvantage of higher cost. In recent years, the rapid growth of 3DP technology has the advantages of higher structural design freedom, lower cost in small-scale production, rapid prototyping of customized products, and saving material waste. These advantages just to make up for the above shortcomings (34).

2.2.3 Training and Education

2.2.3.1 Anatomy teaching tool

3D printed models (3DP) are also powerful tools for education purpose. For medical student, the traditional anatomy teaching is through cadaver dissection or plastinated specimens. Articles discussing the use of 3D printed models as anatomy teaching tools have shown positive and promising results (35-37). These articles have a clear discussion on why 3DP is better than using cadavers or specimens for teaching anatomy. The advantages include easy to store, reproducible, relatively cheap, scalable, capable of showing rare cases, dissectible. Compared to precious cadaver teaching method, a 3D printed model does not have moral or legal issues. Anatomy teaching has also been further improved with the development of 3DP technology. The new generation of 3D printers can print models in a variety of colours, and even use different materials in different parts, which makes the 3DP technology more room for development in the teaching of anatomy. Lim et al. pointed out that 3DP is an innovative and effective way for undergraduate anatomy learning (38). Chen et al. reported that used 3DP as teaching tools for gastrocolic trunk anatomy structure had received positive feedback from students while Ye et al. also reported using 3DP for education is able to improve students' understanding of anatomy (39, 40). Since 2020, many countries and regions adopt distance teaching due to coronavirus disease

pandemic. Students have had no access to cadavers during the pandemic, which used to be the principal way to learn anatomy. Under these circumstances, it is possible for 3DP to become a potential tool for anatomy education. However, there is limited evidence of its educational effectiveness compared to cadaveric dissection (41).

2.2.3.2 Surgical education

Simulated surgery training is another way to help medical students, inexperienced surgeons or residents practice surgery procedures and understand the anatomy of 3DP models. It can also allow trainees to improve their understanding of spatial pathology and explore specific anatomy. In different medical fields, the application of 3D models as training tool had been discussed recent years, including Otolaryngology (42), Orthopaedics (43, 44), Ophthalmology (45, 46), Neurosurgery (47-50), Urology (51, 52), General Surgery (53, 54), Anaesthesia (55). Sun and Wang et al. discussed about 3D printed models used in cardiovascular surgery training simulation and preoperative planning in their review paper (14, 56). In all of these previous studies, they believe that using solid 3D models as training tools is an efficient and helpful training approach. Because the 3DP model is reproducible and replaceable, trainees can learn from their mistakes. This training method provides trainees with a safe and relatively stress-free learning environment, and can be practiced for various special cases.

Despite many positive feedbacks, 3DP simulation models still have their limitations. The accuracy of the model for complex structures, such as hollow vessel models, aneurysms, etc., used to be a major limitation of 3DP (57). But after years of development, most of this problem has been overcome (58, 59). Another limitation is that 3DP usually only prints the lesion or region of interest, lack of description of other

important anatomical surrounding organ and tissue. Also, for small blood vessels and tissues, it cannot be achieved with the current commercially-available technology. (60).

2.2.3.3 Patient education

Currently, the most commonly used diagnostic tools are mainly 2D images. For example, CT and MRI are both two-dimensional images. For patients and their families without professional training, it is relatively difficult to interpret 2D images and understand their own condition. Even though there are many imaging software that can convert 2D images into 3D digital models, a physical 3D model that can be touched is far easier to understand than a 2D image that can only be viewed through a screen (61, 62). Through the demonstration of the 3D model, patients and family members can also understand the upcoming operation in a simple and easy way, figure the risks and reduce unnecessary worries. Compared with commercial mass-produced models, 3D printed models can also express the situation of each different patient more accurately (63).

Andolfi et al. reported that discussed with patient through multicolour 3D printed model is an effective way to help patient understand and get ready for coming treatment (64). Yang et al. used 3D printed liver models for educating children with hepatic tumours and their parents. The results show after presentation with models displayed, parents demonstrated improvements in their understanding of basic liver anatomy, basic liver physiology, tumour characteristic, surgical procedure and associated surgical risks (65). Zhuang et al. randomly separate 45 patients with degenerative lumbar disease into three groups and educated them the lumbar anatomy, physiology and the surgical plan to them (63). The results show the patients educated with personalized 3D models demonstrated an expanded level of understanding and satisfaction than patients educated with CT and MRI imaging and

3D digital reconstruction. Based on the above research and with the increasingly advanced 3D printing technology, the use of personalized 3D models may be the star of the future for patient education.

2.2.4 Preoperative planning and simulation

The obvious answer that using patient-specific 3D printed models as a preoperative guiding tool are helpful is they provide surgeons a physical, touchable model to understand anatomical structure inside patients. The purpose of the simulation is to make the trainees better understand the anatomy and the procedure of the operation, while the preoperative plan is to prepare for the upcoming operation (66). Using a touchable 3DP model at this stage will enable the surgeon to have a more comprehensive understanding and preparation for the upcoming operation, including improves the understanding of the anatomy of individual patients and plans possible surgical methods, map out the best surgical routes, determining the most appropriate tools needed, and evaluates the feasibility of surgical methods through exercises on models (67). Even during the operation, the 3D printed model can be used as an auxiliary surgical tool for immediate correction and adjustment of the treatment plan (68). Thus, these 3D printed anatomic models based on patient-specific anatomy can be used for surgical planning both in and out of the operating room (69).

Compared to traditional 2D images, for example, CT and MRI, an accurate 3D printed model can provide a further non-invasive viewing opportunity and could be easier for doctors to prepare the procedure in certain disease with complex anatomical structure. Several studies have demonstrated that use patient-specific models for treatment planning and intra-operative guiding may potentially avoid making mistakes during surgery, and reduce the operation time (70). Furthermore, the use of preoperative 3D models as preoperative tool may result in fewer complications and

decrease reintervention rate, so patients can save more healthcare expenses by reducing the stays in the hospital after operation (71).

3D models for preoperative treatment planning and guiding become a very popular research area in recent years. Mahaisavariya et al. used 3D printed model as a surgical simulation tool to perform corrective osteotomy for cubitus varus patients (72). Both of their patients were successfully operated as surgical planning without any complication. Huang et al. used 3D models as a guiding tool to pre-shape the stent graft before endovascular aneurysm repair operation for a juxtarenal abdominal aortic aneurysm case (73). To precisely locate the fenestration position, they 3D printed a hollow abdominal aortic aneurysm model and used it to cut the fenestration holes on the stent graft. They claimed this novel approach for 3DP guiding stent graft fenestration is cheap and potentially possible to be used in emergency situation, the most important is, this method is able to improve the accuracy of fenestration on stent graft significantly. Wang et al. create 3D printed models in personalized treatment for complex spinal disorder patients (74). In their research, the use of 3D models reduced operating time and intraoperative blood loss as well as the risk of postoperative complications. 3DP techniques can also be used to create surgical tools and instruments. Sheth et al. print a solid 3D model of a glenohumeral joint with recurrent anterior shoulder instability and complex Bankart and Hill-Sachs lesions (75) because in this kind of complex anatomy structure, 2D image is often inadequate. The model they create was used in the preoperative planning stages of an arthroscopic Bankart repair and remplissage.

These researches present positive outcomes about the use of 3DP in health care application. It may able to decrease the cost of operative and reduce the time spent in surgery room. More and more research of 3D printed model for preoperative planning

and guiding are published. However, most of their methods still have not been widely admitted as an effective way due to insufficient patients and samples. Besides, most hospitals do not have on-site 3D printers and lack operators who have both 3DP and medical knowledge. Despite there are still a lot of space to improve the clinical 3DP application technology, these studies prove that 3DP is a powerful manufacturing technology that full of different possibility to be used in health care domain.

2.3 3D printing and Aortic dissection

3D printed models have proven to be highly accurate in replicating normal anatomy and cardiac pathology, personalized 3D printed models created from cardiac imaging data, primarily from cardiac CT images, are increasingly used in cardiovascular diseases, mainly for preoperative planning and simulation of complex surgical procedures and medical education (31, 76) (14). To achieve a medical 3DP model, the workflow can be separated into five steps: image acquisition, image segmentation, surface mesh generation, Standard Tessellation Language (STL) post processing, and printing (58, 77, 78) (**Figure 2.2**). Image data can be acquired in a number of ways, the most common being CT and MRI. Import the image data into the software for image segmentation, dividing the original image into multiple segments. The image segmentation process aims to simplify image data, locate regions of interest, and confirm boundaries by labelling each pixel as a distinct segment. Pixels in the same segment have certain characteristics (79-81). After image segmentation, the image becomes more meaningful and easier to analyse. Surface mesh generation creates the surface structure of the model for 3DP based on the segmented dataset, and converts this file to the STL file format, which describes the surface geometry and mesh data. Due to the characteristics of the STL file format, it has been widely used in computer-aided manufacturing and 3DP. STL is also a standard file for most 3DP machines. The

step after surface mesh generation is STL post-processing, during which the STL file is checked and repaired to ensure it is printable. For example, repair holes and gaps in model surfaces, repair discontinuous surfaces, and verify wall thickness. In the final step, the STL file will be transferred to the press and a physical haptic model will be generated.

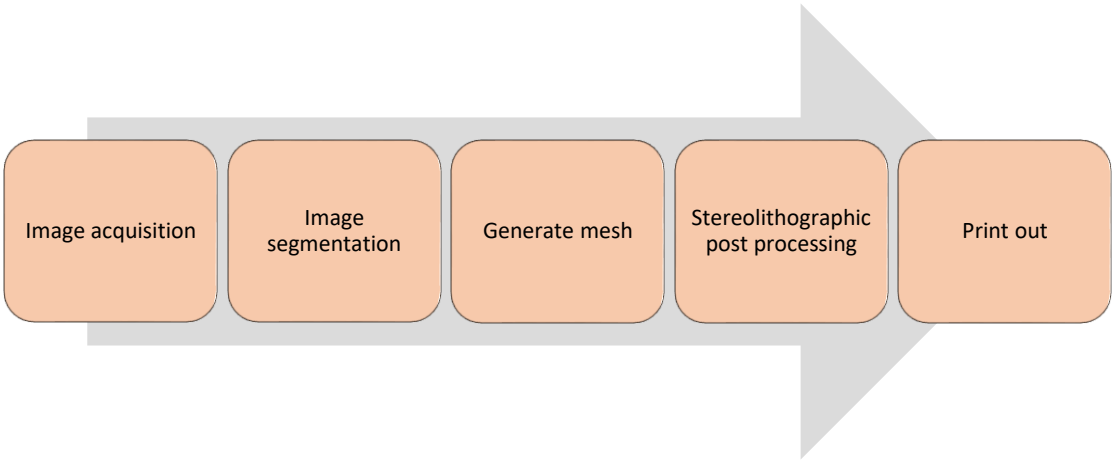

Figure 2.2 Five steps to produce a patient-specific 3D printed model: image acquisition, image segmentation, surface mesh generation, stereolithographic (STL) post processing, and printing.

2.4 Limitations of making 3D printed AD models

Some previous studies created AD models for various purpose, Lei et al. used 3D printed model for customized patient-specific aortic stent graft (82). Gomes and his colleague use 3D printed AD model to guide creation of fenestrations in stent graft (83). Zhang et al. also proved that fenestrations diameter could be reduced by guiding with 3D printed model (84). Hossien et al. created 3D printed models in preplanning of Type A AD (85). Finotello et al. investigated a twelve- year follow up post TEVAR patient through 3D printed model (86). Despite many researches used to manufacture 3D printed AD models, however, some of them did not provide a complete segmentation method, some of them did not create a hollow model, and in some studies, the printing material did not have mechanical property close to real aorta. Due

to the complex anatomy structure and thin thickness of intimal flap, for those without relevant basic experience, segmentation of AD could be quite challenging (**Figure 2.3**). In general, hollow models are more practical than solid ones. However, under contrast enhancement CT, the edge of the wall is hard to be identified and the aortic wall is difficult to be delineated.

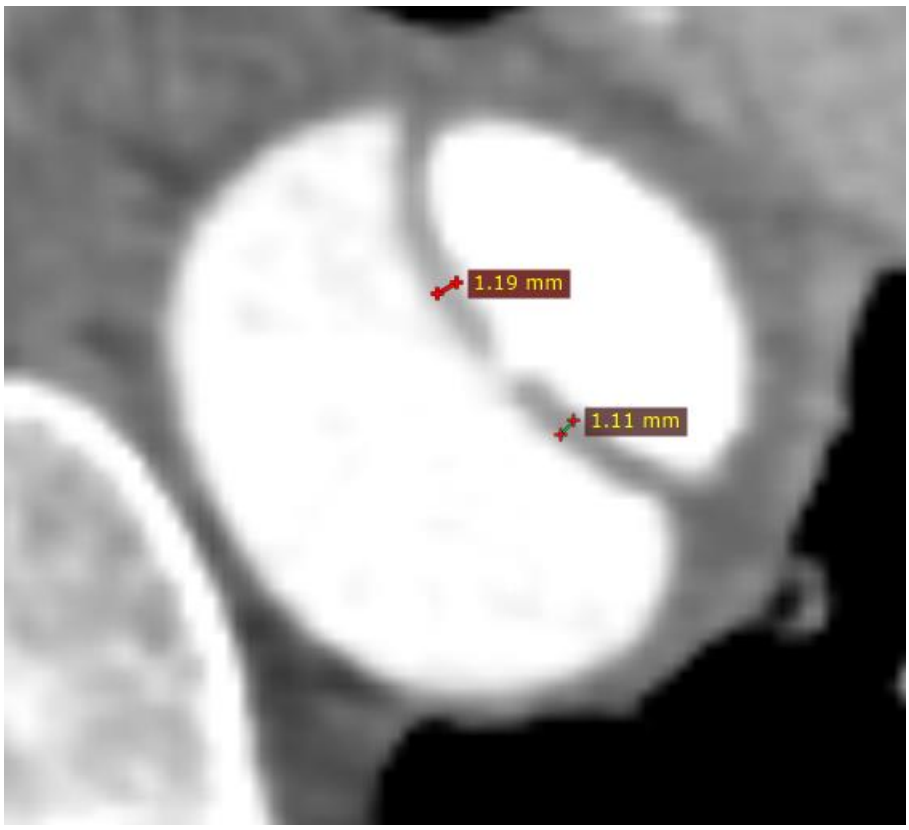

Figure 2.3 Because of the thin thickness of intimal flap and unclear aortic wall, AD segmentation is challenging.

In recent years, many open-source software have updated the hollow function. As long as the TL and FL can be segmented out, hollow function is able to transfer it into hollow model by just one click. Since TL and FL are treated as two distinct objects, the intimal flap is double-counted when performing the hollow function. As **Figure 2.4** shows, since TL and FL are hollowed out respectively, the thickness of intimal flap has doubled. Incorrect thickness can still be seen despite after merged post-processing,

plus, much post-processing can easily change the reality and accuracy of the model. Segment the model as close to the original image as possible without excessive post-processing is another aim.

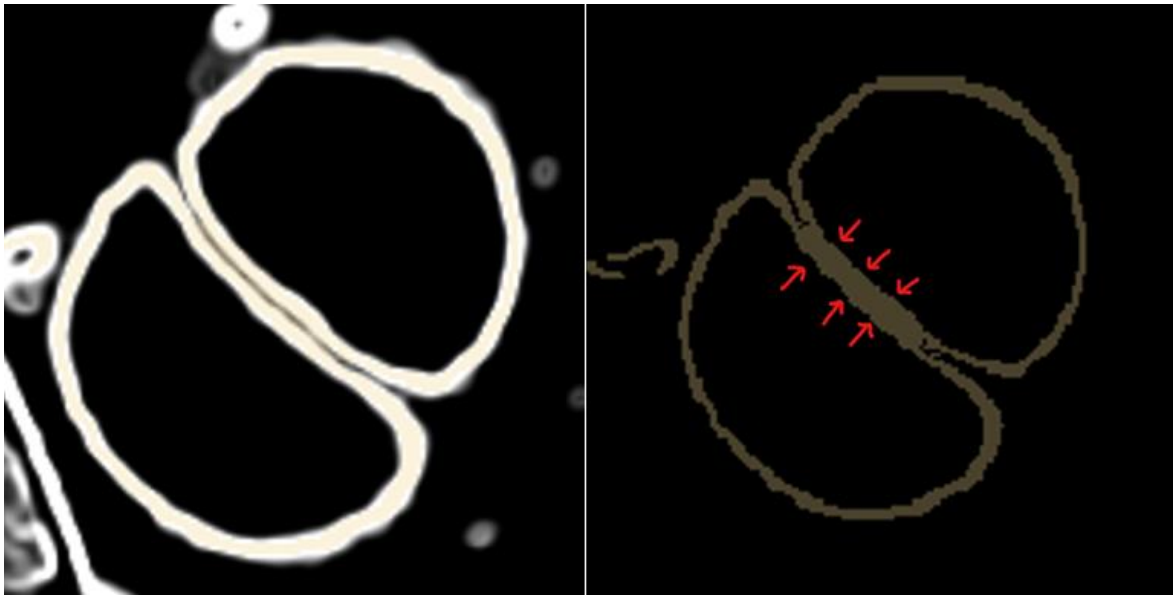

Figure 2.4 Left: The intimal flap is doubled thickness after hollow function. Right: After transfer to segmentation mode and limited post-processing, intimal flap is still thicker than original image.

In order to make 3DP easier to use in clinical practice, besides reducing the cost of 3DP, a simple and fast segmentation protocol that can be used on open-source software is also necessary. Therefore, in this research we tried to verify a proper segmentation method of using 3D printed model for AD research, find a suitable printing material which has mechanical and radiological properties close to real human body for AD phantom model. We also use AD model as a phantom to optimise follow up CT scan parameters for post TEVAR patients, which further improve the value of 3D printed models in medical domain.

Due to complex anatomy and controversial treatment modalities, patient-specific 3D printed model has the potential to be a powerful tool for AD patients. From

treatment planning, educating patients to simulating surgical procedures, an accurate patient-specific 3D printed model can provide greatly assistance. However, in addition to the exorbitant printing cost, there are still some limitations before high-quality 3DP that can widely assist clinical treatment.

2.5 Accuracy and segmentation process of AD models

Although 3DP has been proven to use CT, MRI and other medical images to create high-accuracy models, however, compared with other diseases, the anatomy of AD involves intimal flap that make segmentation process more difficult, especially to make a hollow model. Because of the thin thickness, intimal flap in AD could be a great challenge in segmentation (87), plus, there were no readily available published guidelines or standardized methods for medical image segmentation and the methods of segmentation need to be improved to achieve a higher quality model in less time (77, 88). In **Chapter 3**, the development of an efficient segmentation protocol for AD cases is proposed and investigated. To address the current lack of published guidance for AD image segmentation, a protocol designed for accurate and efficient segmentation of intimal flap in CT images is proposed and evaluated (89). In this study, there is a focus on using open source software so this method is made easier for replication by people who are not familiar with image segmentation or do not have access to proprietary processing software.

2.6 3D printing materials selection

With the vigorous development of 3DP technology, many companies in the market have developed various printers and different printing materials (**Figure 2.5**). Due to the different operating principles of 3D printers, the materials that can be used are different, and the finished products produced have different characteristics and qualities. In **Chapter 4**, we use the model produced to simulate the situation of real

patients, and we are committed to pursuing a model with mechanical and radiological properties close to the real patient's aorta (90). More realistic mechanical properties make the model more tactile and can also be used for pre-operative simulation or as educational equipment. Since CT scans are a common routine examination in AD patients regardless of preoperative and postoperative, models with radiological properties similar to real blood vessels can be used as phantom for CT scan experiments instead of repeatedly scan real patients. Riedle et al. compared commercial 3D-printed elastomers and found that the mechanical property of TangoPlus Flex is closest to aortic tissues (91). Follow their suggestions, we investigated some different commercial printing materials with different hardness to determine a proper material for AD model.

Figure 2.5 To test mechanical and radiological properties, models were printed through different printing materials.

2.7 Further investigation of the value of 3D printed models

In current CT examinations, the pre-set scanning parameters and doses used for preoperative examination and postoperative follow-up of AD patients usually are the same. However, since postoperative patients need regular and long-term follow-up, reducing the CT examination dose will greatly reduce the risk caused by radiation. In order to further verify the value of 3D models in the medical area, we used the 3D printed AD models as the phantom and repeatedly scanned the same model with different CT scan parameters, try to reduce the dose to postoperative patients by analysing the data from these scans. A quantitative assessment was performed in **Chapter 5**, as a result a recommend optimized scanning protocol is found by comparing the signal-to-noise ratio (SNR) in different images (92). However, an image with lower image quality does not mean that it has no diagnostic value. To verify the diagnostic value of image datasets with different scan parameters, a number of radiology technicians and radiologists were invited to perform a qualitative assessment in **Chapter 6**. All images were anonymised, and participants filled out questionnaires to express whether they thought the images had diagnostic value. Through the studies in Chapters 5 and 6, we found better tracking scan parameters for postoperative AD patients. These studies further demonstrate the value of 3DP for clinical research.

References

1. Kodama H. Automatic method for fabricating a three-dimensional plastic model with photo-hardening polymer. Review of Scientific Instruments. 1981;52(11):1770-3.
2. Shahrubudin N, Lee TC, Ramlan R. An overview on 3D printing technology: Technological, materials, and applications. Procedia Manufacturing. 2019;35:1286-96.
3. Murphy SV, Atala A. 3D bioprinting of tissues and organs. Nature Biotechnology. 2014;32(8):773-85.
4. Sakin M, Kiroglu YC. 3D Printing of Buildings: Construction of the Sustainable Houses of the Future by BIM. Energy Procedia. 2017;134:702-11.
5. Rowe C, Katstra W, Palazzolo R, Giritlioglu B, Teung P, Cima M. Multimechanism oral dosage forms fabricated by three dimensional printing™. Journal of Controlled Release. 2000;66(1):11-7.
6. Curodeau A, Sachs E, Caldarise S. Design and fabrication of cast orthopedic implants with freeform surface textures from 3-D printed ceramic shell. Journal of Biomedical Materials Research: An Official Journal of The Society for Biomaterials, The Japanese Society for Biomaterials, and The Australian Society for Biomaterials and the Korean Society for Biomaterials. 2000;53(5):525-35.
7. Melican MC, Zimmerman MC, Dhillon MS, Ponnambalam AR, Curodeau A, Parsons JR. Three-dimensional printing and porous metallic surfaces: A new orthopedic application. Journal of Biomedical Materials Research: An Official Journal of The Society for Biomaterials, The Japanese Society for Biomaterials, and The Australian Society for Biomaterials and the Korean Society for Biomaterials. 2001;55(2):194-202.
8. Hong S-B, Eliaz N, Leisk G, Sachs E, Latanision R, Allen S. A new Ti-5Ag alloy for customized prostheses by three-dimensional printing (3DP™). Journal of Dental Research. 2001;80(3):860-3.
9. Wilasrusmee C, Suvikrom J, Suthakorn J, Lertsithichai P, Sitthiseriprapip K, Proprom N, et al. Three-dimensional aortic aneurysm model and endovascular repair: an educational tool for surgical trainees. The International Journal of Angiology: official publication of the International College of Angiology, Inc. 2008;17(3):129.
10. Bruyere F, Leroux C, Brunereau L, Lermusiaux P. Rapid prototyping model for percutaneous nephrolithotomy training. Journal of Endourology. 2008;22(1):91-6.
11. Sodian R, Schmauss D, Markert M, Weber S, Nikolaou K, Haeberle S, et al. Three-dimensional printing creates models for surgical planning of aortic valve replacement after previous coronary bypass grafting. The Annals of Thoracic Surgery. 2008;85(6):2105-8.
12. Sodian R, Weber S, Markert M, Loeff M, Lueth T, Weis FC, et al. Pediatric cardiac

transplantation: three-dimensional printing of anatomic models for surgical planning of heart transplantation in patients with univentricular heart. The Journal of Thoracic and Cardiovascular Surgery. 2008;136(4):1098-9.

13. Ballard DH, Trace AP, Ali S, Hodgdon T, Zygmont ME, DeBenedectis CM, et al. Clinical applications of 3D printing: primer for radiologists. Academic Radiology. 2018;25(1):52-65.

14. Sun Z. Clinical Applications of Patient-Specific 3D Printed Models in Cardiovascular Disease: Current Status and Future Directions. Biomolecules. 2020;10(11):1577.

15. Perica ER, Sun Z. A systematic review of three-dimensional printing in liver disease. Journal of Digital Imaging. 2018;31(5):692-701.

16. Yan Q, Dong H, Su J, Han J, Song B, Wei Q, et al. A review of 3D printing technology for medical applications. Engineering. 2018;4(5):729-42.

17. Ionita CN, Mokin M, Varble N, Bednarek DR, Xiang J, Snyder KV, et al., editors. Challenges and limitations of patient-specific vascular phantom fabrication using 3D Polyjet printing. Medical Imaging 2014: Biomedical Applications in Molecular, Structural, and Functional Imaging. 2014;9038: 164-75.

18. Hazelaar C, van Eijnatten M, Dahele M, Wolff J, Forouzanfar T, Slotman B, et al. Using 3D printing techniques to create an anthropomorphic thorax phantom for medical imaging purposes. Medical Physics. 2018;45(1):92-100.

19. Craft DF, Kry SF, Balter P, Salehpour M, Woodward W, Howell RM. Material matters: analysis of density uncertainty in 3D printing and its consequences for radiation oncology. Medical Physics. 2018;45(4):1614-21.

20. Ratinam R, Quayle M, Crock J, Lazarus M, Fogg Q, McMenamin P. Challenges in creating dissectible anatomical 3D prints for surgical teaching. Journal of Anatomy. 2019;234(4):419-37.

21. Zhang F, Zhang H, Zhao H, He Z, Shi L, He Y, et al. Design and fabrication of a personalized anthropomorphic phantom using 3D printing and tissue equivalent materials. Quantitative Imaging in Medicine and Surgery. 2019;9(1):94-100.

22. Aimar A, Palermo A, Innocenti B. The role of 3D printing in medical applications: a state of the art. Journal of Healthcare Engineering. 2019;2019.

23. Klebe RJ. Cytoscribing: a method for micropositioning cells and the construction of two- and three-dimensional synthetic tissues. Experimental Cell Research. 1988;179(2):362-73.

24. Landers R, Hübner U, Schmelzeisen R, Mülhaupt R. Rapid prototyping of scaffolds derived from thermoreversible hydrogels and tailored for applications in tissue engineering. Biomaterials. 2002;23(23):4437-47.

25. Wilson Jr WC, Boland T. Cell and organ printing 1: protein and cell printers. The Anatomical

Record Part A: discoveries in molecular, cellular, and evolutionary biology. 2003;272(2):491-6.

26. Dhariwala B, Hunt E, Boland T. Rapid prototyping of tissue-engineering constructs, using photopolymerizable hydrogels and stereolithography. Tissue Engineering. 2004;10(9-10):1316-22.

27. Jayasinghe SN, Qureshi AN, Eagles PA. Electrohydrodynamic jet processing: an advanced electric-field-driven jetting phenomenon for processing living cells. Small. 2006;2(2):216-9.

28. Skardal A, Mack D, Kapetanovic E, Atala A, Jackson JD, Yoo J, et al. Bioprinted amniotic fluid-derived stem cells accelerate healing of large skin wounds. Stem Cells Translational Medicine. 2012;1(11):792-802.

29. Noor N, Shapira A, Edri R, Gal I, Wertheim L, Dvir T. 3D printing of personalized thick and perfusable cardiac patches and hearts. Advanced Science. 2019;6(11):1900344.

30. Cai H. Application of 3D printing in orthopedics: status quo and opportunities in China. Annals of Translational Medicine. 2015;3(Suppl 1).

31. Nadagouda MN, Rastogi V, Ginn M. A review on 3D printing techniques for medical applications. Current Opinion in Chemical Engineering. 2020;28:152-7.

32. Burnard JL, Parr WC, Choy WJ, Walsh WR, Mobbs RJ. 3D-printed spine surgery implants: a systematic review of the efficacy and clinical safety profile of patient-specific and off-the-shelf devices. European Spine Journal. 2020;29(6):1248-60.

33. Dall'Ava L, Hothi H, Di Laura A, Henckel J, Hart A. 3D printed acetabular cups for total hip arthroplasty: a review article. Metals. 2019;9(7):729.

34. Ribeiro D, Cimino SR, Mayo AL, Ratto M, Hitzig SL. 3D printing and amputation: a scoping review. Disability and Rehabilitation: Assistive Technology. 2019:1-20.

35. Torres K, Staśkiewicz G, Śnieżyński M, Drop A, Maciejewski R. Application of rapid prototyping techniques for modelling of anatomical structures in medical training and education. Folia Morphologica. 2011;70(1):1-4.

36. Li Z, Li Z, Xu R, Li M, Li J, Liu Y, et al. Three-dimensional printing models improve understanding of spinal fracture—A randomized controlled study in China. Scientific Reports. 2015;5:11570.

37. O'Reilly MK, Reese S, Herlihy T, Geoghegan T, Cantwell CP, Feeney RN, et al. Fabrication and assessment of 3 D printed anatomical models of the lower limb for anatomical teaching and femoral vessel access training in medicine. Anatomical Sciences Education. 2016;9(1):71-9.

38. Lim KHA, Loo ZY, Goldie SJ, Adams JW, McMenamin PG. Use of 3D printed models in medical education: a randomized control trial comparing 3D prints versus cadaveric materials for

learning external cardiac anatomy. Anatomical Sciences Education. 2016;9(3):213-21.

39.Chen Y, Qian C, Shen R, Wu D, Bian L, Qu H, et al. 3D Printing Technology Improves Medical Interns' Understanding of Anatomy of Gastrocolic Trunk. Journal of Surgical Education. 2020;77(5):1279-84.

40.Ye Z, Dun A, Jiang H, Nie C, Zhao S, Wang T, et al. The role of 3D printed models in the teaching of human anatomy: a systematic review and meta-analysis. BMC Medical Education. 2020;20(1):1-9.

41.Iwanaga J, Loukas M, Dumont AS, Tubbs RS. A review of anatomy education during and after the COVID-19 pandemic: Revisiting traditional and modern methods to achieve future innovation. Clinical Anatomy. 2021;34(1):108-14.

42.Chen G, Jiang M, Coles-Black J, Mansour K, Chuen J, Amott D. Three-dimensional printing as a tool in otolaryngology training: a systematic review. The Journal of Laryngology & Otology. 2020;134(1):14-9.

43.Morgan C, Khatri C, Hanna SA, Ashrafian H, Sarraf KM. Use of three-dimensional printing in preoperative planning in orthopaedic trauma surgery: A systematic review and meta-analysis. World Journal of Orthopedics. 2020;11(1):57.

44.Weidert S, Andress S, Suero E, Becker C, Hartel M, Behle M, et al. 3D printing in orthopedic and trauma surgery education and training: possibilities and fields of application. Der Unfallchirurg. 2019;122(6):444-51.

45.Akkara JD, Kuriakose A. The magic of three-dimensional printing in ophthalmology. Kerala Journal of Ophthalmology. 2018;30(3):209-15.

46.Scawn RL, Foster A, Lee BW, Kikkawa DO, Korn BS. Customised 3D printing: an innovative training tool for the next generation of orbital surgeons. Orbit. 2015;34(4):216-9.

47.Clifton W, Nottmeier E, Edwards S, Damon A, Dove C, Refaey K, et al. Development of a novel 3d printed phantom for teaching neurosurgical trainees the freehand technique of c2 laminar screw placement. World Neurosurgery. 2019;129:812-20.

48.Chiriac A, Iencean A, Ion G, Stan G, Munteanu S, Poeata I. Current applications of 3d printing in neurosurgery. Romanian Neurosurgery. 2019:417-23.

49.Davids J, Manivannan S, Darzi A, Giannarou S, Ashrafian H, Marcus HJ. Simulation for skills training in neurosurgery: a systematic review, meta-analysis, and analysis of progressive scholarly acceptance. Neurosurgical Review. 2020:1-15.

50.Joseph FJ, Weber S, Raabe A, Bervini D. Neurosurgical simulator for training aneurysm microsurgery—a user suitability study involving neurosurgeons and residents. Acta Neurochirurgica. 2020;162(10):2313-21.

51.Smith B, Dasgupta P. 3D printing technology and its role in urological training. World Journal

of Urology. 2020;38(10):2385-91.

52.Cacciamani GE, Okhunov Z, Meneses AD, Rodriguez-Socarras ME, Rivas JG, Porpiglia F, et al. Impact of three-dimensional printing in urology: state of the art and future perspectives. A systematic review by ESUT-YAUWP group. European Urology. 2019;76(2):209-21.

53.Bruns N, Krettek C. 3D-printing in trauma surgery: planning, printing and processing. Der Unfallchirurg. 2019;122(4):270-77.

54.Watson RA. A low-cost surgical application of additive fabrication. Journal of Surgical Education. 2014;71(1):14-7.

55.Chao I, Young J, Coles-Black J, Chuen J, Weinberg L, Rachbuch C. The application of three-dimensional printing technology in anaesthesia: a systematic review. Anaesthesia. 2017;72(5):641-50.

56.Wang C, Zhang L, Qin T, Xi Z, Sun L, Wu H, et al. 3D printing in adult cardiovascular surgery and interventions: A systematic review. Journal of Thoracic Disease. 2020;12(6):3227-37.

57.Khan IS, Kelly PD, Singer RJ. Prototyping of cerebral vasculature physical models. Surgical Neurology International. 2014;5:11.

58.Ho D, Squelch A, Sun Z. Modelling of aortic aneurysm and aortic dissection through 3D printing. Journal of Medical Radiation Sciences. 2017;64(1):10-7.

59.Sun Z, Squelch A. Patient-specific 3D printed models of aortic aneurysm and aortic dissection. Journal of Medical Imaging and Health Informatics. 2017;7(4):886-9.

60.Kim PS, Choi CH, Han IH, Lee JH, Choi HJ, Lee JI. Obtaining informed consent using patient specific 3D printing cerebral aneurysm model. Journal of Korean Neurosurgical Society. 2019;62(4):398-404.

61.Wake N, Rosenkrantz AB, Huang R, Park KU, Wysock JS, Taneja SS, et al. Patient-specific 3D printed and augmented reality kidney and prostate cancer models: impact on patient education. 3D Printing in Medicine. 2019;5(1):1-8.

62.Chen MY, Skewes J, Woodruff MA, Dasgupta P, Rukin NJ. Multi-colour extrusion fused deposition modelling: a low-cost 3D printing method for anatomical prostate cancer models. Scientific Reports. 2020;10(1):1-5.

63.Zhuang Y-d, Zhou M-c, Liu S-c, Wu J-f, Wang R, Chen C-m. Effectiveness of personalized 3D printed models for patient education in degenerative lumbar disease. Patient Education and Counseling. 2019;102(10):1875-81.

64.Andolfi C, Plana A, Kania P, Banerjee PP, Small S. Usefulness of three-dimensional modeling in surgical planning, resident training, and patient education. Journal of Laparoendoscopic & Advanced Surgical Techniques. 2017;27(5):512-5.

65.Yang T, Tan T, Yang J, Pan J, Hu C, Li J, et al. The impact of using three-dimensional printed

liver models for patient education. Journal of International Medical Research. 2018;46(4):1570-8.

66. Waran V, Narayanan V, Karuppiah R, Owen SL, Aziz T. Utility of multimaterial 3D printers in creating models with pathological entities to enhance the training experience of neurosurgeons. Journal of Neurosurgery. 2014;120(2):489-92.

67. Liu Y-f, Xu L-w, Zhu H-y, Liu SS-Y. Technical procedures for template-guided surgery for mandibular reconstruction based on digital design and manufacturing. Biomedical Engineering Online. 2014;13(63):1-15.

68. Nie W, Gu F, Wang Z, Wu R, Yue Y, Shao A. Preliminary application of three-dimension printing technology in surgical management of bicondylar tibial plateau fractures. Injury. 2019;50(2):476-83.

69. Matsumoto JS, Morris JM, Rose PS. 3-dimensional printed anatomic models as planning aids in complex oncology surgery. JAMA Oncology. 2016;2(9):1121-2.

70. Perica E, Sun Z. Patient-specific three-dimensional printing for pre-surgical planning in hepatocellular carcinoma treatment. Quantitative Imaging in Medicine and Surgery. 2017;7(6):668-77.

71. O'Brien EK, Wayne DB, Barsness KA, McGaghie WC, Barsuk JH. Use of 3D printing for medical education models in transplantation medicine: a critical review. Current Transplantation Reports. 2016;3(1):109-19.

72. Mahaisavariya B, Sitthiseripratip K, Oris P, Tongdee T. Rapid prototyping model for surgical planning of corrective osteotomy for cubitus varus: report of two cases. Injury Extra. 2006;37(5):176-80.

73. Huang J, Li G, Wang W, Wu K, Le T. 3D printing guiding stent graft fenestration: a novel technique for fenestration in endovascular aneurysm repair. Vascular. 2017;25(4):442-6.

74. Wang Y-T, Yang X-J, Yan B, Zeng T-H, Qiu Y-Y, Chen S-J. Clinical application of three-dimensional printing in the personalized treatment of complex spinal disorders. Chinese Journal of Traumatology. 2016;19(1):31-4.

75. Sheth U, Theodoropoulos J, Abouali J. Use of 3-dimensional printing for preoperative planning in the treatment of recurrent anterior shoulder instability. Arthroscopy techniques. 2015;4(4):311-6.

76. Sun Z. Insights into 3D printing in medical applications. Quantitative Imaging in Medicine and Surgery. 2019;9(1):1-5.

77. Foley TA, El Sabbagh A, Anavekar NS, Williamson EE, Matsumoto JM. 3D-Printing: Applications in Cardiovascular Imaging. Current Radiology Reports. 2017;5(9).

78. Witowski J, Sitkowski M, Zuzak T, Coles-Black J, Chuen J, Major P, et al. From ideas to long-

term studies: 3D printing clinical trials review. International Journal of Computer Assisted Radiology and Surgery. 2018;13(9):1473-8.

79. Casey RG, Lecolinet E. A survey of methods and strategies in character segmentation. IEEE Transactions on Pattern Analysis and Machine Intelligence. 1996;18(7):690-706.

80. Kovács T, Cattin P, Alkadhi H, Wildermuth S, Székely G, editors. Automatic segmentation of the aortic dissection membrane from 3D CTA images. International Workshop on Medical Imaging and Virtual Reality; 2006: Springer.

81. Farooqi KM, Lengua CG, Weinberg AD, Nielsen JC, Sanz J. Blood Pool Segmentation Results in Superior Virtual Cardiac Models than Myocardial Segmentation for 3D Printing. Pediatric Cardiology. 2016;37(6):1028-36.

82. Lei Y, Chen X, Li Z, Zhang L, Sun W, Li L, et al. A new process for customized patient-specific aortic stent graft using 3D printing technique. Medical Engineering and Physics. 2020;77:80-7.

83. Gomes EN, Dias RR, Rocha BA, Santiago JAD, Dinato FJdS, Saadi EK, et al. Use of 3D printing in preoperative planning and training for aortic endovascular repair and aortic valve disease. Brazilian Journal of Cardiovascular Surgery. 2018;33:490-5.

84. Zhang M, Tong Y-H, Liu C, Li X-Q, Liu C-J, Liu Z. Treatment of Stanford type A aortic dissection with triple pre-fenestration, reduced diameter, and three-dimensional-printing techniques: A case report. World Journal of Clinical Cases. 2021;9(1):183.

85. Hossien A, Gelsomino S, Maessen J, Autschbach R. The interactive use of multi-dimensional modeling and 3D printing in preplanning of type A aortic dissection. Journal of Cardiac Surgery. 2016;31(7):441-5.

86. Finotello A, Marconi S, Pane B, Conti M, Gazzola V, Mambrini S, et al. Twelve-year Follow-up Post–Thoracic Endovascular Repair in Type B Aortic Dissection Shown by Three-dimensional Printing. Annals of Vascular Surgery. 2019;55(309):13-9.

87. Kovács T, Cattin P, Alkadhi H, Wildermuth S, Székely G. Automatic segmentation of the vessel lumen from 3D CTA images of aortic dissection. Bildverarbeitung für die Medizin 2006. 2006;Springer:161-5.

88. Giannopoulos AA, Steigner ML, George E, Barile M, Hunsaker AR, Rybicki FJ, et al. Cardiothoracic applications of 3D printing. Journal of Thoracic Imaging. 2016;31(5):253-72.

89. Wu C-A, Squelch A, Sun Z. Optimal image segmentation protocol for 3D printing of aortic dissection through open-source software. Journal of 3D Printing in Medicine. 2021;5(1):37-49.

90. Wu C-A, Squelch A, Sun Z. Investigation of three-dimensional printing materials for printing aorta model replicating type B aortic dissection. Current Medical Imaging. 2021;17(7):843-

9.

91. Riedle H, Mukai B, Molz P, Franke J, editors. Determination of the Mechanical Properties of Aortic Tissue for 3D Printed Surgical Models. 2018 11th Biomedical Engineering International Conference (BMEiCON); 2018: IEEE.

92. Wu C-A, Squelch A, Jansen S, Sun Z. Optimization of computed tomography angiography protocols for follow-up type B aortic dissection patients by using 3D printed model. Applied Sciences. 2021;11(15):6844.

CHAPTER 3

OPTIMAL IMAGE SEGMENTATION PROTOCOL FOR 3D PRINTING OF AORTIC DISSECTION THROUGH OPEN-SOURCE SOFTWARE

To determine the optimal image segmentation protocol that minimizes the amount of manual intervention and correction required while extracting 3D model geometries suitable for 3D printing of aortic dissection (AD) using open-source software. Materials & methods: Computed tomography images of two type B AD (TBAD) cases were selected with images segmented using a 3D Slicer to create a hollow model containing the aortic wall and intimal tear. A workflow composed of filters, lumen extraction and outer surface creation was developed. Results & conclusion: The average difference in measurements at 14 anatomical locations between the Standard Tessellation Language file and the computed tomography image for cases 1 and 2 were 0.29 and 0.32 mm, respectively. The workflow for the image segmentation of TBAD was able to produce a high-accuracy 3D-printed model in a short time through open-source software.

3.1 Introduction

Aortic dissection (AD) is one of the most dangerous and fatal cardiovascular diseases that require urgent treatment. Acute AD (AAD) is the separation of the layers between the aortic walls. Blood flow tears any breach on the aortic wall, and blood enters into the space between intimal and media layer creating two passages for blood flow, the true lumen and false lumen. Based on the anatomical location, AAD can be classified into Stanford type A or type B. The dissections that occur at the ascending aorta are classified as type A, whereas TBAD involves only distal to the left subclavian artery. For type A AD, if the situation is left untreated, early mortality can be increased by >1% per h. 50% of patients with type A AD die within 3 days, 75% die within 2 weeks, and the mortality within 3 months can be >95% (1-3).

Patients with Stanford type A AAD need immediate surgery after diagnosis because of high mortality and various complications. For patients with TBAD, the management of treatment is controversial, as it can be treated either medically or through endovascular stent-graft surgery, depending on the clinical presentation (3-9). Therefore, further research for managing the best patient-specific treatment is necessary. A touchable 3D-printed model has potential to be a powerful tool for investigating the best treatment options for patients with AAD. 3D printing (3DP) is a rapidly developing technology that can produce a physical and touchable model from 3D computer digital model through material layering (10-15). This technology is becoming more and more mature and has increasing applications in a wide range of areas (16, 17). The 3D-printed models have great potential in the medical field. They can be used in a variety of areas including preoperative and planning and simulation, training and education of medical students and residents, improving doctor-patient communication, and developing optimal computed tomography (CT) protocols (18-23).

Studies have shown that 3DP heart models are able to reduce the risk of perioperative complications (24, 25). Due to its performance of improving the understanding of anatomical structures, 3DP models also improve the efficiency of surgery (26, 27).

To achieve a medical 3DP model, the workflow can be designed with five steps: image acquisition, image segmentation, surface mesh generation, Standard Tessellation Language (STL) post processing and printing **(Figure 3.1**) (16, 17, 28, 29). The image data can be acquired in various ways, and the most common methods are CT and MRI. The image data are imported into the software to perform image segmentation, at the end of which the original image will be separated into multiple segments. The image segmentation process aims to simplify the image data, locate the regions of interest and confirm boundaries by labelling every pixel into appropriate segments. Pixels that are in the same segment have certain characteristics (30-32). The image will become more meaningful and easier to analyse after image segmentation. Surface mesh generation creates the surface structure of the model for 3DP based on the segmented dataset and converts this file into the STL file format, which describes surface geometry and mesh data. Owing to the characteristics of the STL file format, it has been widely used for computer-aided manufacturing and 3DP.

Image segmentation plays an important role in the conversion of digital images into surface meshes. Even with a high-resolution image source, a physical model cannot be printed if segmentation has not been performed well. However, if the image resolution of the original source is poor, the image segmentation process could be unsuccessful in some particular locations or diseases that require higher resolution. Kov´acs et al. proposed a computer-aided method to segment the true and false lumen on AD segmentation. Their algorithm can fully automatically capture true and false lumen on AD cases with regular-shaped aortas (31). With the development of deep

learning algorithm, Li et al. and Cao et al. used convolutional neural network and 3D U-net, respectively, to segment cases with AD (33, 34). They annotated true and false lumen using open-source software and provided fully automatic methods to segment dissection aorta. Yet, none of them provided further details of annotation protocols.

The availability of a protocol to segment aorta from AD cases using open-source software could be helpful for future research as it would lower the barriers of segmentation learning. There are no readily available published guidelines or standardized methods for medical image segmentation, and the methods of segmentation need to be improved to achieve a higher quality model in a shorter time (35, 36). Therefore, this study focuses on the development and optimization of the procedure of image segmentation through open-source software, which is essential for the successful generation of STL models suitable for the 3DP of relevant medical models.

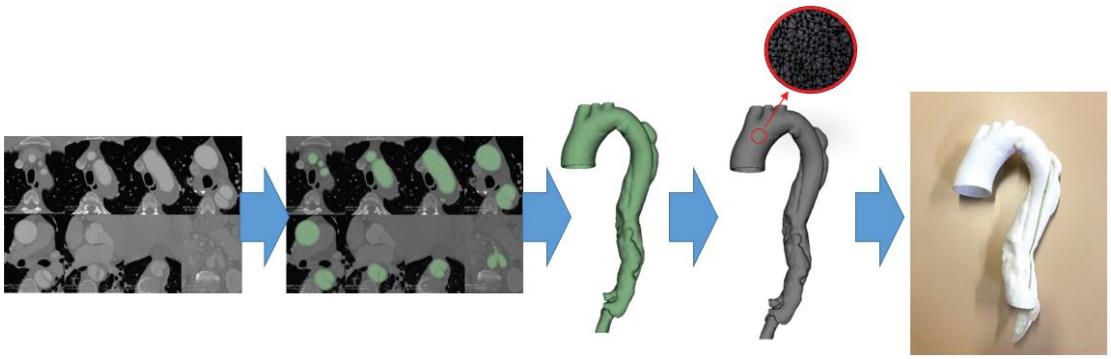

Figure 3.1 A medical 3D-printed model can be produced through five steps: image acquisition, image segmentation, surface mesh generation, Standard Tessellation Language post processing and printing. STL: Standard Tessellation Language.

3.2 Materials & methods

To verify a proper workflow for TBAD segmentation, appropriate patient data were selected to provide the subject matter expert for development and evaluation of the 3DP model workflow. The proposed workflow requires preparation and processing

of the patient image data to facilitate lumen segmentation and ultimately creation of the STL model. All post-processing steps were conducted through open-source software. The suitability of the workflow is validated by comparing equivalent locations in the patient CT scan data and the STL model. This study was approved by the Curtin Human Research Ethics Committee (approval number: HRE2018-0087).

3.2.1 Patient data selection

Contrast-enhanced CT image data of 11 patients who underwent type B AAD between November 2015 and March 2016 were de-identified and retrieved from a public hospital. One of the patient datasets (contrast-enhanced CT performed on a 128-slice CT with a 120 kVp tube potential, 128 reference mAs and 1.0 mm reconstructed slice thickness) was selected to develop an optimal segmentation workflow, performs uneven distribution between true and false lumen, which is one of the challenges in AD segmentation. Additionally, the difference in Hounsfield unit (HU) between the descending aorta and the abdominal aorta is large in this case. Another patient dataset (120 kVp tube potential, 184 reference mAs and 1.0 mm reconstructed slice thickness) with an even contrast distribution was selected to validate the devised workflow.

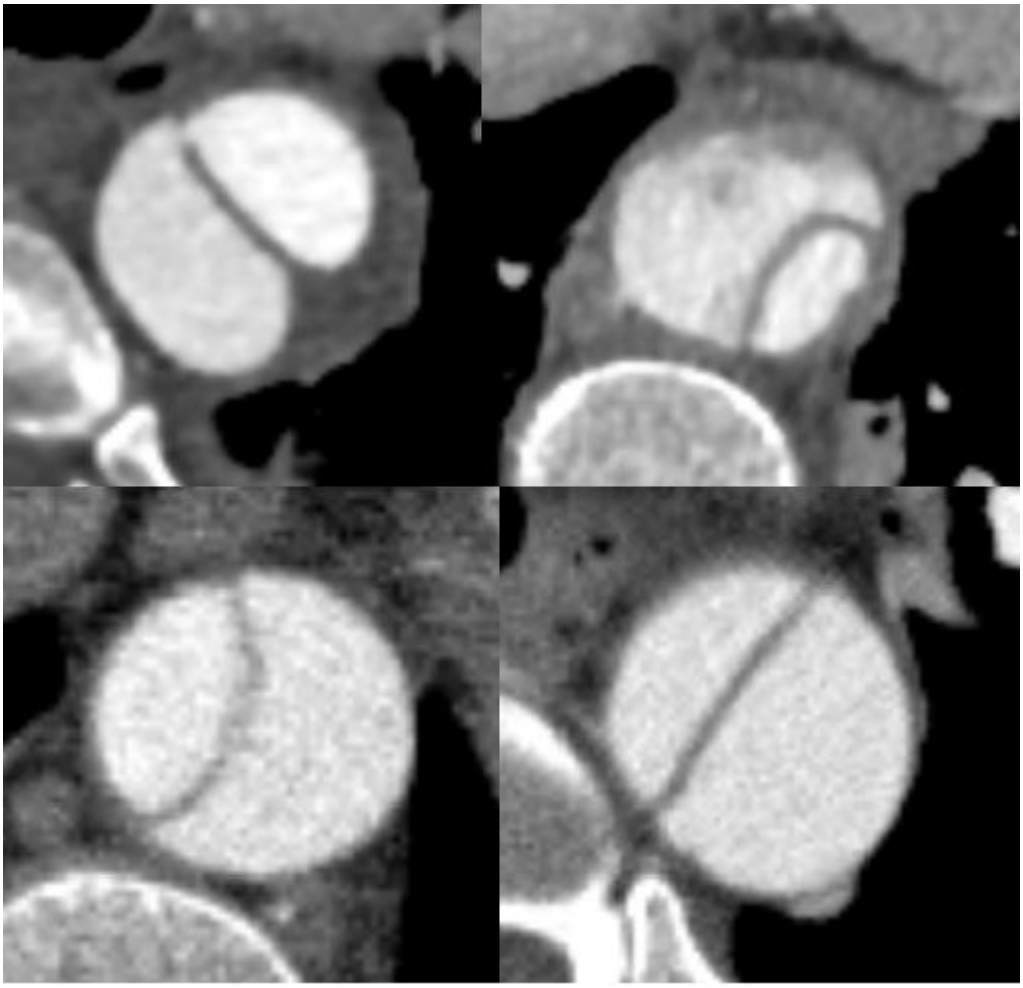

Figure 3.2 Middle segment of the aorta in selected patient 1 and patient 2. Patient 1 haduneven distribution of contrast enhancement between true and false lumen (upper left) and blurred aorta borders (upper right). Patient 2 had more complete performance of aorta CTA image than Patient 1 (lower left and right).

Authors chose these two cases because of better image quality and images describing the regions of interest clearly (true and false lumen, intimal flap and fenestration). Images of patient 1 were selected because of the high contrast difference between true and false lumen with significantly lower CT attenuation in the false lumen. In contrast, patient 2 images represent a good example of better contrast enhancement in both true and false lumens. In the remaining nine cases some of them are not applicable to this method since their false lumen has no contrast difference

with surrounding organ. Other cases have low image quality that causes the blur edge on the image, thus it is difficult to be measured even in the original images.

3.2.2 Post processing

All patients' image datasets were transferred to a desktop PC with Intel Core processor (4 × 3.0 GHz), 8 GB RAM and an Intel(R) HD Graphics 630 display adapter for post processing. Thresholding is the most common function used to conduct an automatic segmentation process. However, due to the scanning time and the complex anatomic structure of the dissection aorta, the distribution of contrast can be uneven between true and false lumen. To solve this problem, a protocol was devised for optimizing type B AAD segmentation as shown in **Figures 3.2 and 3.3**. One of the criteria applied in the selection of software for this study was that it should be easily acquired and able to run on most modern desktop or laptop workstations. Therefore, all selected software is open-source and available for download online. After comparison of different open-source software, with all the necessary function for this workflow in the default package, 3D Slicer was considered as suitable post processing software for this study. 3D Slicer (version 4.10.0, www.slicer.org; MA, USA) is free software for medical image visualization and computing (37). It should be noted that the available 3D-slicer programs such as Slicer are not currently US FDA approved, and therefore, their use is not in current practice in clinical cardiac medicine.

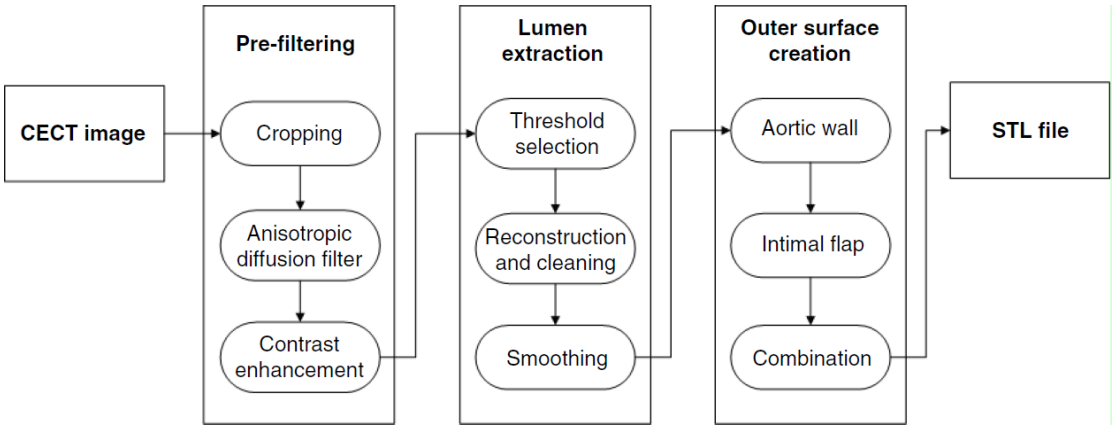

Figure 3.3 A protocol devised for optimizing type B acute aortic dissection segmentation.

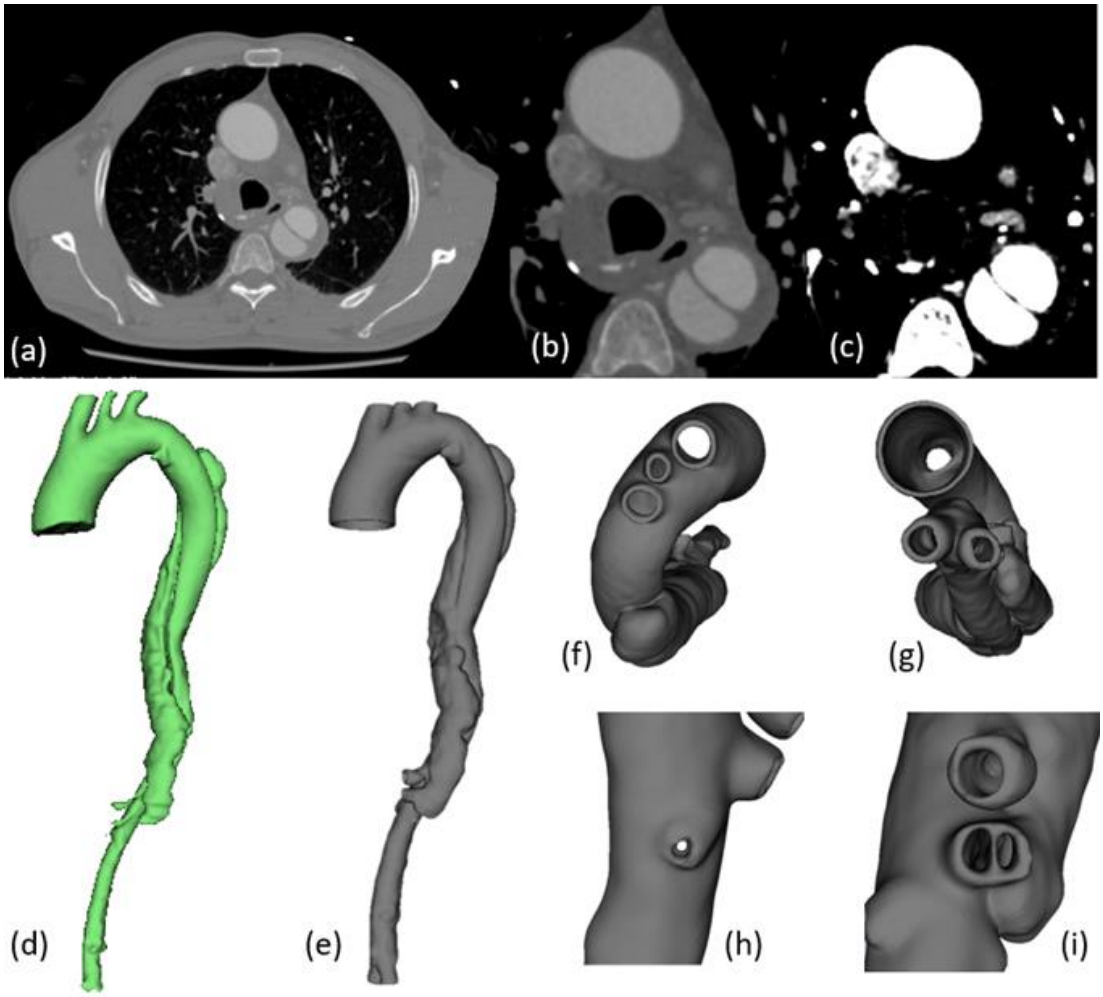

Figure 3.4 Developed protocol for image processing and segmentation of type B aortic dissection. (A) Original computed tomography image. (B) Image cropping. (C) Image after applied de-noising and contrast enhancement filters. (D) Reconstruction and extraction of the lumen. (E) Final outcome of the Standard Tessellation Language (STL) model. (F) STL model top view. (G) STL model bottom view. (H) Renal artery on the STL model. (I) Celiac trunk and superior mesenteric artery on the STL model.

3.2.3 Image filters & enhancement

In order to increase the efficiency of detection for lumen segmentation, it is recommended that image filters and image enhancements are applied before using any auto-segmentation function. These include cropping, anisotropic diffusion filter and contrast enhancement.

Cropping: A typical initial action is to crop the image data to remove unnecessary peripheral parts of the images and to extract the region of interest. Using a crop image tool to reduce the image volume will improve the efficiency of any subsequent processing steps by removing unwanted regions of the image data and increasing the processing speed for the remaining region of interest. For CT image series, a volume cropping function is the most efficient option to achieve the desired outcome rather than cropping individual images one at a time. For TBAD, the region of interest should include the whole aorta. Considering the clinical value of the physical 3DP model, the segmentation should include the ascending thoracic aorta, aorta arch, descending thoracic aorta and abdominal aorta. In addition, the base of the brachiocephalic trunk, left common carotid artery and left subclavian artery should be included at the top and, if applicable, the common iliac artery should be included as well.

Anisotropic diffusion filter: This filter is used to reduce the noise in digital images. Anisotropic diffusion reduces noise in a similar way to Gaussian blurring using the same diffusion coefficient; however, in the case of anisotropic diffusion, the diffusion remains inside the applied region and the blurring is prevented from going across strong edges. Using this filter efficiently reduces the digital noise while at the same time relatively increasing the clarity of edges. After anisotropic diffusion, the range of HU inside the lumen is reduced and the edge becomes sharper, so it will be easier for subsequent image processing steps to detect the edge.

Contrast enhancement: The Intensity Windowing Image Filter applies a linear transformation algorithm to the intensity levels of the input image within a user-defined interval. Values below this interval will be set to a constant, and values higher than this interval will be set to a different constant. In this study, the HU range of lumen is set as 60–400. Thus, the input minimum is set to 60, and the input maximum is set to 400. To ensure that the HU of the new enhanced image has a contrast that is strong enough to separate lumen and other unwanted regions, the output minimum is set to 0 and the output maximum is set to 10000. After the Intensity Windowing Image Filter is applied, all the pixels with HU values <60 are set to 0 and all the pixels with HU values >400 are set to 10000. The pixels which originally had HU values between 60 and 400 now have a new HU value from 0 to 10000 based on the linear transformation algorithm. This means that the unwanted region has been set to constant values and the useful part of interest (HU between 60 and 400) not only has been retained but also has a stronger contrast that is more easily segmented.

Lumen extraction: Image segmentation is applied to the cropped and filtered image data that underwent specific contrast enhancement to separate the lumen. However, there are still some unwanted regions in the image data that are also in the original HU range between 60 and 400, such as the heart, branches of aorta, organs that are connected to branches of the aorta, bones in the chest and the abdomen. The overlapping of HU values makes it hard to remove them through the application of the Intensity Windowing Image Filter. Therefore, the next step is to remove these unwanted parts and then extract the lumen.

Threshold selection: The fastest and simplest way to begin the segmentation process is to apply a ‘threshold’ function. A threshold is selected to exclude specific range or ranges of HU values. In this study, the threshold has been chosen as 2000–

10000. Visual inspection of the image data indicates that the majority of the lumen region has HU values within this selected interval. Excluding pixels that have HU between 0 and 2000 does cause a part of lower lumen to be eliminated, and some darker parts in the lumen where thrombus and turbulence are present. Nonetheless, the selected threshold range does efficiently rule out a significant amount of the unwanted regions such as many branches of aorta, some parts of heart and organs that connect with aorta.

Reconstruction and cleaning: The objective of this step is to extract the entire lumen and remove unwanted parts. Using a 3Dpreview or rendering tool before cleaning will reduce the difficulty associated with the cleaning process. An efficient cleaning method is achieved by using two basic image segmentation tools: scissors and identify islands. Scissors is a tool used to clip segments. Identification of islands can create a unique segment for each connected region of the selected segment. The main approach is indicated in **Figure 3.4**, where the scissors function is used to cut off the connections between aorta lumen and unwanted parts, followed by identifying islands to isolate the lumen. Typically, the connections that need to be cut off include all of the organs and branches connected by aorta, such as the heart, kidneys, coeliac trunk, superior mesenteric artery (SMA) and inferior mesenteric artery. Unexpected connections such as tiny branches, can occur between the spine and aorta sometimes.

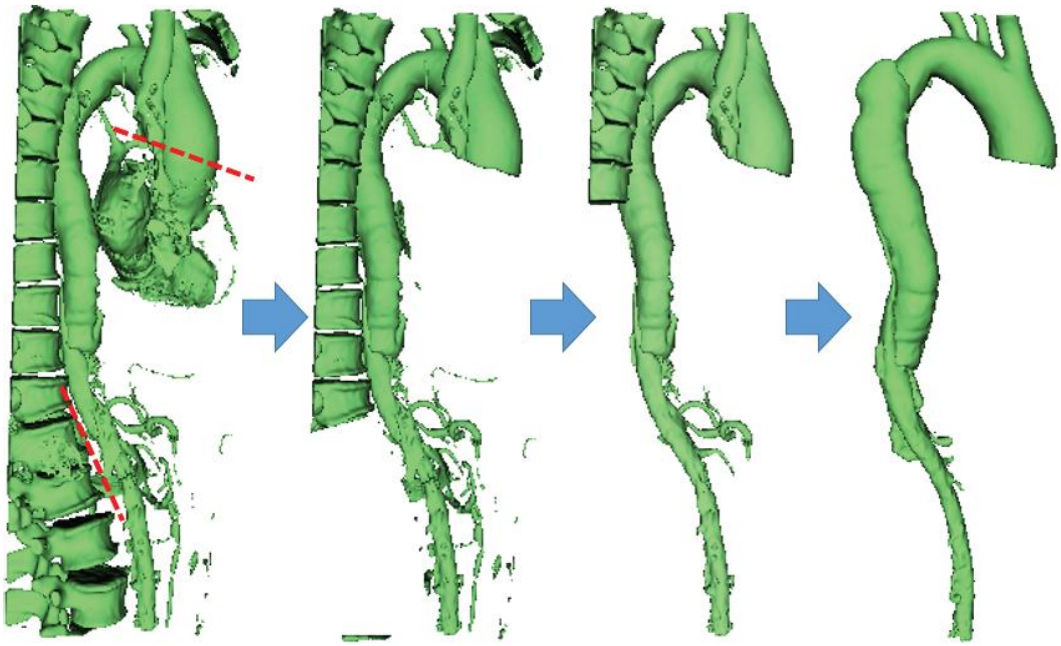

Figure 3.5 Lumen extraction. The scissors function is used to cut off connections between aorta lumen and unwanted parts and switch to identifying islands to isolate the lumen.

Smoothing: Applying a smoothing function before creating the outer surface is recommended. It can make the final outer surface smoother and less spikes are generated that need to be fixed. The smoothing in this step should be carried out by a median filter with kernel size <2 mm (3 × 3 × 3 pixels). The anatomic structure tends to be changed if a big kernel size is applied. The Gaussian filter has a powerful smoothing effect but tends to change the shape and reduce the accuracy of the model. The Closing (fill holes) filter can be applied as well, and the kernel size should be <2 mm or the structure around tears will be changed.

Outer surface creation: A solid aorta lumen model is initially produced through reconstruction and cleaning. To achieve a hollow model, the next step is to create an aortic wall and intimal flap. The average aortic wall thickness is about 2.7 mm (33). The aortic wall can be created using the hollow function to generate a 2.7 mm outside surface of the lumen. However, since intimal flap thickness is usually <2.7 mm, using

the hollow function tends to lead to the disappearance of the intimal flap. Therefore, the aortic wall and the intimal flap should be created separately.

Aortic wall: In their study of aortic wall thickness, Liu et al. found that the average aortic wall thickness for patients with hypertension is about 2.7 mm (38). There are two methods to create aortic wall with automatic function in open-source software. In 3D Slicer, the hollow function can create a 2.7 mm outer surface based on solid lumen segment. In most open-source software, if a hollow function is not available, dilate is an alternative function available to create an aortic wall. Dilate applied to the lumen creates a dilated (i.e., wider diameter) version of the lumen, and from this, the original lumen can be subtracted to produce the aortic wall, which is close to the one generated by the hollow function method.

Intimal flap: The dilated lumen segment can be used as a mask to find the intimal flap. After the lumen is dilated, this segment includes original lumen, intimal flap and aortic wall. **Figure 3.5** shows the use of the threshold function to identify the low contrast area inside the dilated lumen. Through this approach, one can find the intimal flap segment.

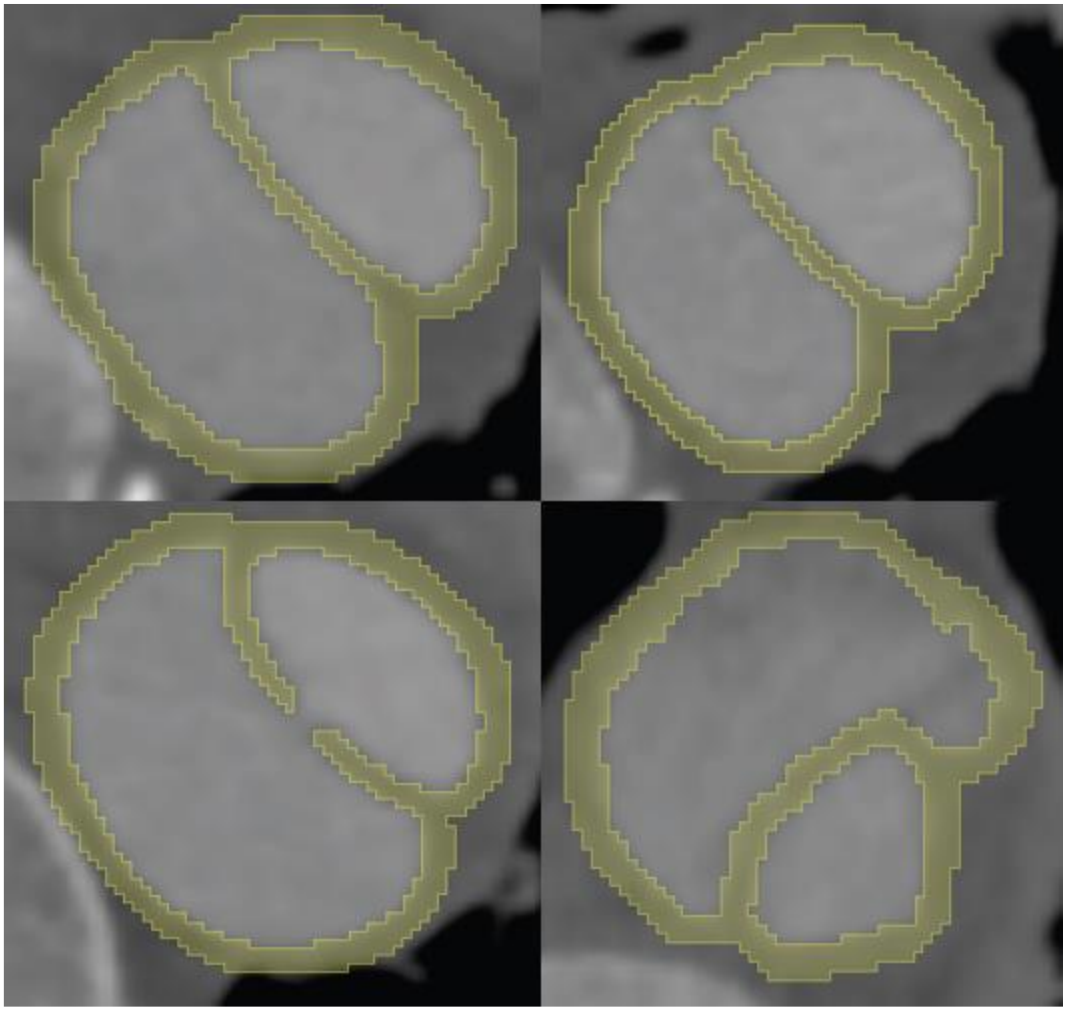

Figure 3.6 Using threshold function to identify low contrast area inside dilated lumen. (A) Location of near aortic arch. (B & C) Locations of flap tears. (D) Location above the superior mesenteric artery.

Combination: The aortic wall segment and the intimal flap segment can be combined together through the logical operators function in 3D Slicer. This combined segment with aortic wall and intimal flap is the final 3D model outcome before the complete geometry is exported as an STL file. A final anatomic structure check should be performed at this stage including checking the shape of true and false lumen, tear of flap, and location of branches. Smoothing is an optional operation that can be applied in this step or it can be applied after the model has been exported as an STL file.

3.2.4 Validation

The STL files of the two patients were re-imported into 3D Slicer and reconstructed as a tomography slice image to compare with original CT images. Fourteen different anatomical locations were measured with measurements taken from the inner lumen of the aorta and were recorded in **Table 3.1**, which included three branches on the aortic arch, abdominal artery and three points selected between the aortic arch and abdominal artery. The internal diameters of the true and false lumen were calculated by taking the average of the two axis measurements. Since the smoothing function was applied before transferring the file to printing, the segmented data is the same as STL. Only holes fixing approach was used in the pre-printing checking. One has to admit that the intimal tears are sometimes difficult to be detected by the software due to its tiny structure and fibrous member features which present challenges for both visualization and image post processing and segmentation. However, in this study, through the contrast enhancement filter, the possibility of missing intimal tear was greatly reduced. Authors did not encounter any issue of segmenting the true lumen from the false lumen across the flap with our developed workflow, neither did our segmentation approach lead to 'false fenestrations' or 'erroneously closing true fenestrations'. The accuracy measurements were conducted by two experienced 3D Slicer software users and the output STL file was checked by an experienced vascular and endovascular surgeon.

Table 3.1 Measurements taken at fourteen different anatomical locations for comparison and validation.

	Patient 1			**Patient 2**			**Average**		
Anatomical location	STL (mm)	DICOM (mm)	Error (mm)	STL (mm)	DICOM (mm)	Error (mm)	STL (mm)	DICOM (mm)	Error (mm)
Brachiocephalic trunk	17.70	17.30	0.40	18.35	18.60	0.25	18.02	17.95	0.33
Left common carotid	10.00	9.85	0.15	7.94	8.32	0.38	8.97	9.08	0.27

artery									
Left Subclavian artery	12.50	12.50	0.00	12.52	13.03	0.51	12.51	12.76	0.26
Ascending aorta	40.30	40.45	0.15	45.35	45.85	0.50	42.82	43.15	0.33
True lumen 1	18.60	18.55	0.05	18.05	18.35	0.30	18.32	18.45	0.18
False lumen 1	24.50	24.30	0.20	26.15	26.75	0.60	25.32	25.52	0.40
True lumen 2	13.88	14.14	0.26	16.45	16.85	0.40	15.16	15.49	0.33
False lumen 2	23.00	23.65	0.65	22.90	23.30	0.40	22.95	23.47	0.53
True lumen 3	12.60	13.10	0.50	12.64	12.71	0.07	12.62	12.90	0.29
False lumen 3	18.80	19.40	0.60	14.66	15.03	0.37	16.73	17.21	0.49
Abdominal aorta	12.55	13.10	0.55	N/A	N/A	N/A	N/A	N/A	N/A
Intimal flap 1	1.37	1.54	0.17	1.75	1.79	0.04	1.56	1.66	0.11
Intimal flap 2	1.42	1.64	0.22	1.74	1.98	0.24	1.58	1.81	0.23
Intimal flap 3	1.77	1.93	0.16	1.54	1.66	0.12	1.65	1.79	0.14
Average Error			0.29			0.32			

3.3 Results

The measurements were conducted at the base of the brachiocephalic trunk, left common carotid artery and left subclavian artery. The true and false lumen were measured at three different locations: distal of the aortic arch, middle of the thoracic aorta and location above the celiac trunk. For patient 2, diameter of the abdominal aorta cannot be compared since the dissection continues from the thoracic aorta to the iliac artery. Due to variation of the dissection and its extent involving different parts of the abdominal aorta (dissection in patient 1 ends at the SMA, while dissection in patient 2 involves abdominal aorta and extends to the common iliac arteries), authors could not compare the abdominal aorta diameter below SMA between these two cases.

Measurements taken in the CT images were compared with measurements of equivalent features available in the STL files for the two patients. Two scatter plots

shown in **Figures 3.6 and 3.7** were generated from four different datasets. A strong correlation (r = 0.99) was noted in each scatter plot.

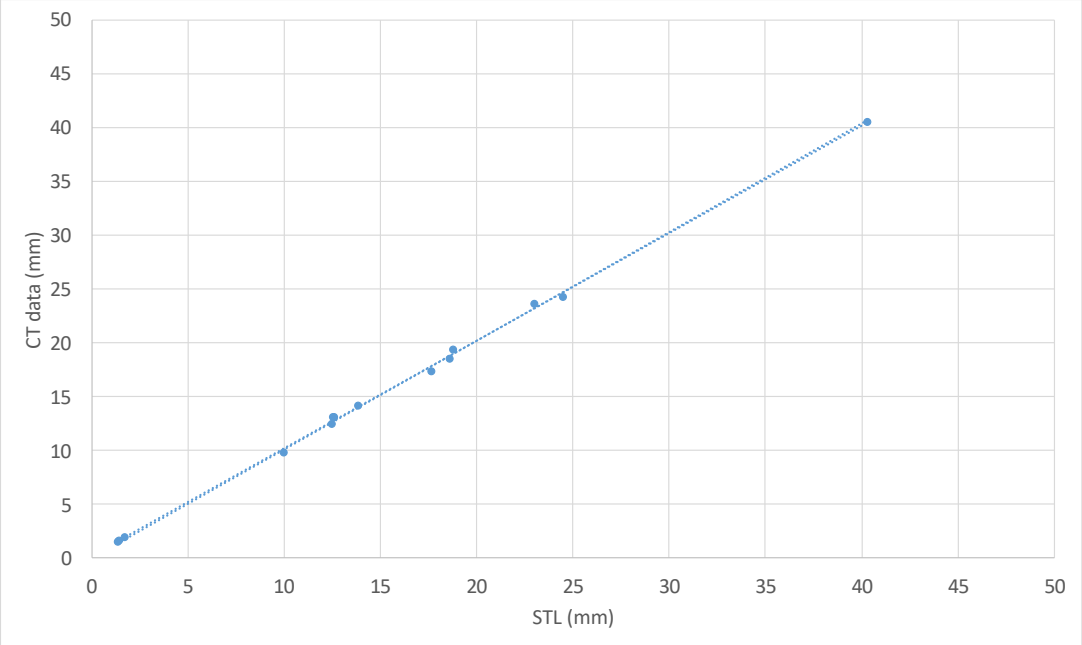

Figure 3.7 Scatter plot of the STL model measurements and CT image measurements of patient 1, with 0.29 mm average difference.

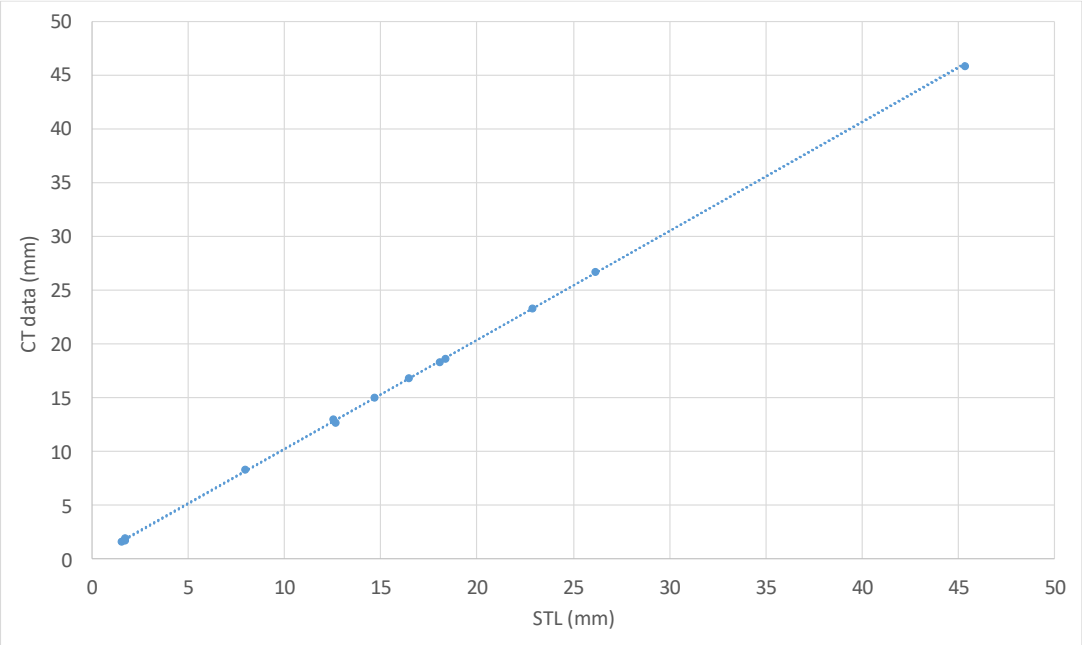

Figure 3.8 Scatter plot of the STL model measurements and CT image measurements of patient 2, with 0.32 mm average difference.

As shown in **Table 3.1**, the average differences between the STL file and the CT image for patient 1 and 2 were 0.29 and 0.32 mm, respectively. The average differences in true lumen between the two patients were 0.27 mm. The average difference of false lumen was 0.48 mm on patient 1 and 0.46 mm for patient 2. At the intimal flap level, measurements showed an average difference of 0.18 and 0.13 mm for patients 1 and 2, respectively. Both patients had a greater average difference of measurements at false lumen. For patient 1, the maximum difference of 0.65 mm occurs at false lumen 2. The maximum difference of 0.6 mm occurs at false lumen 1 for patient 2. The maximum of average error occurs at the false lumen 2 and was 0.525 mm. By following the devised workflow in this study, both comparisons demonstrated a strong correlation (r = 0.99), with all the data points lying closely and exhibiting a perfect correlation line (r = 0.99). Measurement differences between original CT images and STL files could be due to several reasons. First, the error or disagreement in measurements could be simply caused by the measurement variability introduced by manual measurements. Second, pixel selection during image segmentation and processing the final reconstruction and cleaning of volume data could contribute to the measurement discrepancy between CT images and STL files. Third, after smoothing, some of the surface could slightly be changed, the balance between surface roughness and accuracy is an important aspect to be weighed. Fourth, when reimporting STL file back into 3D Slicer for further measurement, the model could be changed because of the file converting process.

3.4 Discussion

The greatest challenge in TBAD segmentation is to distinguish aortic wall, true lumen, false lumen and intimal flap. Kov´acs et al. presented an algorithm which can segment entire aorta and identify the dissection membrane between two lumens (31,

39). This method was very accurate in identifying the aorta and detecting the intimal flap but not accurate if there are irregular-shaped aortas and it is difficult to achieve an accurate identification with open-source software. Thanks to the increasing interest and recent development on machine learning or deep learning, Li et al. (33) and Cao et al. (34) provided another method to segment two lumens. Compared with other methods, deep learning approaches are relatively straightforward since they do not include multiple classical image processing methods. However, for supervised training, deep learning-based methods require a large amount of manually annotated data, which could be very time consuming. Both of these studies used open-source software to achieve annotation, yet none of them has published further details about their annotation protocol.

This study is focused on providing an efficient way to create a high AAD 3DP model by using software accessible for everyone who is interested in 3DP. In many cases, especially in the lower body and false lumen, the HU in the lower aortic lumen is extremely close to the aortic wall because the blood flow may be disordered in patients with AD and some of these patients might have thrombus. Contrast medium can help us understand the movement of blood flow in the aorta; however, only minimal blood flow goes into the thrombus part, which creates images that appear less bright and features of interest that are less distinct. In some cases, the blood flow does not go into thrombus part at all and the HU is exactly the same as aortic wall and other surrounding areas. The dissection also results in disordered and turbulent blood flow. The HU could be unusual when the contrast medium goes turbulent. Second, due to aortic anatomy, blood flow will go through some branches since it leaves the heart including brachiocephalic trunk, left common carotid artery and left subclavian artery, celiac trunk, renal arteries, and superior and inferior mesenteric arteries. After passing

these many arteries, the contrast becomes split. The contrast concentration in the lower body declines owing to the distance it travels in the aorta, which results in darker images from the lower aorta, that is, lower HU values than in the upper aorta. Other reasons that lead to different distributions of contrast medium in the aorta are scanning time and the dosage of contrast. Too early or too late a capture time will affect the location of contrast in the images. In this study, in seven out of 11 cases, upper aorta is brighter than lower aorta. All cases were scanned using the general chest CTA scan protocol (120 kVp tube potential, 150 reference mAs and 1.0 mm reconstructed slice thickness). Their CT images were of sufficient quality and showed a clear depiction of aorta which are sufficient for diagnosis; however, they are not able to rapidly produce a 3DP model without any filters and adjustments of the original image.

Both selected patients did not have thrombus in the false lumen. The workflow presented here was applied to image data for a patient who had dead end false lumen. Due to the thrombus at the end of the false lumen, there was no blood flow in the distal false lumen, and therefore, no contrast was present at the end of false lumen. This problem cannot be solved through this study since there is no contrast inside false lumen, and therefore, it is virtually impossible to detect the shape of false lumen through threshold or other threshold-based segmentation functions.

Two methods were applied to segment a dissection aorta in using the open source software: edge detection and region growing. In general, edge detection methods identify and locate sharp discontinuities in an image. This function can be used for human organ recognition in medical images (40). Edge detection can be used to detect and extract a normal aorta; however, it is not a suitable function for a dissection aorta since it has two lumens that are separated only by a thin membrane.

Applying edge detection on a dissection aorta can cause the intimal flap to be generated considerably thicker than its actual thickness because it is detected twice at the true lumen and false lumen sides. Furthermore, edge detection will separate the true and false lumen into two individual segments, which will affect the accuracy of the created 3D model due to the difficulty in identifying the original aortic wall location. Additionally, the aorta surface will connect to the spine or other organs when trying to make an outside surface using an edge detection function.

Region growing is a general region-based image segmentation function that has a wide usage in medical image segmentation (41, 42). It can classify the pixels on the image into different segments based on features of the pixels selected in the initial seed. This method has potential to process segmentation faster than the threshold function since it does not need to clean the superfluous bones, arteries and organs. Furthermore, the aortic wall and flap can be generated directly through this method, so it can save the time needed to create them. Uccheddu et al. created 3D-printed models for cardiovascular interventions through the region growing function (43). They proved the potential usefulness of the 3D-printed models in cardiovascular disease diagnosis and treatment planning. However, their work did not include AD cases. In our study, it is difficult to perform region growing on patients with TBAD due to the long anatomic structure of aorta and the uneven contrast situation. When applying region growing, the effect worsens as the growing region moves away from the initial seed. Since the aorta is a long anatomic structure, initial seeds had to be drawn at least every twenty slices for proper functioning of region growing. In some locations of lower aorta, the seeds had to be painted every ten or fewer slices because of the complicated dissection structure and low image quality. Owing to the uneven contrast distribution, there were times when some additional slices needed to be

painted because of the blurred edges and thin intimal flap. Applying region growing might save time in cleaning unnecessary parts and creating wall and flap segments, but it takes too long to draw the required seeds and manual fixing. Thus, region growing is not the best option for segmenting a dissection aorta. This function might have potential for use in reconstruction and cleaning process to shorten the manual fixing time cost. The benefits of region growing applied to the segmentation of AD cases could be investigated in future studies. With the fast development of imaging processing, newly released filters and functions provide various potential ways to conduct segmentation efficiently.

The workflow in this study provides an efficient way to segment AD aorta through open-source software. By adding the filters before applying the threshold, this workflow provides an efficient way to segment a dissection aorta with high accuracy through accessible open-source software. In the two selected cases, their segmented files were exported to the STL format and imported to Meshmixer (v3.4.35; Autodesk, Inc., CA, USA. www.meshmixer.com) for pre-printing checking (44). By using the auto-check function in Meshmixer, <5 errors were detected, and these could be automatically fixed by the software. There were no evident significant flaws in the models after being converted into the STL file format.

In this study, authors focused on the improvement of the efficiency of dissection aortic segmentation with use of open-source software. In previous studies, researchers tend to solve the challenges of dissection segmentation through artificial intelligence or new algorithms (26, 28, 29). However, these approaches are not easy to achieve for open-source software user. Therefore, authors did not describe specific function or algorithm in our workflow. Instead, authors provided some basic functions that can be easily applied in most of the open-source software applications. Therefore,

our workflow is helpful for users who do not have medical image segmentation knowledge to improve their understanding of the workflow of dissection segmentation. For an experienced software user with difficulty in dissection segmentation, it also provides them with an efficient way to process the segmentation.

There are some limitations in this study that should be acknowledged. In this study, authors chose these two cases from 11 cases because they have better image quality and their images describe the regions of interest clearly (true & false lumen, intimal flap and fenestration). Patient 1 images were selected because of the low contrast difference between true and false lumen. This problem is quite challenging. In contrast, patient 2 images represented a good example of better contrast enhancement in both true and false lumens. It was chosen to validate the workflow on nonchallenging case. Authors agree that the low number of model is the main limitation of this study. Further, to perform quantitative and qualitative assessments of the 3D-printed model accuracy, in addition to including more cases, more assessors, preferably experts on AD will be invited in the future study to enable robust statistical analysis of results. In this study, due to limited case number (only two cases), Pearson's correlation is sufficient to show comparison of the accuracy between STL and original CT images. With more cases to be collected in further studies, Bland-Altman plots with limits of agreement should be used to allow generation of results with better statistical analysis.

This study is focused on creating a high-quality dissection STL model suitable for 3DP. Model wall thickness is also an important factor that needs to be considered carefully to find balance between actual tissue properties and printability, especially for the extremely thin part like the intimal flap. Any holes and flaws have to be avoided before STL post fixing to increase accuracy of replicating anatomical structures. The

pixel size also needed to be considered due to 3D printer's limitation. Our objective is the development of a segmentation protocol that facilitates the generation of STL models directly suitable for 3DP that require a minimal amount of manual intervention or correction during the entire workflow. Our future work will verify the model accuracy by reimporting the STL mesh models into the 3D Slicer software to check the overlapping with the volumetric data.

3.5 Conclusion

In this study, we devised a workflow for the segmentation of TBAD. Application of this protocol to relevant CT image data can produce a high accuracy 3D model geometry suitable for 3DP. In addition, this result is achieved in a shorter time owing to the reduced time required for the segmentation task. All needed functions in this method are available through open-source software with the default toolkit. Because of the limitation of the threshold function, this workflow cannot be used in some circumstances, such as complete thrombus in the false lumen or when there is no difference in the HU value between lumen and the surrounding organs. This workflow could be helpful for anyone who does not possess commercial software but who is interested in producing 3D-printed models of AD cases. This method can be reproduced by someone who has general knowledge of performing image post processing and segmentation using software tools.

References

1. Dake MD, Kato N, Mitchell RS, Semba CP, Razavi MK, Shimono T, et al. Endovascular stent–graft placement for the treatment of acute aortic dissection. New England Journal of Medicine. 1999;340(20):1546-52.
2. Hagan PG, Nienaber CA, Isselbacher EM, Bruckman D, Karavite DJ, Russman PL, et al. The International Registry of Acute Aortic Dissection (IRAD): new insights into an old disease. Jama. 2000;283(7):897-903.
3. Fattori R, Montgomery D, Lovato L, Kische S, Di Eusanio M, Ince H, et al. Survival after endovascular therapy in patients with type B aortic dissection: a report from the International Registry of Acute Aortic Dissection (IRAD). JACC: Cardiovascular Interventions. 2013;6(8):876-82.
4. Jia X, Guo W, Li TX, Guan S, Yang RM, Liu XP, et al. The results of stent graft versus medication therapy for chronic type B dissection. Journal of Vascular Surgery. 2013;57(2):406-14.
5. Brunkwall J, Kasprzak P, Verhoeven E, Heijmen R, Taylor P, Trialists A, et al. Endovascular repair of acute uncomplicated aortic type B dissection promotes aortic remodelling: 1 year results of the ADSORB trial. European Journal of Vascular Endovascular Surgery. 2014;48(3):285-91.
6. Pape LA, Awais M, Woznicki EM, Suzuki T, Trimarchi S, Evangelista A, et al. Presentation, diagnosis, and outcomes of acute aortic dissection: 17-year trends from the International Registry of Acute Aortic Dissection. Journal of the American College of Cardiology. 2015;66(4):350-8.
7. Qin Y-L, Wang F, Li T-X, Ding W, Deng G, Xie B, et al. Endovascular repair compared with medical management of patients with uncomplicated type B acute aortic dissection. Journal of the American College of Cardiology. 2016;67(24):2835-42.
8. Huang C-Y, Hsu H-L, Chen P-L, Chen I-M, Hsu C-P, Shih C-C. The Impact of Distal Stent Graft–Induced New Entry on Aortic Remodeling of Chronic Type B Dissection. The Annals of Thoracic Surgery. 2018;105(3):785-93.
9. Zhao Y, Yin H, Chen Y, Wang M, Zheng L, Li Z, et al. Restrictive bare stent prevents distal stent graft-induced new entry in endovascular repair of type B aortic dissection. Journal of Vascular Surgery. 2018;67(1):93-103.
10. Schubert C, van Langeveld MC, Donoso LA. Innovations in 3D printing: a 3D overview from optics to organs. British Journal of Ophthalmology. 2014;98(2):159-61.
11. Ventola CL. Medical applications for 3D printing: current and projected uses. Pharmacy and Therapeutics. 2014;39(10):704-11.

12. Baskaran V, Štrkalj G, Štrkalj M, Di Ieva A. Current applications and future perspectives of the use of 3D printing in anatomical training and neurosurgery. Frontiers in Neuroanatomy. 2016;10:69.

13. Byrne N, Velasco Forte M, Tandon A, Valverde I, Hussain T. A systematic review of image segmentation methodology, used in the additive manufacture of patient-specific 3D printed models of the cardiovascular system. JRSM Cardiovascular Disease. 2016;5:2048004016645467.

14. Sindi R, Wong YH, Yeong CH, Sun Z. Development of patient-specific 3D-printed breast phantom using silicone and peanut oils for magnetic resonance imaging. Quantitative Imaging in Medicine and Surgery. 2020;10(6):1237-48.

15. Langridge B, Momin S, Coumbe B, Woin E, Griffin M, Butler P. Systematic review of the use of 3-dimensional printing in surgical teaching and assessment. Journal of Surgical Education. 2018;75(1):209-21.

16. Lupulescu C, Sun Z. A systematic review of the clinical value and applications of three-dimensional printing in renal surgery. Journal of Clinical Medicine. 2019;8(7):990.

17. Witowski J, Sitkowski M, Zuzak T, Coles-Black J, Chuen J, Major P, et al. From ideas to long-term studies: 3D printing clinical trials review. International Journal of Computer Assisted Radiology and Surgery. 2018;13(9):1473-8.

18. Sun Z. Insights into 3D printing in medical applications. Quantitative Imaging in Medicine Surgery. 2019;9(1):1-5.

19. Sun Z. Clinical Applications of Patient-Specific 3D Printed Models in Cardiovascular Disease: Current Status and Future Directions. Biomolecules. 2020;10(11):1577.

20. Hossien A, Gesomino S, Maessen J, Autschbach R. The Interactive Use of Multi-Dimensional Modeling and 3D Printing in Preplanning of Type A Aortic Dissection. Journal of Cardiac Surgery. 2016;31(7):441-5.

21. Wu C-A, Squelch A, Sun Z. Investigation of three-dimensional printing materials for printing aorta model replicating type B aortic dissection. Current Medical Imaging. 2021;17(7):843-9.

22. Gomes EN, Dias RR, Rocha BA, Santiago JAD, Dinato FJdS, Saadi EK, et al. Use of 3D printing in preoperative planning and training for aortic endovascular repair and aortic valve disease. Brazilian Journal of Cardiovascular Surgery. 2018;33:490-5.

23. Sun Z, Squelch A. Patient-specific 3D printed models of aortic aneurysm and aortic dissection. Journal of Medical Imaging and Health Informatics. 2017;7(4):886-9.

24. Schmauss D, Schmitz C, Bigdeli AK, Weber S, Gerber N, Beiras-Fernandez A, et al. Three-dimensional printing of models for preoperative planning and simulation of transcatheter

valve replacement. The Annals of Thoracic Surgery. 2012;93(2):31-3.

25. Gallo M, D'Onofrio A, Tarantini G, Nocerino E, Remondino F, Gerosa G. 3D-printing model for complex aortic transcatheter valve treatment. 2016.

26. Schmauss D, Gerber N, Sodian R. Three-dimensional printing of models for surgical planning in patients with primary cardiac tumors. The Journal of Thoracic and Cardiovascular Surgery. 2013;145(5):1407-8.

27. Olivieri L, Krieger A, Chen MY, Kim P, Kanter JP. 3D heart model guides complex stent angioplasty of pulmonary venous baffle obstruction in a Mustard repair of D-TGA. International Journal of Cardiology. 2014;172(2):297-8.

28. Pepe A, Li J, Rolf-Pissarczyk M, Gsaxner C, Chen X, Holzapfel GA, et al. Detection, segmentation, simulation and visualization of aortic dissections: A review. Medical Image Analysis. 2020;65:101773.

29. Ho D, Squelch A, Sun Z. Modelling of aortic aneurysm and aortic dissection through 3D printing. Journal of Medicine Radiation Science. 2017;64(1):10-7.

30. Casey RG, Lecolinet E. A survey of methods and strategies in character segmentation. IEEE Transactions on Pattern Analysis and Machine Intelligence. 1996;18(7):690-706.

31. Kovács T, Cattin P, Alkadhi H, Wildermuth S, Székely G, editors. Automatic segmentation of the aortic dissection membrane from 3D CTA images. International Workshop on Medical Imaging and Virtual Reality; 2006: Springer.

32. Farooqi KM, Lengua CG, Weinberg AD, Nielsen JC, Sanz J. Blood Pool Segmentation Results in Superior Virtual Cardiac Models than Myocardial Segmentation for 3D Printing. Pediatric Cardiology. 2016;37(6):1028-36.

33. Li Z, Feng J, Feng Z, An Y, Gao Y, Lu B, et al., editors. Lumen segmentation of aortic dissection with cascaded convolutional network. International Workshop on Statistical Atlases and Computational Models of the Heart; 2018: Springer.

34. Cao L, Shi R, Ge Y, Xing L, Zuo P, Jia Y, et al. Fully automatic segmentation of type B aortic dissection from CTA images enabled by deep learning. European Journal of Radiology. 2019;121:108713.

35. Giannopoulos AA, Steigner ML, George E, Barile M, Hunsaker AR, Rybicki FJ, et al. Cardiothoracic applications of 3D printing. Journal of thoracic imaging. 2016;31(5):253.

36. Foley TA, El Sabbagh A, Anavekar NS, Williamson EE, Matsumoto JM. 3D-Printing: Applications in Cardiovascular Imaging. Current Radiology Reports. 2017;5(9).

37. Fedorov A, Beichel R, Kalpathy-Cramer J, Finet J, Fillion-Robin J-C, Pujol S, et al. 3D Slicer as an image computing platform for the Quantitative Imaging Network. Magnetic Resonance Imaging. 2012;30(9):1323-41.

38. Liu C-Y, Chen D, Bluemke DA, Wu CO, Teixido-Tura G, Chugh A, et al. Evolution of aortic wall thickness and stiffness with atherosclerosis: long-term follow up from the multi-ethnic study of atherosclerosis. Hypertension. 2015;65(5):1015-9.

39. Kovács T, Cattin P, Alkadhi H, Wildermuth S, Székely G. Automatic segmentation of the vessel lumen from 3D CTA images of aortic dissection. Bildverarbeitung für die Medizin 2006. Springer;2006:161-5.

40. Lee LK, Liew SC, Thong WJ. A review of image segmentation methodologies in medical image. Advanced Computer and Communication Engineering Technology: Springer; 2015:1069-80.

41. Zanaty E, Ghoniemy S. Medical image segmentation techniques: an overview. International Journal of Informatics and Medical Data Processing. 2016;1(1):16-37.

42. Masood S, Sharif M, Masood A, Yasmin M, Raza M. A survey on medical image segmentation. Current Medical Imaging Reviews. 2015;11(1):3-14.

43. Uccheddu F, Gallo M, Nocerino E, Remondino F, Stolocova M, Meucci F, et al. Cardiovascular interventions planning through a three-dimensional printing patient-specific approach. Journal of Cardiovascular Medicine. 2019;20(9):584-96.

44. Schmidt R, Singh K, editors. Meshmixer: an interface for rapid mesh composition. ACM SIGGRAPH 2010 Talks; 2010: ACM.

CHAPTER 4

INVESTIGATION OF THREE-DIMENSIONAL PRINTING MATERIALS FOR PRINTING AORTA MODEL REPLICATING TYPE B AORTIC DISSECTION

This study aims to determine a printing material that has both elastic property and radiology equivalence close to the real aorta for simulation of endovascular stent-graft repair of aortic dissection (AD). With the rapid development of three-dimensional (3D) printing technology, a patient- specific 3D printed model is able to help surgeons to make a better treatment plan for Type B AD (TBAD) patients. However, the radiological properties of most 3D printing materials have not been well characterized. This study aims to investigate the appropriate materials for printing human aorta with mechanical and radiological properties similar to the real aortic computed tomography (CT) attenuation.

4.1 Introduction

Three-dimensional (3D) printing is a popular technology that is increasingly used in the medical domain within the last decade (1-5). 3D-printed models are widely used in different medical applications, such as preoperative guiding and planning (6), educating students and inexperienced surgeons (7), and creating a phantom for academic research (8). Patient-specific models have shown clinical value in pre-surgical planning of endovascular stent-graft repair of aortic aneurysm and AD (9-11). Kim et al., reported that the 3D-printing technique could benefit the surgical outcome on the repair of an extensive thoracoabdominal aortic disease, hence improving surgical outcomes in the presence of challenging anatomy (9). Tong et al., advanced the application of 3D printing in fenestrated endovascular repair of AD and aneurysm in 34 patients (11). They achieved accurate planning of fenestrated endovascular repair by developing personalised approaches for individual cases based on measurement of the fenestration sizes using 3D-printed aorta models. Their results showed successful treatment of these complicated thoracoabdominal aortic diseases, thus highlighting the clinical value of the use of 3D printed aortic models to guide aortic disease treatment. These studies indicate that patient-specific models play an important role in assisting clinical-decision making by delivering precision medicine to individual patients with complex aortic disease, including AD, thus improving the quality of patient care.

Acute aortic dissection (AAD) is the most common life threatening catastrophe of the aorta. Stanford's classification system is most commonly used to classify AD into Type A and Type B based on its anatomic location (12). It can also be used to decide the treatment for AAD patients (13). Mortality in AAD varies rapidly in time, anatomic location and complications. Early mortality of Type A AAD increases at 1% per hour

and it can reach 90% at 3 months if the patients are left untreated (14, 15). For Type B AAD, the overall in-hospital mortality is reported to be 11%. Type A

AAD patients tend to need urgent surgical treatment because of their high mortality data. In contrast, treatment management for Type B is controversial. The comparison between medical therapy, surgical treatment and endovascular treatment has been widely discussed (16-18). A 3D-printed model can be used to assist in designing stent grafts or be applied to select a suitable stent graft system and simulate the implantation procedure as a personalized model (19, 20). Thus, a 3D-printed TBAD model has the potential value to become a helpful tool for making patient-specific treatment decisions (21).

A 3D-printed aorta model can replicate anatomical details of aortic structure with high accuracy (11, 22). To mimic the artery properties, printing materials have to possess high elasticity and flexibility. Soft 3D printing materials, Visijet CE-NT and Visijet CE-BK from 3D Systems (Valencia, CA, USA), can be printed with different hardness and have close mechanical properties to the artery (23). Riedle et al., compared commercial 3D-printed elastomers and found that the mechanical property of TangoPlus Flex is closest to aortic tissues (24). Stratasys Agilus (Eden Prairie, MN, USA) is also a flexible 3D printing material with variable hardness (25, 26). Most of the current studies focus on clinical applications of 3D printing in aortic disease (9-11, 19-23), while, the discussion of commercial materials' radiological properties is limited in the current literature. These materials accurately replicate normal anatomy and pathology, such as aortic aneurysm and AD on 3D- printed physical models; however, it remains to be determined whether the materials have physical and tissue properties similar to real patient data. Since the 3D-printed models are starting to be used as

imaging phantom for research or assessment model for CT reconstruction algorithms, more studies of 3D printing materials' radiological properties are needed (27, 28).

This study aimed to evaluate the performance of 3Dprinted TBAD phantoms under CT scan and to find out suitable materials to print the aorta model by replicating the TBAD case. A 3D printing material, which has both mechanical and radiological properties close to the real patients' aorta, is valuable to clinical treatment planning and helpful for future studies as an imaging phantom.

4.2 Materials and Methods

A short segment of the TBAD model was created at the workstation based on a real patient's imaging data. Four models were printed out with two different materials, which were selected based on their mechanical properties and appearance. All of the models were CT scanned twice, with and without contrast inside. After scanning, Hounsfield units (HU) were measured in five different reference points inside the image datasets. These measurements were compared with the original patient image to see if they have significant differences.

4.2.1 Model Design

Contrast-enhanced CT image data of 11 patients who underwent acute TBAD were retrospectively reviewed and selected for this study. Depending on the description of the true lumen, false lumen and intimal tear, one of the patients who had relatively better image quality was selected. The CT image dataset was imported into 3D Slicer (Version 4.9.0, www.slicer.org; Massachusetts, USA) to proceed with image post-processing and segmentation. A 25-mm segment located at the proximal segment of the descending aorta, between the aortic arch and celiac trunk, was selected (**Figure 4.1**). This segment had a perfect description of both lumens and intimal flap and the border of the aortic wall could be clearly identified. The segment

was cut out and transferred into a Standard Tessellation Language (STL) format for printing. All of the models were directly ordered from the online customer service of each company.

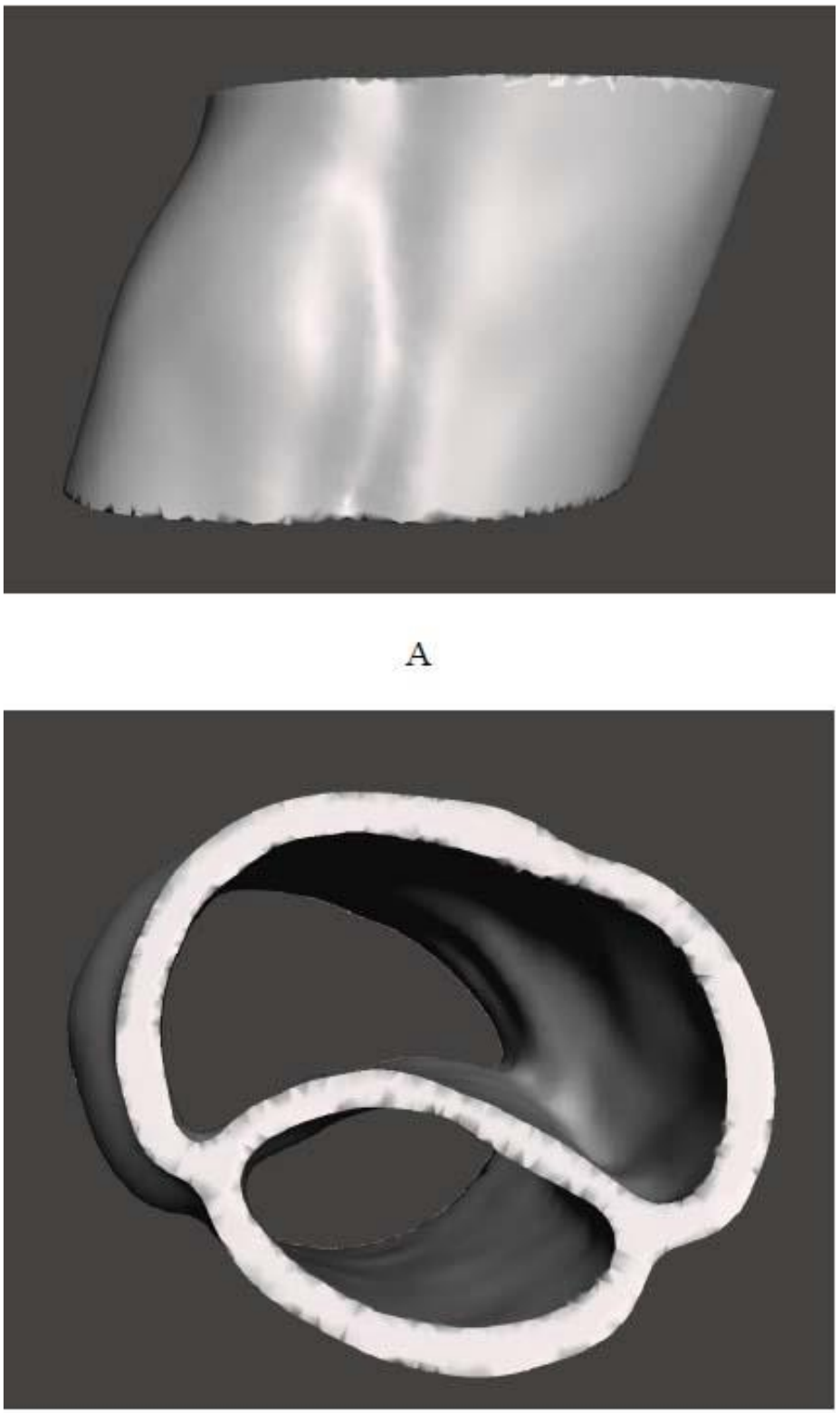

Figure 4.1 A 25-mm segment located at the proximal of the descending aorta was selected. Standard Tessellation Language (STL) file of the segmented aorta with frontal view (A) and inferior view of the true lumen, false lumen and intimal flap (B).

4.2.2 Material Selection

The selection of materials depended on two considerations: mechanical properties and transparency. To make a model that has a mechanical property approach to a real human aorta, the model's materials have to be elastic and flexible. The tensile strength of elderly cardiovascular disease patients should be around 0.39 and modulus of elasticity 0.628 (23). Elongation at break of the aorta is around 82% to 140% and hardness is between Shore A12 and A18, including the ascending aorta, descending aorta and abdominal aorta (24). In terms of transparency, a transparent material is the best option for an aorta model. It is able to provide an excellent vision of the intravascular structure and will be helpful in academic and clinic settings. However, a transparent elastomer printing material is not available at commercial companies; therefore, translucent materials are the second option.

Based on the mechanical properties, two kinds of elastomers were selected, namely, Agilus (Stratasys) and Visijet CE-NT (3D Systems). Both of these materials are soft rubber-like photopolymer resin that can be mixed with another hard photopolymer resin during printing to create various elasticity products. The mechanical properties of these materials are recorded in **Table 4.1**. Agilus models were printed out with two different degrees of hardness, Shore A40 and A50. The elongation at break for A40 was from 150% to 170% and for A50 between 130% and 150%. Both of these models have a tensile strength between 0.5 and 1.5 (29).

Table 4.1 Mechanical properties of materials.

Materials Properties/ 3D Printing Materials	Selected 3D Printing Materials			
	Agilus A40	Agilus A50	Visijet CE-NT	Visijet CE-NT
Transparency	Opaque Black	Opaque Black	Translucent	Translucent
Tensile Strength	0.5-1.5	0.5-1.5	0.2-0.4	0.75-1.1
Elongation at Break	150-170	130-150	160-230	50-80
Shore (Scale A)	28-40	36-50	27-33	66-75

3D Systems has two different soft rubber-like materials that are suitable for producing aorta-like models, namely, Visijet CE-NT and Visijet CE-BK. Both have similar mechanical properties but in different colours. Compared to CE-BK, a black and opaque material, CE-NT is better for this study since it has a natural light yellow and translucent appearance. Two Visijet CE-NT models with different hardness were printed, A30 and A70. A30 has a tensile strength between 0.2 and 0.4, which is close to elderly cardiovascular disease patients. To produce a model to mimic a younger human's aorta, A90 would be the best choice which has a tensile strength of around 1.4 to 1.9. However, as a model which aims to simulate the aorta, A90 has a less flexible ability; hence, A70 was selected instead (30).

4.2.3 CT Scanning

Four 3D-printed aortic segment models were scanned by 192-slice Siemens CT scanner (Somatom Force, Siemens Healthcare, Forchheim, Germany) with routine CT angiography scanning parameters: 120 kVp tube potential, 150 reference mAs, 0.75 mm slice thickness, and 0.5 mm reconstruction spacing. The actual scanning parameters are controlled through Siemens' automatic dosing programme (**Figure 4.2**).

2A

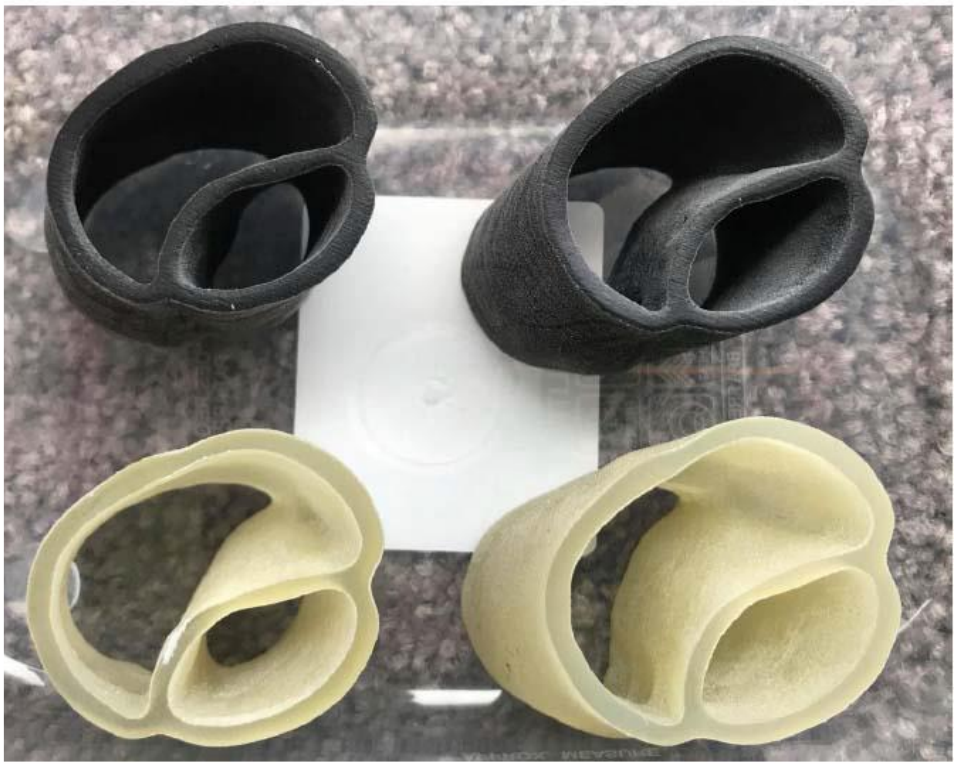

2B

Figure 4.2 Computed tomography scanning parameters were set at 120 kVp tube potential, 150 reference mAs, 0.75-mm slice thickness and 0.5 mm reconstruction spacing. A: the models were placed in a plastic container with a superior view. B: inferior view of these 3D printed models. Upper black models from left to right are Agilus A40 and A50. Lower translucent models from left to right are Visijet CE-NT A30 and A70.

The scan was conducted twice. The first was a direct scan without any contrast. To mimic the real patient's scan, water mixed with 6% contrast medium was added inside the true and false lumens of the models. The open ends of the models were sealed by removable adhesive. Duck fat (30-mm thick) was placed on top of the models to mimic body fat.

4.2.4 Data Analysis

Five reference points inside the aortic wall were selected, including the middle of the true lumen, middle of the false lumen, two junctions between the true and false lumens and the middle of the intimal flap. A 1.5 mm diameter (1.77 mm2) circular region of interest (ROI) was placed inside each point to measure the average HU (**Figure 4.3**). The shape of ROI could be changed, but it was maintained in the same area because of the thickness of the intimal flap. Each point had measured in triplicate and the average value was reported. The comparison between the patient's aorta and models was performed through a paired-sample t-test. Image data of the original patient aortic wall was compared with that of the models with and without contrast. A total of eight comparisons were reported. A p-value less than 0.05 was considered statistically significant.

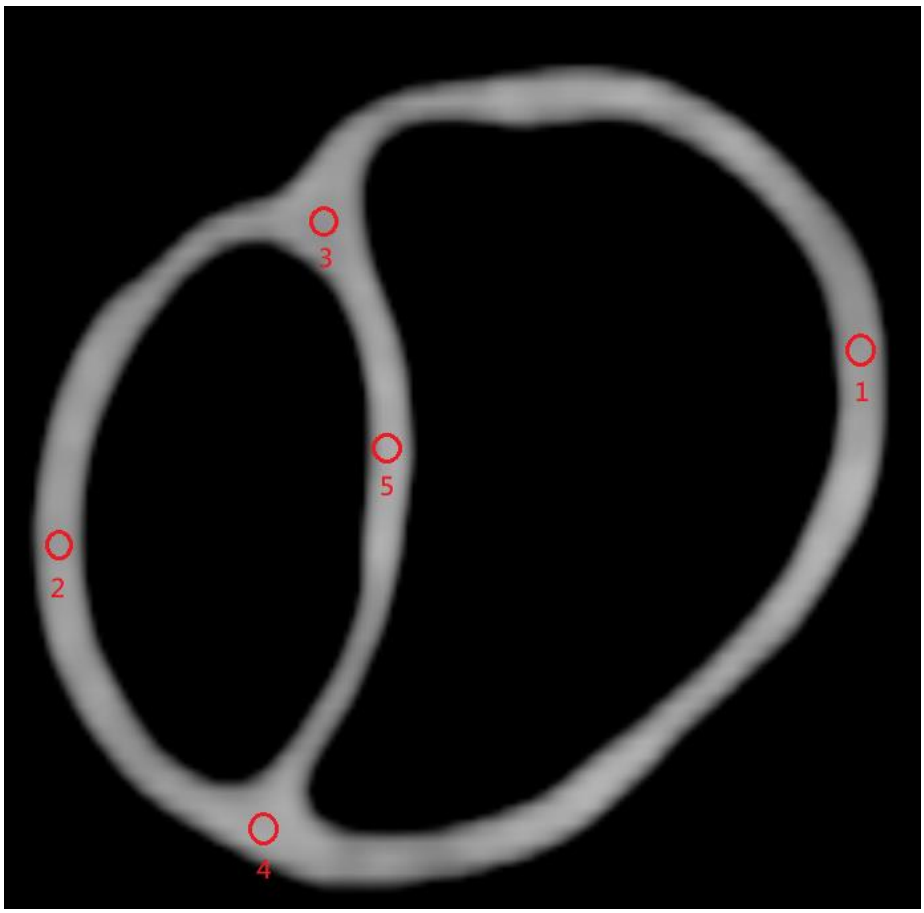

Figure 4.3 Five regions of interest with the same area were put inside the middle of the true lumen, false lumen, junctions between true and false lumens and middle of the intimal flap to measure the Hounsfield units of patient's aorta and 3D printed models. (A higher resolution / colour version of this figure is available in the electronic copy of the article).

4.3 Results

The average of three measurements was recorded in **Table 4.2**. The average of all measurements of the original image was 80.7 HU. Under a noncontrast situation, Agilus A50 had an average of 82.6 HU, which is closest to measurement on the original images. On the other hand, Visijet CE-NT A30 had an average of 90.6 HU, which is closest to the original image after adding contrast inside the models. Agilus models had a greater average HU than Visijet CE-NT models, whether with or without contrast. All of the measurements became higher after adding contrast. The measurements at the intimal flap (point 5) tend to lower than other reference points when CT scans were performed without contrast. This happened opposite after adding contrast as the

intimal flap measurements became higher than other points, which was close to the real-patient scanning situation. The measurements at the junction between true and false lumens (points 3 and 4) had higher HU than measurements inside the middle of true and false lumens (points 1 and 2) after adding contrast.

Table 4.2 Average Hounsfield unit measurements on the original patient image and models. ROI: region of interest.

Printing Materials/ROI	Five References Points for Measurements				
	point 1	point 2	point 3	point 4	point 5
Original aortic wall	70.5 + 11.9	75.5 ± 1.92	76 ± 15.88	73.75 + 3.95	107.5 ± 3.54
Agilus A40 (without contrast)	62 ±12.2	56.86 ±2.91	66.34 ±5.37	68.28 + 6.67	44.38 ± 8.74
Agilus A50 (without contrast)	72.67 ±6.6	74 ±9	109.42 ± 9.21	78.15 ±8.16	78.75 ± 6.24
Visijet CE-NT A30 (without contrast)	40.72 ± 4.96	40.15 ±7.2	32.29 ±2.21	41.5 ±2.35	23.25 ±9.16
Visijet CE-NT A70 (without contrast)	46.23 ± 8.24	48.34 ±8.85	59.63 ±4.28	47 ± 4.79	35.38 ±5
Agilus A40 (with contrast)	99.75 ± 17.83	73.34 ± 18.72	128 ±6.36	166 ±3.98	178 ±7.55
Agilus A50 (with contrast)	97.76 ± 18.65	79.41 ± 13.13	128.75 ±3.86	178.71 ± 5.09	190.5 ± 8.85
Visijet CE-NT A30 (with contrast)	47 ± 9.47	43.6 ± 8.84	108.5 ± 10.67	105.25 ± 7.41	148.5 ± 15.44
Visijet CE-NT A70 (with contrast)	97.8 ± 14.47	103.75 ± 14.11	137 ± 5.478	136.71 ± 6.9	172.5 ±9.36

The measurements at the intimal flap (point 5) tend to lower than other reference points when CT scans were performed without contrast. This happened opposite after adding contrast as the intimal flap measurements became higher than other points, which was close to the real-patient scanning situation. The measurements at the junction between true and false lumens (points 3 and 4) had higher HU than

measurements inside the middle of true and false lumens (points 1 and 2) after adding contrast.

Through paired-sample t-test, Agilus A40 and A50 without contrast that have a p-value greater than 0.05 showed that they are not statistically significant with the original aorta image. Two Visijet CE-NT models have significant differences from the original image since their p-values were lower than 0.05. After adding contrast inside the models, the CT attenuation measured in all of the models is significantly higher than that of the original images, except for the material of Visijet CE-NT A30, the only model with the mean CT attenuation showing no significant difference from that of original CT images ($p>0.05$).

4.4 Discussion

This study shows that under the noncontrast situation, Agilus A40 and A50 did not have significant differences from the original aorta. On the other hand, Visijet CE-NT A30 is the only one that had no significant differences from the original patient with contrast. Since the second scan with contrast inside is more close to the clinical situation, Visijet CE-NT A30 could be considered as an excellent elastic 3Dprinted material for the TBAD model because of its performance under CT scan.

The mechanical properties are another criterion of printing material selection. According to Riedle et al., elongation at break of the aorta is around 82% to 140%, and hardness is between Shore A12 and A18, including the ascending aorta, descending aorta and abdominal aorta (24). In 3D Systems and Stratasys, the softest elastomer is Shore A30 hardness. There are no 3D-printed materials from the selected companies that have the hardness/softness of a real aorta while maintaining a strong enough elasticity. Agilus A40 and A50 were chosen because of elongation and tensile strength. Visijet CE-NT A30 has excellent elongation, which is greater than a human aorta and

tensile strength approach to elderly patients' arteries. Visijet CE-NT A70 was selected since it has a tensile strength close to young human arteries, but it does not perform well on elongation. Based on the mechanical properties, both materials with low hardness can be applied for clinical purposes, such as treatment planning or pre-surgical guidance. On the other hand, high hardness elastomers might not be as useful as the soft materials on pre-surgery guiding and it can still be used for education purposes such as teaching aids or helping explain patients' situations to their families since it is a patient-specific model.

Whether for clinical application or education purposes, a transparent model is always the best choice. In thoracic endovascular aortic repair, a transparent model is able to provide a clear vision of the inside of the arteries. This advantage is helpful for pre-surgery guiding or stent pre-shaping. However, there is no available transparent elastic printing material product from the selected companies right now. The only available Agilus colour from Stratasys' official website is opaque black, which is not an ideal colour for an aorta model since it could be used for clinical purposes. On the other hand, the appearance of a Visijet CE-NT model is translucent light yellow. Judging by the colour, Visijet CE-NT with low hardness could be a nice material for the purpose of making an aorta model for pre-surgery guiding usage.

According to Knollmann et al., the aortic wall can be measured from 33 to 91 HU on AD patients (31). All of the reference point measurements were from the original image datasets located within this range, except for the intimal flap. The average measurements reported had higher HU than other reference points. Meanwhile, for situations without contrast, the intimal flap measurements had lower HU than the other points. Compared with situations without contrast, intimal flap measurements tend to have the same performance as the original image after adding contrast inside,

and HU is greater than the other points. This difference happens because of the thickness of the intimal flap. When ROI was placed into the intimal flap, both sides of the ROI were very close to the true and false lumens as the intimal flap was too thin. Therefore, when there is no contrast inside the lumen, both sides of the ROI become darker than the middle area. This leads to lower HU results after calculating the average inside ROI. On the contrary, in the original image and models with contrast, the true and false lumens were full of contrast, so both sides of the ROI become lighter than the middle area. For this reason, the intimal flap had higher HU than other points after perfusion of contrast inside both lumens. This kind of effect can be seen not only in the intimal flap but also in other reference points; however, the influence is not as strong as the intimal flap because only one of its sides is attached to the lumen and the aortic wall is thicker than intimal flap. Because of this effect, overall HU measurements with contrast inside were higher than without contrast.

Contrast inside the lumen has a big influence on HU measurements. Although in the first scan without contrast, the Agilus A40 and A50 models did not produce significantly different results, the second scan results with contrast inside can be more valuable since it is closer to real-patient scanning datasets. Based on the data analysis, Visijet CENT A30 is the only one that has no significant difference from the original aorta image. Thus, compared with other materials, Visijet CE-NT A30 is a 3D-printed elastic material that provides HU close to a real patients' image under CT scanning.

It takes time from the design of the 3D models to print out and to perform CT scanning. Over time, the density of the model could change (32). In this study, the first CT scanning was conducted 4 weeks after printing and 6 weeks after the second scanning. Thus, the density of the models could have been changed and introduced the errors of HU measurements. Another point to consider is that the scanning

protocol is auto-adjusted through Siemens workstation. In this study, the models were scanned without a human body phantom. Duck fat was used to mimic the fat inside the human body, but there is nothing to represent other organs inside the chest. Thus, both outcome dosages were lower than the original patient. The scanning images of the models were unable to completely represent a real-patient scanning.

In the future study, some different materials can be selected to test the performance under CT scans, such as a softer 3D printable elastomer like silicone-based materials or any transparent elastic materials. The phantom of scanning should be improved to mimic the in vivo circumstance, which includes bone, fat, air, soft tissue and other organs surrounding the aorta. This allows for the investigation of optimal CT scanning protocols for detection of AD and assessment of stent-graft position in relation to the aortic branches with minimization of radiation and contrast medium doses as shown in other studies with the use of personalized 3D printed models (33-37).

4.5 Conclusion

Both Visijet CE-NT and Agilus have tensile strength and elongation close to real patients' tissue properties, although their hardness is still a bit higher than the actual aorta. In CT scanning, Visijet CE-NT A30 was considered as it had no significant differences from real dissection aorta based on measurements of Hounsfield unit with contrast inside the model. However, the scanning circumstances in this study are not able to represent the real-patient scanning because of the lack of body phantom and surrounding anatomical structures. Further research with the simulation of realistic body environment should be conducted to address these limitations.

References

1. Witowski J, Sitkowski M, Zuzak T, Coles-Black J, Chuen J, Major P, et al. From ideas to long-term studies: 3D printing clinical trials review. International Journal of Computer Assisted Radiology and Surgery. 2018;13(9):1473-8.
2. Sun Z. Insights into 3D printing in medical applications. Quantitative Imaging in Medicine and Surgery. 2019;9(1):1-5.
3. Langridge B, Momin S, Coumbe B, Woin E, Griffin M, Butler P. Systematic review of the use of 3-dimensional printing in surgical teaching and assessment. Journal of Surgical Education. 2018;75(1):209-21.
4. Lau IWW, Liu D, Xu L, Fan Z, Sun Z. Clinical value of patient-specific three-dimensional printing of congenital heart disease: Quantitative and qualitative assessments. PloS One. 2018;13(3):0194333.
5. Sun Z, Liu D. A systematic review of clinical value of three-dimensional printing in renal disease. Quantitative Imaging in Medicine and Surgery. 2018;8(3):311-25.
6. Ryan JR, Almefty KK, Nakaji P, Frakes DH. Cerebral Aneurysm Clipping Surgery Simulation Using Patient-Specific 3D Printing and Silicone Casting. World Neurosurg. 2016;88:175-81.
7. Yi X, Ding C, Xu H, Huang T, Kang D, Wang D. Three-Dimensional Printed Models in Anatomy Education of the Ventricular System: A Randomized Controlled Study. World Neurosurgery. 2019;125:891-901.
8. Yang Y, Liu X, Xia Y, Wu W, Xiong H, Zhang H, et al. Impact of spatial characteristics in the left stenotic coronary artery on the hemodynamics and visualization of 3D replica models. Scientific Reports. 2017;7(1):1-13.
9. Kim WK, Kim T, Lee S, Yang DH, Kim GB, Kim N, et al., editors. 3D-printing-based open repair of extensive thoracoabdominal aorta in severe scoliosis. Seminars in Thoracic and Cardiovascular Surgery; 2019: Elsevier.
10. Huang J, Li G, Wang W, Wu K, Le T. 3D printing guiding stent graft fenestration: a novel technique for fenestration in endovascular aneurysm repair. Vascular. 2017;25(4):442-6.
11. Tong Y-H, Yu T, Zhou M-J, Liu C, Zhou M, Jiang Q, et al. Use of 3D printing to guide creation of fenestrations in physician-modified stent-grafts for treatment of thoracoabdominal aortic disease. Journal of Endovascular Therapy. 2020;27(3):385-93.
12. Sebastià C, Pallisa E, Quiroga S, Alvarez-Castells A, Dominguez R, Evangelista A. Aortic dissection: diagnosis and follow-up with helical CT. Radiographics. 1999;19(1):45-60.
13. Tien M, Ku A, Martinez-Acero N, Zvara J, Sun EC, Cheung AT. The Penn classification predicts hospital mortality in acute Stanford type A and type B aortic dissections. Journal of Cardiothoracic and Vascular Anesthesia. 2020;34(4):867-73.

14. Tran TP, Khoynezhad A. Current management of type B aortic dissection. Vascular Health and Risk Management. 2009;5:53-63.

15. Apostolakis E, Baikoussis NG, Georgiopoulos M. Acute type-B aortic dissection: the treatment strategy. Hellenic Journal of Cardiology. 2010;51(4):338-47.

16. Qin Y-L, Wang F, Li T-X, Ding W, Deng G, Xie B, et al. Endovascular repair compared with medical management of patients with uncomplicated type B acute aortic dissection. Journal of the American College of Cardiology. 2016;67(24):2835-42.

17. Kamman AV, Brunkwall J, Verhoeven EL, Heijmen RH, Trimarchi S, Kasprzak P, et al. Predictors of aortic growth in uncomplicated type B aortic dissection from the Acute Dissection Stent Grafting or Best Medical Treatment (ADSORB) database. Journal of Vascular Surgery. 2017;65(4):964-71.

18. Li F-R, Wu X, Yuan J, Wang J, Mao C, Wu X. Comparison of thoracic endovascular aortic repair, open surgery and best medical treatment for type B aortic dissection: A meta-analysis. International Journal of Cardiology. 2018;250:240-6.

19. Perica E, Sun Z. Patient-specific three-dimensional printing for pre-surgical planning in hepatocellular carcinoma treatment. Quantitative Imaging in Medicine and Surgery. 2017;7(6):668.

20. Lei Y, Chen X, Li Z, Zhang L, Sun W, Li L, et al. A new process for customized patient-specific aortic stent graft using 3D printing technique. Medical Engineering and Physics. 2020;77:80-7.

21. Sun Z, Squelch A. Patient-specific 3D printed models of aortic aneurysm and aortic dissection. Journal of Medical Imaging and Health Informatics. 2017;7(4):886-9.

22. Ho D, Squelch A, Sun Z. Modelling of aortic aneurysm and aortic dissection through 3D printing. Journal of Medicine Radiation Science. 2017;64(1):10-7.

23. Ratinam R, Quayle M, Crock J, Lazarus M, Fogg Q, McMenamin P. Challenges in creating dissectible anatomical 3D prints for surgical teaching. Journal of Anatomy. 2019;234(4):419-37.

24. Riedle H, Mukai B, Molz P, Franke J, editors. Determination of the Mechanical Properties of Aortic Tissue for 3D Printed Surgical Models. 2018 11th Biomedical Engineering International Conference (BMEiCON); 2018: IEEE.

25. Shearn AI, Yeong M, Richard M, Ordoñez MV, Pinchbeck H, Milano EG, et al. Use of 3D models in the surgical decision-making process in a case of double-outlet right ventricle with multiple ventricular septal defects. Frontiers in Pediatrics. 2019:330.

26. Hussein N, Kasdi R, Coles JG, Yoo S-J. Use of 3-dimensionally printed heart models in the planning and simulation of surgery in patients with Raghib syndrome (coronary sinus defect

with left superior vena cava). JTCVS Techniques. 2020;2:135-8.

27. Bieniosek MF, Lee BJ, Levin CS. Characterization of custom 3D printed multimodality imaging phantoms. Medical Physics. 2015;42(10):5913-8.

28. Solomon J, Ba A, Bochud F, Samei E. Comparison of low-contrast detectability between two CT reconstruction algorithms using voxel-based 3D printed textured phantoms. Medical Physics. 2016;43(12):6497-506.

29. Agilus30 Material Data Sheet: Stratasys Ltd.; [Available from: https://www.stratasys.com/materials/search/agilus30.

30. Projet MJP 5600 Tech Specs.: 3D Systems; [Available from: https://www.3dsystems.com/materials/visijet-ce-nt-elastomeric-natural.

31. Knollmann FD, Lacomis JM, Ocak I, Gleason T. The role of aortic wall CT attenuation measurements for the diagnosis of acute aortic syndromes. European Journal of Radiology. 2013;82(12):2392-8.

32. Craft DF, Kry SF, Balter P, Salehpour M, Woodward W, Howell RM. Material matters: analysis of density uncertainty in 3D printing and its consequences for radiation oncology. Medical Physics. 2018;45(4):1614-21.

33. Sun Z. Use of three-dimensional printing in the development of optimal cardiac CT scanning protocols. Current Medical Imaging. 2020;16(8):967-77.

34. Sun Z, Jansen S. Personalized 3D printed coronary models in coronary stenting. Quantitative Imaging in Medicine and Surgery. 2019;9(8):1356.

35. Aldosari S, Jansen S, Sun Z. Patient-specific 3D printed pulmonary artery model with simulation of peripheral pulmonary embolism for developing optimal computed tomography pulmonary angiography protocols. Quantitative Imaging in Medicine and Surgery. 2019;9(1):75.

36. Aldosari S, Jansen S, Sun Z. Optimization of computed tomography pulmonary angiography protocols using 3D printed model with simulation of pulmonary embolism. Quantitative Imaging in Medicine and Surgery. 2019;9(1):53-62.

37. Sun Z, Ng CK, Squelch A. Synchrotron radiation computed tomography assessment of calcified plaques and coronary stenosis with different slice thicknesses and beam energies on 3D printed coronary models. Quantitative Imaging in Medicine and Surgery. 2019;9(1):6-22.

CHAPTER 5

OPTIMIZATION OF COMPUTED TOMOGRAPHY ANGIOGRAPHY PROTOCOLS FOR FOLLOW-UP TYPE B AORTIC DISSECTION PATIENTS BY USING 3D PRINTED MODEL

Thoracic endovascular aortic repair (TEVAR) is a life-saving therapy for type B aortic dissection (TBAD). However, surveillance computed tomography (CT) scans in post-TEVAR patients are associated with high radiation dose, thus resulting in potential risk of radiation-induced malignancy. In this study, we developed a patient-specific three-dimensional (3D) printed phantom with stent grafts in situ, then scanned the phantom with different CT protocols to determine the optimal scanning parameters for post-treatment patients.

5.1 Introduction

Thoracic endovascular aortic repair (TEVAR) can be a life-saving therapy for treating aortic disease. Compared to open surgical repair, TEVAR is a valid therapeutic option for TBAD because of its lower mortality, morbidity, and paraplegia rate in the past decade (1-3). However, management algorithms remain controversial and long-term follow up is required to determine outcomes and re-intervention rates (4-7).

Computed tomography angiography (CTA) is currently the preferred imaging modality for diagnosis, treatment planning, and follow up for AD patients. With improved spatial and temporal resolution available with modern computed tomography (CT) scanners, CTA plays an important role in the diagnosis and follow up of aortic dissection (AD) (8, 9). However, the high radiation dose associated with CTA is still a concern for the well-being of patients (10-12). To monitor patients after TEVAR, the pursuit of high-resolution and higher-quality images may bring unnecessary radiation doses. Therefore, it is necessary to reduce the radiation dose while maintaining the quality of CT images.

Finding a balance between image quality and radiation risk has always been a challenging issue in achieving optimal scanning protocols. A number of studies describe different strategies to lower the radiation dose including the use of iterative reconstruction (IR) for reducing image noise, use of low tube kilovoltage peak (kVp), and use of high-pitch protocols with fast speed CT scanners (13-15). Despite these studies providing promising results, research is still limited with regard to the reduction of radiation dose for AD patients who require repeat scanning for many years.

Compared with preoperative planning when detail is paramount, postoperative patients could receive a lower dose for routine follow-up examinations to reduce

cumulative radiation dose. Thus, the purpose of this study was to investigate the optimal CTA protocols for surveillance of TBAD patients after EVAR. We employed a patient-specific three-dimensional (3D) printed TBAD model with a stent-graft TEVAR in situ.

Patient-specific 3D printed phantoms have been proven to be valuable in multiple medical applications (16-21). In our previous study, we described how we developed a patient-specific 3D printed TBAD aortic model, and confirmed its accuracy in resembling the mechanical and radiological properties of in vivo imaging under CT scanning modalities (22). In this study, we extended our application of a 3D printed aorta model to focus on the study of optimal CT protocols by deploying a bespoke stent graft inside the true lumen of the AD aorta model to simulate the TEVAR process, and then scanning the model with different CT protocols.

5.2 Materials and Methods

Suitable patient data and materials were required for the preparation and implementation of the 3D printed aorta model used in the study. These components were identified and then utilized as per the methods outlined in the following sections.

5.2.1 Selection of Sample Case and Segmentation

Contrast-enhanced CT (CECT) image data of 11 patients who had TBAD were de-identified and retrieved from public hospital records between November 2015 and March 2016 after ethics approval (Curtin Human Research Ethics (HRE) Committee, approval number: HRE2018-0087). One of the patient datasets (CECT performed on a 128-slice CT with 120 kVp tube potential, 128 reference mAs, and 1.0 mm reconstructed slice thickness) was selected due to high image quality and contrast medium being present in the false lumen, allowing for identification of the aortic shape. The selected CT image dataset was imported into 3D Slicer (Version 4.9.0,

www.slicer.org accessed on 26 July 2021; MA, USA) to proceed with segmentation. The chosen segment had a perfect description of both lumens and intimal flap and the border of the aortic wall could be clearly identified (**Figure 5.1**). After segmentation, a 3D outer surface reconstruction model was generated. Post-processing of the 3D reconstruction model was necessary to ensure model integrity and printing success including checking the thickness, filling of defects (for example, holes inside the models, discontinuous surfaces), and surface smoothing. The 3D reconstruction model was transferred into the stereolithography (STL) format for post cleaning and preprint checking. The final model was directly ordered from the online customer service of 3D Systems Inc. (Valencia, CA, USA).

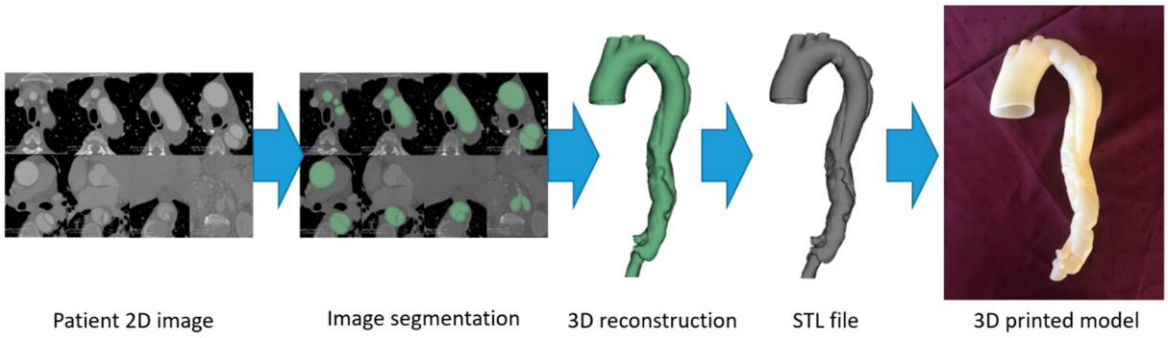

Figure 5.1 A 3D printed model was produced by the following five steps: image acquisition, image segmentation, surface mesh generation, stereolithographic (STL) post-processing, and printing.

5.2.2 Selection of 3D Printing Materials

The selection of a suitable printing material depends on three considerations: the mechanical properties, radiological properties, and transparency. To represent the mechanical properties of the human aorta, the material of the model must have similar flexibility and elasticity. The tensile strength in elderly patients with cardiovascular disease should be around 0.39 MPa and have a modulus of elasticity of 0.628 (23). The elongation at breaking point of the aorta is around 82% to 140% and

the hardness is between Shore A12 and A18 throughout the ascending, descending, and abdominal aorta (24).

Based on our previous study, we chose four different 3D printing materials that had mechanical properties close to that of patients with AD (22). In terms of transparency, a completely transparent model would enhance stent graft deployment without the need for imaging and contrast. This would enable good vision of intravascular structures and be useful in academic applications. However, a transparent elastomer printing material was not available from commercial companies, therefore, a translucent material was the next best option. After scanning samples of several available materials with the current clinical thoracic CTA protocol, one of the materials, Visijet CE-NT (3D systems Inc., Wilsonville, OR, USA), was selected as it had the same radiological properties to in vivo aorta (22). The reason for choosing Visijet CE-NT is due to the following reasons: first, it is a rubber-like material suitable for printing aorta-like models. Second, it has a light yellow and translucent appearance allowing for visualization of the deployed stent grafts inside the aorta. Third, the Visijet CE-NT material has two different hardness, A30 and A70, with A30 having a tensile strength between 0.2 and 0.4, which is close to elderly cardiovascular tissue properties. Finally, our recent study confirms that Visijet CE-NT A30 is the most appropriate material for printing aorta models because its CT attenuation is similar to that of the contrast-enhanced CT images of AD (22).

5.2.3 Deployment of Stent Graft

Three commercially available thoracic stent grafts (Medtronic) were deployed into the model after planning and sizing by an experienced vascular surgeon. The proximal piece deployed into the arch to cover the subclavian artery measured a length of 150 mm and diameter tapering from 42 to 38 mm, which was placed in the

aortic arch. The second overlapping piece was 90 mm long by 31 mm in diameter. The final distal piece measured 94 mm in length and 25 mm in diameter (**Figure 5.2**).

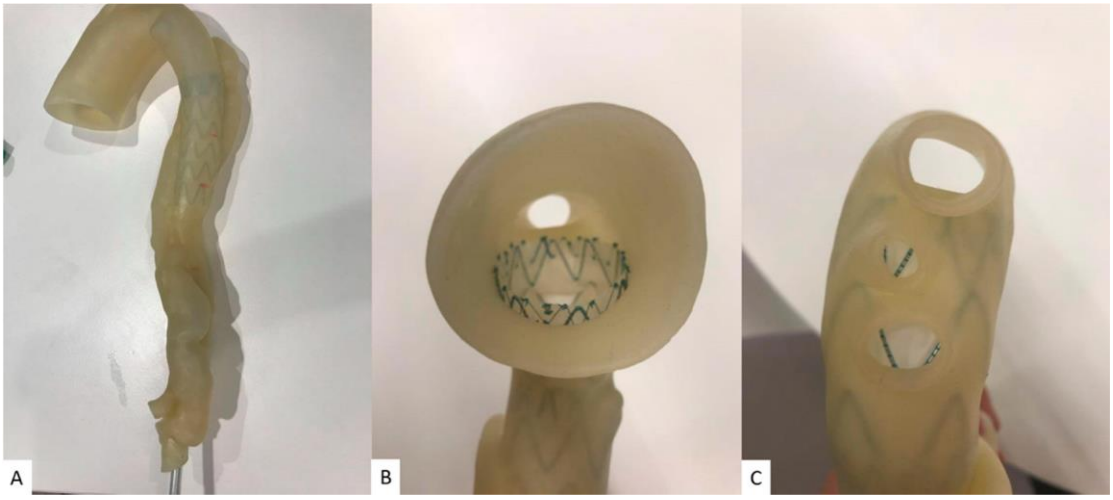

Figure 5.2 Stent graft deployed in the 3D printed model. (A) Deployed stent graft visible through model wall. (B) Axial view from proximal arch. (C) Caudal view down arch vessels.

5.2.4 Aortic CTA Scanning Protocols

The 3D printed TBAD model was placed in a plastic container that was filled with a contrast medium to simulate CECT examinations. Due to the flexibility of the model, air bubbles inside the model were expelled by aspiration via a syringe (**Figure 5.3**). The iohexol contrast medium OmnipaqueTM 350 (GE Healthcare Australia Pty Ltd., New South Wales, Australia), which is routinely used in contrast-enhanced CT scans, was diluted to 7% with a resulting CT attenuation of 300 HU, similar to that of routine CECT. The model was scanned by a 192-slice CT scanner (Siemens Force, Siemens Healthcare, Forchheim, Germany). The CECT scans were conducted with different kVp and pitch values (80, 100, 120 kVp and pitch of 1.2, 1.5, 2.0, 2.5), resulting in a total of 12 datasets. A slice thickness of 1.0 mm with a 0.5 mm reconstruction interval was applied to all images. An iterative reconstruction technique was used (advanced modelled iterative reconstruction (ADMIRE) algorithm with level 3, Siemens Healthcare) and a tissue convolution kernel of Bv40.

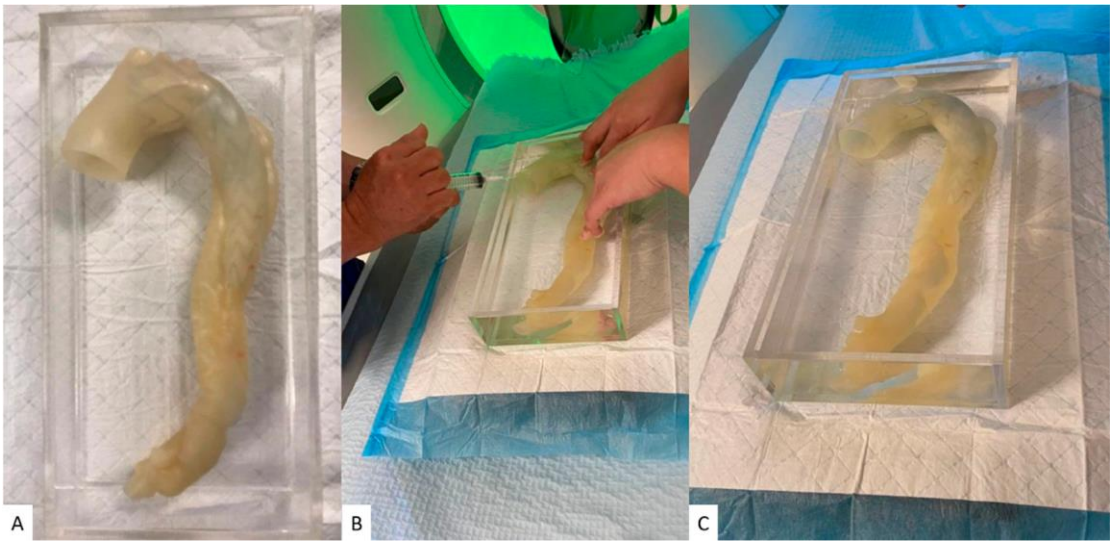

Figure 5.3 The CT scans were performed on the post stent graft deployed aorta model with different scanning protocols. (A) The model placed in a customized acrylic box for scanning. (B) The process of using the syringe to extract the internal air bubbles after pouring the contrast. (C) The final model ready to be scanned.

5.2.5 Quantitative Assessment of Image Quality

In order to determine the image quality in these CTA protocols, the image quality was quantitatively evaluated by measuring the signal-to-noise ratio (SNR) of the proximal and middle descending aorta. Regions of interest (ROI) were placed in the true and false lumens with an area of 25 mm2 (containing at least 300 voxels) to measure SNR. **Figure 5.4** shows the ROI measurement of SNR in the aorta of the model. To minimize the difference between observers, the SNR measurement was repeated three times at each location, and the average value was used to minimize the difference between observers, and the average value between two observers was used as the final result.

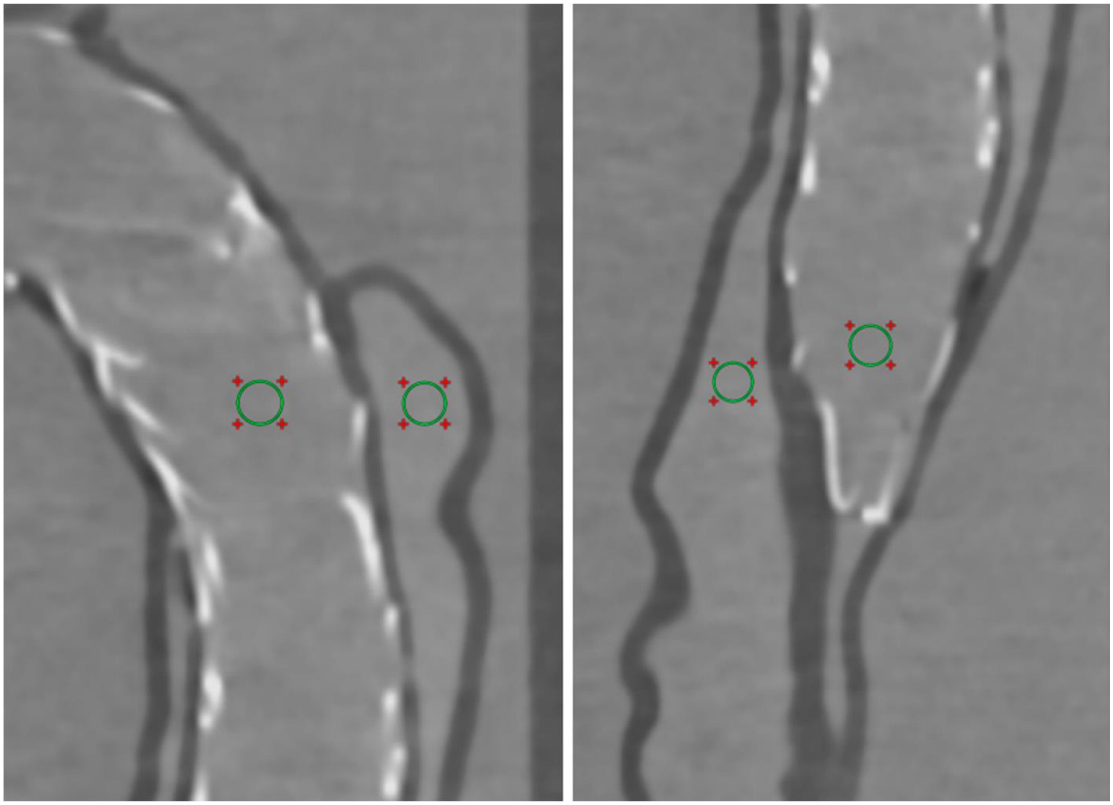

Figure 5.4 ROIs were placed inside the aortic model scan data to measure SNR. Four measuring points were used in each dataset including true and false lumen at proximal and middle descending aorta. ROIs: regions of interest, SNR: signal-to-noise ratio.

5.2.6 Radiation Dose

The volume CT dose index (CTDIvol) and dose length product (DLP) were recorded and compared between different CTA scanning protocols. The effective dose was calculated using a tissue conversion coefficient of 0.014 mSv/mGy/cm, which is commonly used for the calculation of chest CT dose (25).

5.2.7 Statistical Analysis

All data were imported into SPSS 26.0 (IBM Corporation, Armonk, NY, USA) for statistical analysis. A paired sample t-test was used to determine whether there were any significant differences in SNR measured with different CPA protocols. A P value of less than 0.05 indicated a statistically significant difference.

5.3 Results

Different CTA imaging protocols were successfully tested on the 3D printed model. All measurements were performed by two observers, with excellent correlation between the observers. **Table 5.1** shows the SNR measurements at images acquired with different CTA protocols. SNR measurements did not vary significantly when the kVp value range was close such as a comparison between 80 and 100 kVp or between 100 and 120 kVp ($p > 0.05$), regardless of the pitch values. However, the measurements showed that at pitch 1.5, 2.0, and 2.5, SNR at 120 kVp was significantly higher than 80 kVp ($p < 0.05$) in both true and false lumens. SNR showed no significant differences between different kVp when the pitch value was 1.2. At low pitch values such as 1.2 and 1.5, a decrease in kVp from 120 to 80 led to a significant effective dose reduction by more than 20%.

Table 5.1 SNR measurements at images acquired with different CTA protocols. SNR, signal-to-noise ratio; CTDIvol, volume CT dose index; DLP, dose length product.

Tube Voltage	**80 kVp**				**100 kVp**				**120 kVp**			
Pitch	1.2	1.5	2.0	2.5	1.2	1.5	2.0	2.5	1.2	1.5	2.0	2.5
Image Quality(T)	3.00 ± 0.77	2.90 ± 0.54	4.20 ± 0.40	3.80 ± 0.75	3.60 ± 0.66	3.10 ± 0.54	3.50 ± 0.81	3.10 ± 0.81	3.60 ± 0.70	3.20 ± 0.60	3.80 ± 0.60	3.30 ± 0.46
Image Quality(R)	3.17 ± 0.37	3.00 ± 0.58	4.00 ± 0.58	3.50 ± 0.96	3.17 ± 0.69	3.33 ± 0.47	3.17 ± 0.69	3.50 ± 0.50	3.50 ± 0.76	3.00 ± 0.58	3.33 ± 0.47	3.33 ± 0.47
Diagnostic Value	2.83 ± 0.69	2.83 ± 0.37	4.00 ± 0.58	3.50 ± 0.69	3.00 ± 0.58	3.17 ± 0.69	3.33 ± 0.47	3.33 ± 0.75	3.33 ± 0.47	2.83 ± 0.37	3.33 ± 0.47	3.17 ± 0.69
SNR	34.77±1.88	32.06±1.00	24.45±3.10	24.63±3.51	36.79±4.38	33.81±3.28	27.3±4.01	25.62±3.72	38.57±3.66	37.26±3.18	29.09±3.72	27.45±2.99
CTDIvol (mGY)	0.07	0.08	0.06	0.05	0.09	0.08	0.07	0.06	0.11	0.09	0.08	0.07
DLP (mGY/cm)	1.8	1.5	1.4	1.4	2.1	2	1.7	1.6	2.2	2.2	1.8	1.8
Effective dose (mSv)	0.0250	0.021	0.0196	0.0196	0.0294	0.0280	0.0238	0.0224	0.0308	0.0308	0.0252	0.0252

Unlike kVp, a variation of pitch values can significantly affect SNR measurements. When the kVp value is kept constant, SNR showed significant differences with different pitch values. SNR measured significantly higher in images acquired with low pitch values such as 1.2 and 1.5, compared to those acquired with the high 2.0 and 2.5 protocols ($p < 0.05$), regardless of the location of measurements. SNR measurements showed that image quality significantly dropped when the pitch value increased from 1.5 to 2.0 in all kinds of kVp protocols ($p < 0.05$). SNR dropped 30% when pitch value was raised from 1.2 to 2.5 at 80 kVp, and 20% at 120 kVp. In contrast, SNR dropped only 3.9% when kVp was reduced from 120 to 80 at pitch 1.2, and 15.9% at pitch 2.5.

Under low pitch protocols such as 1.2 and 1.5, there were no significant differences in SNR measurements between the proximal and middle descending aorta. In contrast, t high pitch value protocols such as 2.0 and 2.5, the proximal descending aorta tended to have a higher image quality than the middle descending aorta, especially in the false lumen. **Figure 5.5** is an example showing the reformatted images of these CTA protocols. When kVp decreased to 80, image noise was increased with the use of high pitch value protocols such as 2.0 and 2.5, as shown in **Figure 5.5**. However, the shape of the stent graft and the location of the intimal flap are clearly displayed in these images, despite the use of low-dose protocols.

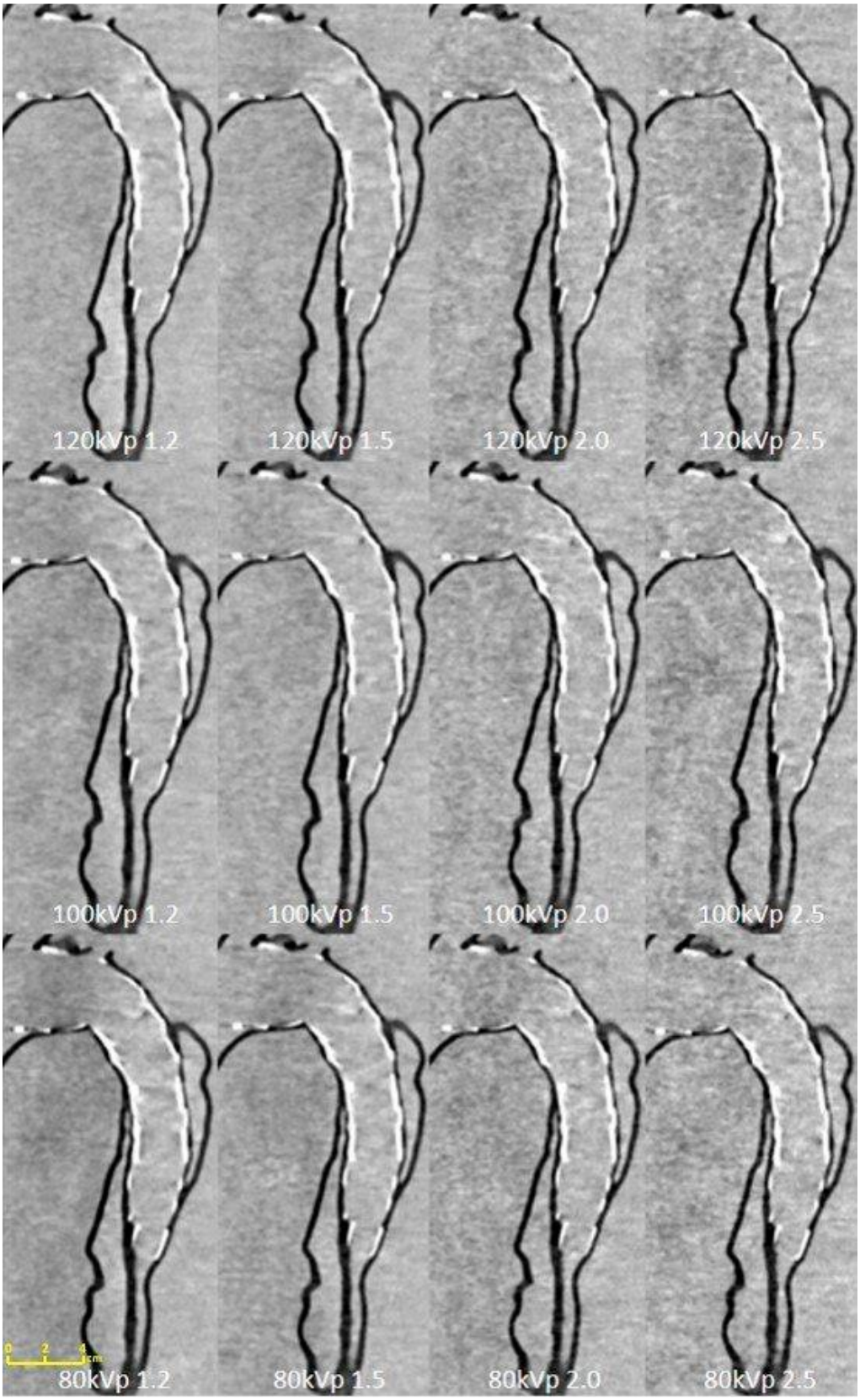

Figure 5.5 Sagittal reformatted images of the CTA protocols. When kVp decreased to 80, image noise increased with the use of high pitch value protocols such as 2.0 and 2.5. CTA: computed tomography angiography, kVp: kilovoltage peak.

5.4 Discussion

In this study, we simulated a post procedural surveillance CT scan of a patient with TBAD with different scanning protocols on a 3D printed aortic model. Quantitative assessment of image quality showed no significant differences between different kVp when the pitch value was 1.2. Compared to the change in kVp, image quality had significant differences between low and high pitch values, although there was no significant impact on the visualization of the stent graft and other structures. Thus, a low-dose aortic CTA is suggested for the follow-up of patients after EVAR.

For patients with AD, follow-up CT is mandatory and continues for many years (8, 11, 26). Various dose-reduction strategies continue to develop with the advancement of CT imaging technology, striving to reduce the risk of patients being exposed to excessive radiation while maintaining image quality including low kVp, use of IR algorithms, tube current modulation, high-pitch protocol, and use of dual energy CT (10, 15, 25). Low-dose CTA using low kVp and high-pitch protocols has been proven to achieve diagnostic image quality compared to the standard aortic CTA protocol while significantly reducing radiation dose (10, 13, 27). However, the image quality research for post TEVAR follow-up patients is still limited (28, 29). This study adds valuable information to the current literature by exploring a variety of CTA protocols and supporting the value of patient-specific 3D printed phantoms.

A CT protocol with high-pitch is available with fast speed CT scanners and will decrease radiation dose significantly when the pitch is increased. However, pitch value also significantly affects image quality with compromising spatial resolution; higher pitch leads to an increase in image noise, which could possibly affect the diagnostic quality. This has been confirmed by our study as image noise was significantly raised when the pitch was increased (**Figure 5.5**). Despite this potential limitation, some

other studies have still shown the possibility of using high-pitch CTA protocols in the diagnosis of AD without losing image quality (10). Shen et al. claimed that the use of a proper iterative reconstruction algorithm is able to maintain image quality while reducing the dose by using a low kVp, high pitch scanning protocol (13). Freyhardt et al. also investigated low-kV CT protocols with IR, allowing for CTA of the entire aorta with excellent image quality and diagnostic confidence with a dose reduction of up to 80% compared to 120 kV (27). In our study, we showed the influence of pitch value on image quality, which is more obvious than adjusting kVp, especially at low kVp.

The novelty of this study lies in the use of a personalized 3D printed aortic model to simulate TEVAR of TBAD. Use of 3D printed models to study optimal CT scanning protocols has been supported in previous studies including the assessment of coronary artery plaques (30), coronary stenting (31) and detection of pulmonary embolism (32, 33). In order to evaluate the impact of different protocols on radiation dose and image quality, CT scans have to be conducted multiple times with different scanning parameters. However, it would be unethical to scan the same patient multiple times and performing this experiment with different patients would lose accuracy due to different body types. With the development of 3D printing technology and the advancement of its application in the medical field, patient-specific 3D printed models could potentially become the new option for these kinds of experiment (16, 18, 34).

Previous literature has discussed the use of 3D printed models to plan stent graft treatment in patients. Tong et al. deployed stent grafts in short 3D printed aortic models with thoracoabdominal aortic disease. They used these models to guide pre-fenestration of the stent grafts before re-deploying them in patients, believing that 3D printing technology could potentially improve both the accuracy and efficiency of the TEVAR procedure (35). Li et al. also used 3D printed models to guide total endovascular

repair for a patient who had a stent graft incorrectly deployed in the false lumen (36). Zhang et al. performed pre-fenestration on a stent graft in a 3D printed model. They thought stent graft pre-fenestration guided by the 3D printed aortic model provided a new solution for AD treatment planning and claimed that this could improve accuracy of the fenestration location (37). Although these previous studies of stent graft deployment inside 3D models are of interest, most did not specify the materials they used to make the models, or attempted to use materials that have mechanical and radiological properties close to the real human aorta. In our study, we provide a new possibility for the medical application of 3D printing by using 3D printing materials with accuracy in vivo representation to obtain more realistic experimental data.

We recognize that there are some limitations to our experiment. First, despite a realistic 3D printed model being used for studying different CTA protocols, the model was not placed in an environment that simulated normal surrounding anatomic regions such as the lungs, ribs, spinal column, or heart. Therefore, the radiation dose associated with these protocols were lower than the actual values reported by other studies. In addition, the 3D printed aorta model was placed in a customized box and immersed inside a dilute contrast medium instead of the perfusion of contrast medium into the lumen. Furthermore, the contrast was not flowing. Future research could focus on improving this aspect of the model. Connecting the 3D printed aortic model to a pulsatile flow circuit with a cardiac pump or printing a controllable syringe pump could be a solution as this will allow for accurate measurement under more dynamic conditions. This can be addressed by further studies when our printing capabilities meet these requirements. Despite this limitation, the current measurements are still acceptable and consistent with what has been reported in the literature regarding measurements of dimensional accuracy based on 3D printed static cardiovascular

models (21). Second, no contrast-to-noise ratio (CNR) was measured. In this study, only SNR was measured to determine image quality because the model was immersed in the contrast medium. A more robust conclusion could be reached with the measurement of both SNR and CNR when the 3D printed models are placed in a realistic chest phantom in future studies. Third, the measurement of SNR and effective dose could be different in patients. Although we selected a 3D printing material that had mechanical and radiological properties approximating those in the human, due to the limited choice of commercial 3D printing materials, we could not exactly match the human aorta.

Different slice thicknesses, use of IR strengths, and image post-processing algorithms to suppress the artefacts from stents could also affect the SNR measurements. Additionally, we did not undertake a qualitative assessment of image quality in this study. In future research, the application value of 3D printed models could be verified through scoring by clinical imaging professionals.

5.5 Conclusions

In this study, we demonstrated the use of a 3D printed full-sized AD model to investigate the possibility of lower radiation dose for the surveillance of TBAD post TEVAR using CT with different scanning parameters. Low-dose CT with acceptable image quality can be achieved by lowering the tube voltage. Compared to adjusting kVp, increasing the pitch can effectively reduce the radiation dose, but will also reduce the overall image quality. High pitch with medium kVp can effectively reduce the dose while maintaining image quality. The contribution of 3D printing to medical applications was also explored in this study. However, since the model was not placed in a realistic chest cavity environment, the radiation dose reports in this study were

lower than the actual values. Improvements in materials and design could add further details and will be explored in future studies.

References

1. Szeto WY, McGarvey M, Pochettino A, Moser GW, Hoboken A, Cornelius K, et al. Results of a new surgical paradigm: endovascular repair for acute complicated type B aortic dissection. The Annals of Thoracic Surgery. 2008;86(1):87-94.
2. Thrumurthy S, Karthikesalingam A, Patterson B, Holt P, Hinchliffe R, Loftus I, et al. A systematic review of mid-term outcomes of thoracic endovascular repair (TEVAR) of chronic type B aortic dissection. European Journal of Vascular and Endovascular Surgery. 2011;42(5):632-47.
3. Bavaria JE, Brinkman WT, Hughes GC, Khoynezhad A, Szeto WY, Azizzadeh A, et al. Outcomes of thoracic endovascular aortic repair in acute type B aortic dissection: results from the Valiant United States investigational device exemption study. The Annals of Thoracic Surgery. 2015;100(3):802-9.
4. Nienaber CA, Kische S, Rousseau H, Eggebrecht H, Rehders TC, Kundt G, et al. Endovascular repair of type B aortic dissection: long-term results of the randomized investigation of stent grafts in aortic dissection trial. Circulation: Cardiovascular Interventions. 2013;6(4):407-16.
5. Huang C-Y, Hsu H-L, Chen P-L, Chen I-M, Hsu C-P, Shih C-C. The Impact of Distal Stent Graft–Induced New Entry on Aortic Remodeling of Chronic Type B Dissection. The Annals of Thoracic Surgery. 2018;105(3):785-93.
6. Hossack M, Patel S, Gambardella I, Neequaye S, Antoniou GA, Torella F. Endovascular vs. medical management for uncomplicated acute and sub-acute type B aortic dissection: a meta-analysis. European Journal of Vascular and Endovascular Surgery. 2020;59(5):794-807.
7. Burke CR, Bavaria JE, editors. The role of thoracic endovascular repair in chronic type B aortic dissection. Seminars in Thoracic and Cardiovascular Surgery; 2020: Elsevier.
8. Pape LA, Awais M, Woznicki EM, Suzuki T, Trimarchi S, Evangelista A, et al. Presentation, diagnosis, and outcomes of acute aortic dissection: 17-year trends from the International Registry of Acute Aortic Dissection. Journal of the American College of Cardiology. 2015;66(4):350-8.
9. Fukui T. Management of acute aortic dissection and thoracic aortic rupture. Journal of Intensive Care. 2018;6(1):1-8.
10. Apfaltrer P, Hanna EL, Schoepf UJ, Spears JR, Schoenberg SO, Fink C, et al. Radiation dose and image quality at high-pitch CT angiography of the aorta: intraindividual and interindividual comparisons with conventional CT angiography. American Journal of Roentgenology. 2012;199(6):1402-9.
11. Sun Z, Al Moudi M, Cao Y. CT angiography in the diagnosis of cardiovascular disease: a transformation in cardiovascular CT practice. Quantitative Imaging in Medicine and Surgery.

2014;4(5):376-96.

12. Hoffmann A, Engelfriet P, Mulder B. Radiation exposure during follow-up of adults with congenital heart disease. International Journal of Cardiology. 2007;118(2):151-3.

13. Shen Y, Sun Z, Xu L, Li Y, Zhang N, Yan Z, et al. High-pitch, low-voltage and low-iodine-concentration CT angiography of aorta: assessment of image quality and radiation dose with iterative reconstruction. PloS One. 2015;10(2):0117469.

14. Felmly LM, De Cecco CN, Schoepf UJ, Varga-Szemes A, Mangold S, McQuiston AD, et al. Low contrast medium-volume third-generation dual-source computed tomography angiography for transcatheter aortic valve replacement planning. European Radiology. 2017;27(5):1944-53.

15. Euler A, Taslimi T, Eberhard M, Kobe A, Reeve K, Zimmermann A, et al. Computed Tomography Angiography of the Aorta—Optimization of Automatic Tube Voltage Selection Settings to Reduce Radiation Dose or Contrast Medium in a Prospective Randomized Trial. Investigative Radiology. 2021;56(5):283-91.

16. Sun Z. Insights into 3D printing in medical applications. Quantitative Imaging in Medicine and Surgery. 2019;9(1):1-5.

17. Byrne N, Velasco Forte M, Tandon A, Valverde I, Hussain T. A systematic review of image segmentation methodology, used in the additive manufacture of patient-specific 3D printed models of the cardiovascular system. JRSM Cardiovasc Disease. 2016;5:2048004016645467.

18. Foley TA, El Sabbagh A, Anavekar NS, Williamson EE, Matsumoto JM. 3D-Printing: Applications in Cardiovascular Imaging. Current Radiology Reports. 2017;5(9).

19. Giannopoulos AA, Steigner ML, George E, Barile M, Hunsaker AR, Rybicki FJ, et al. Cardiothoracic applications of 3D printing. Journal of Thoracic Imaging. 2016;31(5):253-72.

20. Eshkalak SK, Ghomi ER, Dai Y, Choudhury D, Ramakrishna S. The role of three-dimensional printing in healthcare and medicine. Materials & Design. 2020;194:108940.

21. Sun Z. Clinical applications of patient-specific 3D printed models in cardiovascular disease: current status and future directions. Biomolecules. 2020;10(11):1577.

22. Wu C-A, Squelch A, Sun Z. Investigation of three-dimensional printing materials for printing aorta model replicating type B aortic dissection. Current Medical Imaging. 2021;17(7):843-9.

23. Ratinam R, Quayle M, Crock J, Lazarus M, Fogg Q, McMenamin P. Challenges in creating dissectible anatomical 3D prints for surgical teaching. Journal of Anatomy. 2019;234(4):419-37.

24. Riedle H, Mukai B, Molz P, Franke J, editors. Determination of the Mechanical Properties of

Aortic Tissue for 3D Printed Surgical Models. 2018 11th Biomedical Engineering International Conference (BMEiCON); 2018: IEEE.

25. McCollough CH, Primak AN, Braun N, Kofler J, Yu L, Christner J. Strategies for reducing radiation dose in CT. Radiologic Clinics. 2009;47(1):27-40.

26. Tanaka M, Kimura N, Yamaguchi A, Adachi H. In-hospital and long-term results of surgery for acute type A aortic dissection: 243 consecutive patients. Annals of Thoracic and Cardiovascular Surgery. 2012:1109140082.

27. Freyhardt P, Solowjowa N, Böning G, Kahn J, Aufmesser B, Haage P, et al. CT-angiography of the aorta in patients with Marfan disease-High-pitch MDCT at different levels of tube voltage combined with Sinogram Affirmed Iterative Reconstruction. Clinical Imaging. 2018;51:123-32.

28. Flors L, Leiva-Salinas C, Norton PT, Patrie JT, Hagspiel KD. Imaging follow-up of endovascular repair of type B aortic dissection with dual-source, dual-energy CT and late delayed-phase scans. Journal of Vascular and Interventional Radiology. 2014;25(3):435-42.

29. Karmonik C, Duran C, Shah DJ, Anaya-Ayala JE, Davies MG, Lumsden AB, et al. Preliminary findings in quantification of changes in septal motion during follow-up of type B aortic dissections. Journal of Vascular Surgery. 2012;55(5):1419-26.

30. Sun Z, Ng CK, Squelch A. Synchrotron radiation computed tomography assessment of calcified plaques and coronary stenosis with different slice thicknesses and beam energies on 3D printed coronary models. Quantitative Imaging in Medicine and Surgery. 2019;9(1):6.

31. Sun Z, Jansen S. Personalized 3D printed coronary models in coronary stenting. Quantitative Imaging in Medicine and Surgery. 2019;9(8):1356-67.

32. Aldosari S, Jansen S, Sun Z. Patient-specific 3D printed pulmonary artery model with simulation of peripheral pulmonary embolism for developing optimal computed tomography pulmonary angiography protocols. Quantitative Imaging in Medicine and Surgery. 2019;9(1):75-85.

33. Aldosari S, Jansen S, Sun Z. Optimization of computed tomography pulmonary angiography protocols using 3D printed model with simulation of pulmonary embolism. Quantitative Imaging in Medicine and Surgery. 2019;9(1):53-62.

34. Kim GB, Lee S, Kim H, Yang DH, Kim Y-H, Kyung YS, et al. Three-dimensional printing: basic principles and applications in medicine and radiology. Korean Journal of Radiology. 2016;17(2):182-97.

35. Tong Y-H, Yu T, Zhou M-J, Liu C, Zhou M, Jiang Q, et al. Use of 3D printing to guide creation of fenestrations in physician-modified stent-grafts for treatment of thoracoabdominal aortic disease. Journal of Endovascular Therapy. 2020;27(3):385-93.

36.Li X-R, Tong Y-H, Li X-Q, Liu C-J, Liu C, Liu Z. Total endovascular repair of an intraoperative stent-graft deployed in the false lumen of Stanford type A aortic dissection: A case report. World Journal of Clinical Cases. 2020;8(5):954-62.

37.Zhang M, Tong Y-H, Liu C, Li X-Q, Liu C-J, Liu Z. Treatment of Stanford type A aortic dissection with triple pre-fenestration, reduced diameter, and three-dimensional-printing techniques: A case report. World Journal of Clinical Cases. 2021;9(1):183-9.

CHAPTER 6

ASSESSMENT OF OPTIMIZATION OF COMPUTED TOMOGRAPHY ANGIOGRAPHY PROTOCOLS FOR FOLLOW-UP TYPE B AORTIC DISSECTION PATIENTS BY USING A 3D-PRINTED MODEL

Computed tomography angiography (CTA) is a routine imaging examination to follow-up post thoracic endovascular aortic repair (TEVAR) patients, however, radiation exposure associated with CTA remains a concern for follow-up patients due to cumulative scans. The purpose of this study is to use a patient-specific 3D printed Aortic dissection (AD) model as a phantom for testing a range of aortic CTA protocols, with CT scanned at different tube voltages (80, 100, 120 kVp) and pitch values (1.2, 1.5, 2.0, 2.5). Signal-to-noise ratio (SNR) was measured to quantitatively assess the image quality between these protocols. Six cardiologists and 10 radiological technologists were invited to assess images in terms of both image quality and diagnostic value. This study concludes that low tube voltage with high pitch CTA protocols produce adequate image quality while reducing radiation dose for AD follow-up. Use of patient-specific 3D printed model represents a potential valuable tool for developing optimal CTA protocols.

6.1 Introduction

Aortic dissection (AD) is a complex and highly fatal cardiovascular disease caused by damage to the medial layer of the aortic vessel wall for various reasons (such as high blood pressure or connective tissue defects), resulting in rupture of the intima of the vessel wall, allowing blood to enter into the blood vessel wall. This may cause insufficient blood supply throughout the body, resulting in ischemia of the limbs or brain. In addition, because the periphery of the false lumen is not a complete vascular wall structure, it is relatively fragile, easy to rupture and cause massive haemorrhage or cardiac tamponade (1-3).

Depending on the location of AD, it can be divided into Stanford Type A or type B (4). Compared with Type A, the treatment plan for Type B is more controversial (5-7). With the rapid development, thoracic endovascular aortic repair (TEVAR) is one of the common treatments for Type B AD (TBAD) (8). TEVAR has higher success rate, lower mortality and less stent graft-related complications than open surgery (9-11). More and more researchers show that combining TEVAR and medical treatment is effective, and can improve the long-term prognosis and survival rate of patients (12-15). However, more long-term, prospective clinical studies are still needed to verify whether TEVAR surgery is the best treatment option for TBAD (16, 17).

For surveillance long-term follow-up patients after TEVAR, computed tomography angiography (CTA) is the most commonly used imaging examination. The speed and image resolution of CTA have been continuously improved with the technological developments in CT scanner techniques. Because of its speed and convenience, it has become the mainstream evaluation method for monitoring postoperative AD patients (8, 18, 19). However, the high radiation associated with CTA has always been a risk to consider with this examination (20, 21). Patients after TEVAR must undergo regular

CTA examinations, hence resulting in high cumulative radiation doses to patients which raise concerns. Compared with detailed preoperative planning, postoperative patients can receive routine examinations at lower doses to reduce the cumulative radiation dose. Many studies had discussed and tried various strategies to reduce radiation dose while maintaining image quality, including low tube voltage (22, 23), use high pitch protocols (24, 25), adjust amount of contrast medium (26, 27), and different image post-processing methods (23, 28). Although these studies have provided promising results, research on radiation dose reduction in patients with AD who require repeated scans over many years is not well explored.

In pursuit of a better balance between image quality and radiation dose, 3DP could be a potential method due to its increasing use in the medical domain with capability of printing physical heart and vascular models with high accuracy (29-31). As a phantom, patient-specific models can achieve some research results that cannot be achieved with real patients (29, 30, 32). In our previous study we used open-source software to create an accurate patient-specific AD model (33). A comparison of quantitative assessment was conducted on this model by using different scanning parameters, based on the result, we recommended using medium kVp with high pitch to reduce radiation dose while maintaining image quality. To further reduce the radiation dose will inevitably sacrifice more image quality, however, for follow-up patients, lower image quality is acceptable as long as the doctors are able to diagnose (34). Therefore, a subjective assessment of diagnostic value is necessary.

6.2 Materials & methods

Appropriate patient data and materials were required for the preparation and implementation of the 3D printed aortic model used in the study. These components

were identified and then used according to the methods described in the following sections.

6.2.1 Case selection

This study used the same contrast-enhanced CT (CECT) case as reported in our previous study [34]. One of the patient datasets (CECT performed on a 128-slice CT with 120 kVp tube potential, 128 reference mAs and 1.0 mm reconstructed slice thickness) was selected from other 11 cases because of its high image quality and the presence of the contrast in the false lumen, which allowed identification of the shape of the aorta.

6.2.2 3D printed model

To proceed with segmentation, the selected CT image dataset was imported into 3D Slicer (version 4.9.0, www.slicer.org, MA, USA). We cut out a 20.5-cm-long middle aorta instead of printing the entire aorta due to the printer limitation. The selected segment had a perfect description of both lumens, intimal flap and the edge of the aortic wall was clearly identified. A 3D reconstruction model of the outer surface was created after segmentation. Post processing of the 3D reconstruction model was necessary to ensure the integrity of the model and the success of the printing. This included thickness verification, filling defects (e.g., holes inside the model and discontinuous surfaces), and surface smoothing. The 3D reconstruction model was transferred to stereolithography format for post cleaning and preprint checking. To mimic the elasticity of human aorta, the final model was printed with transparent silicone material.

6.2.3 Deployment of stent graft

We used same method to deploy the stent-graft as our previous paper (34). Due to the short length of this model, only two commercially available thoracic stent grafts

(Medtronic) were deployed into the model. The choice of translucent silicone material made the vision inside the model during deployment was clear, which helps the stent graft deployed at the right place precisely. The proximal piece deployed into the descending aorta measured length of 90 mm and diameter 30 mm. The second overlapping piece was 94 mm long by 24 mm in diameter (**Figure 6.1**).

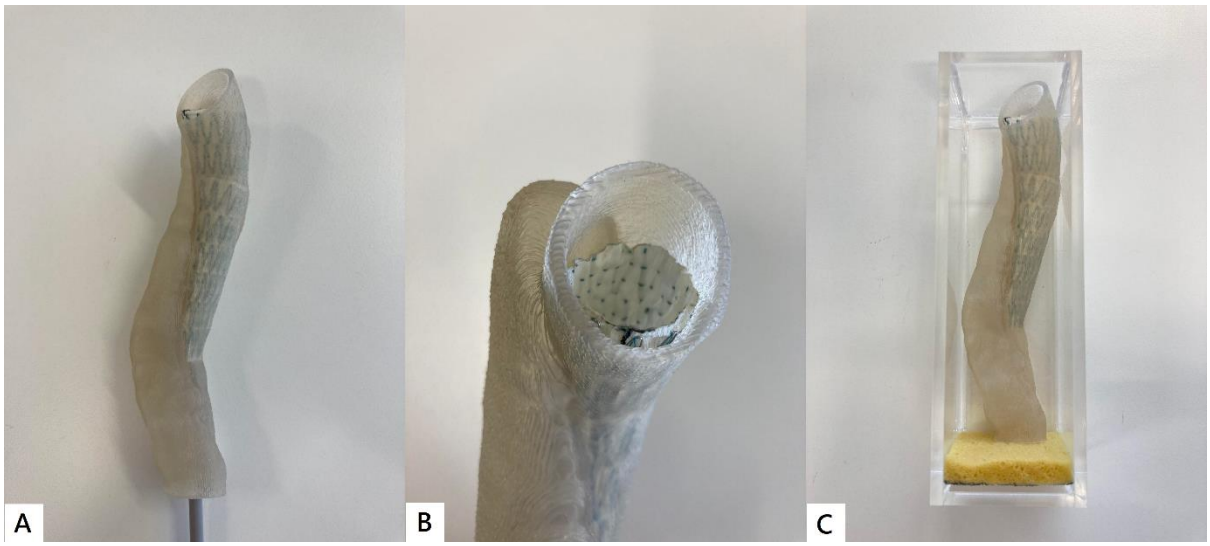

Figure 6.1 Stent graft deployment of 3D printed model. A: Translucent model makes stent graft deployment easier. B: Axial view from proximal descending aorta. C: Model was placed in an acrylic box for CT scanning.

6.2.4 CT image acquisition

The 3D-printed TBAD model was placed in an acrylic container filled with contrast medium to simulate CECT examinations (**Figure 6.1**). The air bubbles inside the model were removed by aspiration with a syringe after the model was immersed in the contrast. Diluted iohexol contrast medium OmnipaqueTM 350 (GE Healthcare Australia Pty Ltd, NSW, Australia) was used and the model was scanned with a 192-slice CT scanner (Somatom Force, Siemens Healthcare, Forchheim, Germany). The default chest CECT scans protocol setting for Siemens was 120 kVp and 2.5 pitch with flash spiral technique, therefore, our CECT scan were performed with three different

kVp (80, 100, 120 kVp) and four different pitch values (pitch of 1.2, 1.5, 2.0, 2.5), resulting in a total of 12 datasets. A slice thickness of 1.0 mm with a reconstruction interval of 0.5 mm was used for all images. An iterative reconstruction technique was used (Sinogram affirmed iterative reconstruction level 3, Siemens Healthcare) and a tissue convolution kernel of Bv40.

6.2.5 Quantitative assessment of image quality

To understand image quality of these image datasets in an objective way, image quality was quantitatively assessed by measuring the signal-to-noise ratio (SNR) of the middle descending aorta. To measure SNR, regions of interest (ROI) with an area of 25 mm^2 (containing at least 1000 voxels) were placed in the true and false lumen (**Figure 6.2**). Four different locations of ROI were measured to get an average SNR value. To minimize the differences between observers, the SNR measurement at each location was measured three times to obtain the average value, and the average value between two observers was used as the final result.

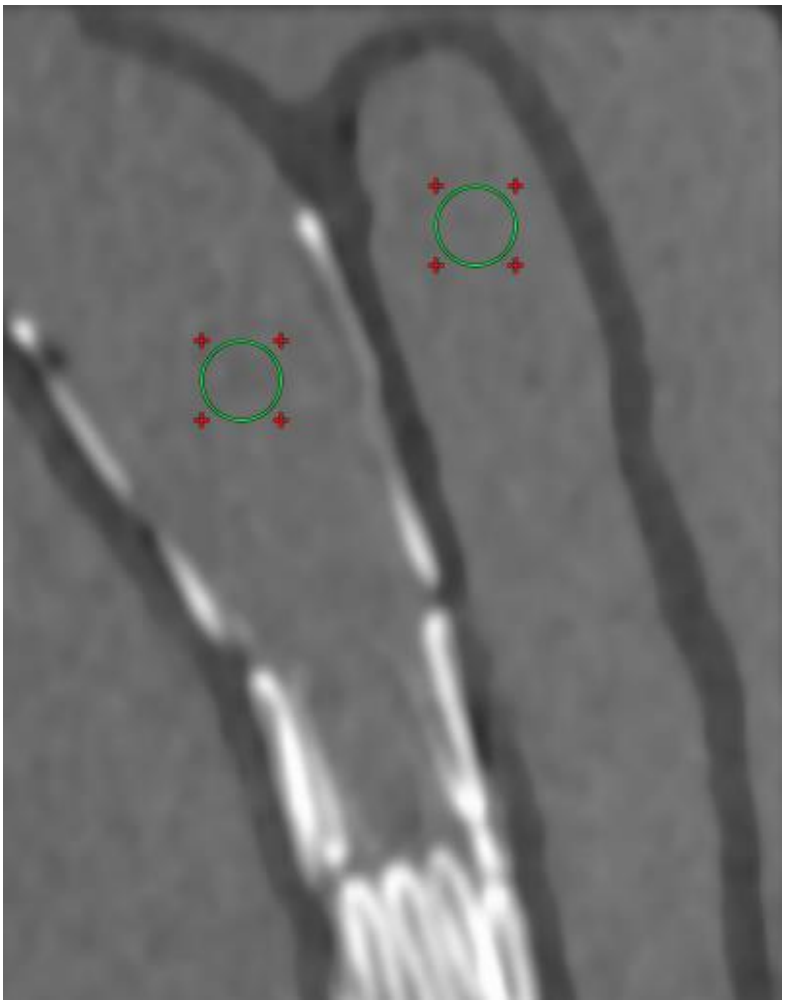

Figure 6.2 SNR measurements were conducted through the ROI placed inside the model scan data. Two ROIs at true lumen and two ROIs at false lumen were used to calculate the average SNR.

6.2.6 Qualitative assessment of image quality

After the information of scanning protocols had been cleared, all image datasets were rearranged and sent to participants. Qualitative assessment was divided into two parts: image quality and diagnostic value (Appendix IX). Ten radiation technologists were invited to evaluate image quality and six radiologists were invited to assess both image quality and diagnostic value (All participants have at least two years of clinical experience). The image quality assessment conducted through a 5-points Likert scale questionnaire (Appendix X), participants score each image dataset according to the following aspects: depiction of the aorta, true lumen and false lumen, depiction of the

dissection lesion. Diagnostic value was also assessed using a questionnaire with a 5-point scale, focusing on whether the image datasets have enough clarity to enable following measurement: Measurement of lumen and wall diameter, wall apposition, measurement of sealing zone lengths and stent clarity (whether stent fracture or kinking is visible). A score of 3 or higher was considered adequate diagnostic image quality.

6.2.7 Radiation dose

In order to understand the effects of dose and image quality. The dose length product (DLP) and volume CT dose index (CTDIvol) were recorded and compared between different CTA scanning protocols. The estimated effective dose was derived from the DLP by using the equation Effective Dose = DLP × k, where k was calculated using a tissue conversion coefficient of 0.014 $mSvmGy^{-1}cm^{-1}$ (35). Due to the lack of human body phantom, the model developed did not comprehensively represent the real human torso, thus, the calculated dose values might be underestimated from the real value. However, this experiment only compared different protocols and associated radiation doses on the same 3D printed model, hence, our results are still valid for developing optimal CT scanning protocols..

6.2.8 Statistical analysis

Scanning data were imported into SPSS 26.0 (IBM Corporation, Armonk, NY, USA) for statistical analysis. Mean and standard deviation were used to represent continuous variables. A paired sample T test was used to determine any significant differences in SNR measurements. A statistically significant difference was reached at a P value of less than 0.05. Inter-observer agreement for quantitative assessment was assessed by Cohen's kappa statistics: poor: $k<0.20$; fair: $k=0.21–0.40$; moderate: $k=0.41–0.60$; good: $k=0.61–0.80$, and excellent agreement $k=0.81–1.00$.

6.3 Results

6.3.1 Quantitative assessment

All CTA scan protocols were successfully performed with the 3D printed model and scan data were collected on **Table 6.1**. All of the measurements had excellent agreement by two observers ($k>0.8$). SNR measurements did not vary significantly at low or high pitch, such as comparison between 1.2 and 1.5 kVp or between 2.0 and 2.5 kVp ($P>0.05$), regardless of the tube voltage. There was a significant gap ($P<0.05$) in SNR between low pitch (1.2 and 1.5) and high pitch (2.0 and 2.5), which is due to the flash scan technology used for high pitch protocols. At 120 kVp with a pitch value of 1.2, the SNR is highest at 38.57, and the lowest value is 24.45 at 80 kVp with a pitch value of 2.5. The SNR increased with increasing kVp, and decreasing the pitch value increases the SNR significantly.

6.3.2 Qualitative assessment

Based on the average score, ten radiological technologists (with clinical work experience of 2 to 28 years) and six radiologists (with work experience of 2 to 20 years) considered that most of the images had sufficient image quality to identify the lesions and anatomical structures. The only exception was the 80 kVp with a pitch value of 1.5, which is the only protocol with an average value less than 3 from technologists. Figure 6.3 is an example showing one of the slices of these CTA protocols.

The score for diagnostic value has a wide gap between low and high pitch at 80 kVp. Both low pitch protocols at 80 kVp were considered to have no diagnostic value by radiologists, whereas high pitch with flash technology protocols at 80 kVp were reviewed as having high diagnostic value. At 80 kVp with pitch of 2.0 was considered as the protocol which had highest diagnostic value. Although pitch of 2.5 got lower score than 2.0, it still had score higher than any other tested protocols (3.5 points). All

of the other protocols at 100 and 120 kVp had sufficient quality for diagnosis except for 120 kVp at pitch 1.5. There was no significant difference of diagnostic value between all of the pitch at 100 kVp ($p > 0.05$). At 120 kVp, significant difference appeared when compared 1.5 pitch with other pitch value ($p < 0.05$). At 80 kVp, a significant difference appeared when the low pitch protocols (1.2 and 1.5) was compared with the other protocols.

6.3.3 Effective dose

The protocol of 80 kVp with a pitch value of 2.0 had the highest score on the quantitative and qualitative assessment, also with a lower effective dose compared with other protocols as shown in Table 6.1. At 120 kVp with 2.5 pitch is one of the common protocols used on thoracic-abdominal CT scan (36). Comparing the results to this protocol, some other tested protocols also had adequate image quality with lower effective doses: 80 kVp with 2.0 and 2.5 pitch value; 100 kVp with 2.0 and 2.5 pitch; and 120 kVp with 2.0 pitch value.

Table 6.1 Score of image quality and diagnostic value, SNR measurements and dose measurements. T, Radiation Technologist; SNR, signal-to-noise ratio; CTDIvol, volume CT dose index; DLP, dose length product.

Tube Voltage	**80 kVp**				**100 kVp**				**120 kVp**			
Pitch	1.2	1.5	2.0	2.5	1.2	1.5	2.0	2.5	1.2	1.5	2.0	2.5
Image Quality(T)	3.00 ± 0.77	2.90 ± 0.54	4.20 ± 0.40	3.80 ± 0.75	3.60 ± 0.66	3.10 ± 0.54	3.50 ± 0.81	3.10 ± 0.81	3.60 ± 0.70	3.20 ± 0.60	3.80 ± 0.60	3.30 ± 0.46
Image Quality(R)	3.17 ± 0.37	3.00 ± 0.58	4.00 ± 0.58	3.50 ± 0.96	3.17 ± 0.69	3.33 ± 0.47	3.17 ± 0.69	3.50 ± 0.50	3.50 ± 0.76	3.00 ± 0.58	3.33 ± 0.47	3.33 ± 0.47
Diagnostic Value	2.83 ± 0.69	2.83 ± 0.37	4.00 ± 0.58	3.50 ± 0.69	3.00 ± 0.58	3.17 ± 0.69	3.33 ± 0.47	3.33 ± 0.75	3.33 ± 0.47	2.83 ± 0.37	3.33 ± 0.47	3.17 ± 0.69
SNR	34.77±1.88	32.06±1.00	24.45±3.10	24.63±3.51	36.79±4.38	33.81±3.28	27.3±4.01	25.62±3.72	38.57±3.66	37.26±3.18	29.09±3.72	27.45±2.99
CTDIvol (mGY)	0.07	0.08	0.06	0.05	0.09	0.08	0.07	0.06	0.11	0.09	0.08	0.07
DLP (mGY/cm)	1.8	1.5	1.4	1.4	2.1	2	1.7	1.6	2.2	2.2	1.8	1.8
Effective dose (mSv)	0.0250	0.021	0.0196	0.0196	0.0294	0.0280	0.0238	0.0224	0.0308	0.0308	0.0252	0.0252

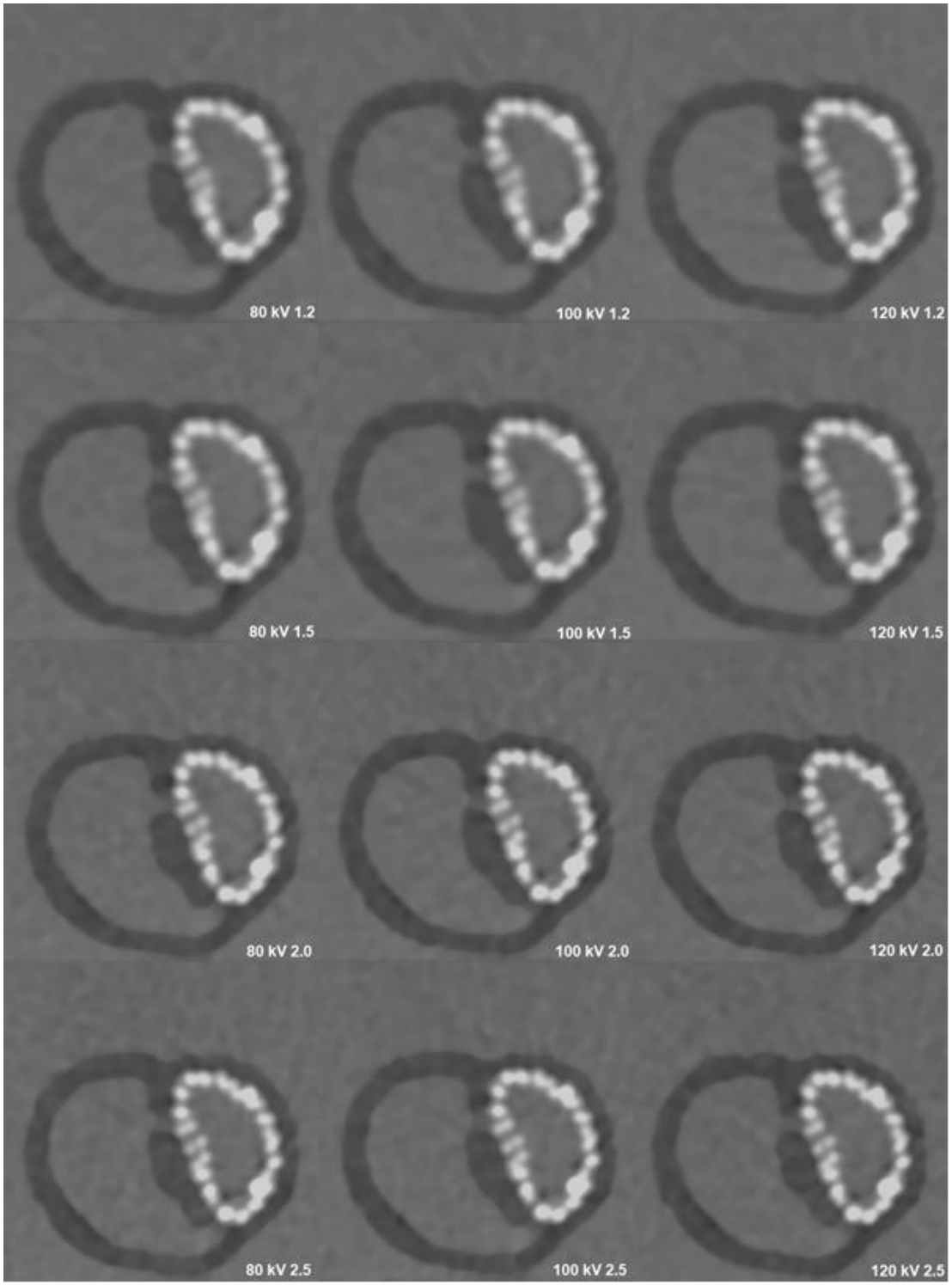

Figure 6.3 Axial reformatted images of the CTA protocols (80, 100, 120 kVp and pitch value of 1.2, 1.5, 2.0, 2.5). These selected slices include true and false lumen, stent-graft and two of the intimal flap tears.

6.4 Discussion

The quantitative assessment indicates that image quality does not show significant difference between different tube voltages, on the other hand, the adjustment of pitch value could have a great impact on the image quality. From the comparison of low pitch and high pitch, there is a huge gap of SNR between using flash technology high pitch protocol (pitch of 2.0 and 2.5) and low pitch protocol (pitch of 1.2 and 1.5). However, there may not be an absolute relationship between SNR and diagnostic value. To understand the relationship between diagnostic value and SNR, we invited medical imaging specialists to give their qualitative assessment. Based on qualitative assessment results, radiologists agree that the vast majority of protocols have diagnostic value except for low pitch value protocols at 80 kVp and pitch of 1.5 at 120 kVp. As a common clinical protocol used for follow-up patients after TEVAR, the effective dose of 120 kVp with pitch of 2.5 can be regarded as a standard for assessing other protocols. Considering effective dose, quantitative and qualitative assessment, low kVp with high pitch protocols were recommended through this study. Despite the low SNR, the image is still adequate for diagnosis and evaluation.

For post-TEVAR AD patients, CT scan is an important and necessary long-term monitoring modality due to its speed and convenience (18,20). Due to the risk from radiation exposure, achieving a balance between image quality and radiation dose has always been an important issue. As CT-imaging technology advances, various dose reduction strategies are evolving to reduce the risk of patients being exposed to excessive radiation while maintaining image quality (22–28,37). However, the image quality research for post TEVAR follow-up patients is still limited (38,39). In this study, we deployed commercial stent graft into a patient-specific 3D-printed model to simulate patient after TEVAR. To acquire CT images scanned with different parameters,

the test subject must be scanned multiple times in succession, which is impossible to conduct on a real patient. A 3D-printed model addresses ethical concerns and ensures scan consistency.

There are various strategies to reduce the radiation dose for patients. Patel et al. adopted a new radiologist monitored protocol instead of routine abdominopelvic imaging and got an encouraging result that the radiation exposure decreased by reducing routine abdominopelvic imaging without compromising accuracy of diagnosis (37). Boning et al. examined 100 CTAs in 67 patients with EVAR using different protocols, their results showed that low tube voltage, using of adaptive statistical iterative reconstruction can significantly reduce the radiation dose (39). Shen et al. also showed by using an appropriate iterative reconstruction (IR) algorithm, image quality could be maintained while reducing the dose by using a low kVp, high pitch scan protocol (28). The results of Freyhardt et al.'s study showed that the CTA image of the entire aorta gave superior image quality and diagnostic reliability with lower radiation risk when they applied a low tube voltage CT protocol using iterative reconstruction algorithm compared with 120 kV (40). These studies have shown promising results on reducing radiation exposure for patients. Despite our study lacks of clinical accuracy compared with these previous studies, due to the use of 3D-printed model, we ensure consistency of different scans. All of the scans were completed at the same spot on the scanning table with exactly the same model. In our previous study, we also used 3D-printed models to confirm that low kV is an effective and feasible dose reduction method without changing too much image quality (34). 3D printing gives us a different approach to conduct this kind of repetitive and risky experiments.

Patient-specific 3D-printed models based on real medical image data can be used in various medical applications. These models accurately replicate anatomy of the diseases; therefore, they can be beneficial in treatment planning, surgical simulation or education (31). In addition to these main applications, although not discussed to the same extent, the use of 3D-printed models as a scanning phantom is another potential and useful application, especially in aortic disease (41). Aldosari and his colleagues use a 3D-printed pulmonary artery model with simulation of thrombus to optimize protocol of computed tomography pulmonary angiography (42). Abdullah et al. used CT images of anthropomorphic chest phantoms to develop a 3D-printed heart phantom that simulated the anatomy by inserting a filler material into the phantom (43). These studies gave promising results that use of 3D-printed models as a phantom is a harmless way with great development prospect to optimize CT protocols for patients. Except for pulmonary artery and heart, due to the high frequency of CT examination after treatment, aortic disease could also be a development direction for 3D-printed phantom and radiation dose reduction (32,44,45). It could be more informative to use the same model to test different scan parameters than to perform different scan parameters on different patients.

Although this is the first study of using patient-specific 3D-printed model as a phantom to optimize CT protocol for follow-up AD patients, we recognize that there are some limitations to our experiment. In this study, due to equipment limitations, the 3D-printed models were not placed in an anthropomorphic environment. Without the simulation of surrounding anatomic regions such as heart, lungs and ribs, the radiation exposure could be lower than normal scan. Also, the model was immersed into contrast dilute medium instead of perfusion of contrast medium into the lumen, lack of simulation of blood flow might also additionally bring about inconsistent effects

with a real patient. Second, we chose 3D-printed materials with mechanical properties close to humans, but due to the limited choice of commercially available 3DP materials, it was not possible to accurately match the human aorta. Third, plain film is a common way used to diagnose whether a stent graft has been successfully deployed. In this study, we did not provide plain film of each image datasets for qualitative assessment, therefore, some of the radiologists reported that they cannot rely on CT image alone to give an accurate judgment on the success of stent graft deployment.

Owing to the existing cost and time required to print a patient-specific 3D-printedmodel, 3DP is not yet clinically applicable. Especially in the case of patients requiring urgent treatment, it is currently impractical to use 3DP to guide treatment planning. However, for chronic patients, 3DP can make treatment plans more reliable. It has also been shown that preoperative surgical simulation and preoperative fenestration of the stent on a patient-specific 3DP model improves the surgery success rate (46,47). Therefore, if high-speed and lower-cost 3DP technology does become available, 3DP will become a powerful tool for treatment planning. In this study, we prove that 3DP can also be used to improve radiation techniques. However, before it can be used clinically, more data are needed to support the conclusion.

In this study, the recommended protocol of 80 kVp with pitch value of 2.0 can reduce the effective dose by around 22% compared with the suggested setting of SiemensDual Source Flash mode chest CTA protocol (120 kVp with pitch of 2.5). When dual source Flash mode is not available, the suggested protocol of routine spiral mode is 120 kVp and pitch of 0.6 for aorta CT scan, but at the cost of higher radiation dose (48). Therefore, to reduce cumulative radiation exposure in the follow-up of patients after TEVAR, lowering kVp should be considered as an effective strategy for further dose reduction in combination with the high-pitch protocol.

Different slice thicknesses, use of IR strengths and image post processing algorithms to suppress the artefacts from stents could also affect the clarity of the CT image. In future studies, a range of different dose reduction methods and scanning protocols can be tested. A better scanning phantom such as appropriate 3DP material with surrounding organs and scanning environment will also improve the accuracy of the results and the recommended optimal scanning protocol for follow-up patients.

6.5 Conclusions

In conclusion, this study has demonstrated that low tube voltage with high pitch CTA produce adequate image quality while reducing radiation dose. Use of patient-specific 3D-printed model represents a potential valuable tool for developing optimal CTA protocols in patients with AD following TEVAR treatment. Although there are still some limitations in this study, the 3D-printed phantoms have been shown to be valuable tools for determining optimal CT scanning protocols, without giving real patients additional radiation risks. In future research, different 3D-printing materials and phantom design could be tested and further details incorporated.

References

1. Apostolakis E, Baikoussis NG, Georgiopoulos M. Acute type-B aortic dissection: the treatment strategy. Hellenic Journal of Cardiology. 2010;51(4):338-47.
2. Tran TP, Khoynezhad A. Current management of type B aortic dissection. Vascular Health and Risk Management. 2009;5:53-63.
3. Sun Z, Chaichana T. A systematic review of computational fluid dynamics in type B aortic dissection. International Journal of Cardiology. 2016;210:28-31.
4. Sebastià C, Pallisa E, Quiroga S, Alvarez-Castells A, Dominguez R, Evangelista A. Aortic dissection: diagnosis and follow-up with helical CT. Radiographics. 1999;19(1):45-60.
5. Qin Y-L, Wang F, Li T-X, Ding W, Deng G, Xie B, et al. Endovascular repair compared with medical management of patients with uncomplicated type B acute aortic dissection. Journal of the American College of Cardiology. 2016;67(24):2835-42.
6. Brunkwall J, Kasprzak P, Verhoeven E, Heijmen R, Taylor P, Trialists A, et al. Endovascular repair of acute uncomplicated aortic type B dissection promotes aortic remodelling: 1 year results of the ADSORB trial. European Journal of Vascular Endovascular Surgery. 2014;48(3):285-91.
7. Li F-R, Wu X, Yuan J, Wang J, Mao C, Wu X. Comparison of thoracic endovascular aortic repair, open surgery and best medical treatment for type B aortic dissection: A meta-analysis. International Journal of Cardiology. 2018;250:240-6.
8. Nauta FJ, Trimarchi S, Kamman AV, Moll FL, Van Herwaarden JA, Patel HJ, et al. Update in the management of type B aortic dissection. Vascular Medicine. 2016;21(3):251-63.
9. Szeto WY, McGarvey M, Pochettino A, Moser GW, Hoboken A, Cornelius K, et al. Results of a new surgical paradigm: endovascular repair for acute complicated type B aortic dissection. The Annals of Thoracic Surgery. 2008;86(1):87-94.
10. Thrumurthy S, Karthikesalingam A, Patterson B, Holt P, Hinchliffe R, Loftus I, et al. A systematic review of mid-term outcomes of thoracic endovascular repair (TEVAR) of chronic type B aortic dissection. European Journal of Vascular and Endovascular Surgery. 2011;42(5):632-47.
11. Miyairi T, Miyata H, Chiba K, Nishimaki H, Ogawa Y, Motomura N, et al. Influence of timing after thoracic endovascular aortic repair for acute type B aortic dissection. The Annals of Thoracic Surgery. 2018;105(5):1392-6.
12. Song C, Lu Q, Zhou J, Yu G, Feng X, Zhao Z, et al. The new indication of TEVAR for uncomplicated type B aortic dissection. Medicine. 2016;95(25).
13. Schwartz SI, Durham C, Clouse WD, Patel VI, Lancaster RT, Cambria RP, et al. Predictors of late aortic intervention in patients with medically treated type B aortic dissection. Journal

of Vascular Surgery. 2018;67(1):78-84.

14. Kamman AV, Brunkwall J, Verhoeven EL, Heijmen RH, Trimarchi S, Kasprzak P, et al. Predictors of aortic growth in uncomplicated type B aortic dissection from the Acute Dissection Stent Grafting or Best Medical Treatment (ADSORB) database. Journal of Vascular Surgery. 2017;65(4):964-71.

15. Hossack M, Patel S, Gambardella I, Neequaye S, Antoniou GA, Torella F. Endovascular vs. medical management for uncomplicated acute and sub-acute type B aortic dissection: a meta-analysis. European Journal of Vascular and Endovascular Surgery. 2020;59(5):794-807.

16. Patel PB, Marcaccio CL, de Guerre LE, Patel VI, Wang G, Giles K, et al. Complications after thoracic endovascular aortic repair for ruptured thoracic aortic aneurysms remain high compared with elective repair. Journal of Vascular Surgery. 2021.

17. Nienaber CA, Kische S, Rousseau H, Eggebrecht H, Rehders TC, Kundt G, et al. Endovascular repair of type B aortic dissection: long-term results of the randomized investigation of stent grafts in aortic dissection trial. Circulation: Cardiovascular Interventions. 2013;6(4):407-16.

18. Pape LA, Awais M, Woznicki EM, Suzuki T, Trimarchi S, Evangelista A, et al. Presentation, diagnosis, and outcomes of acute aortic dissection: 17-year trends from the International Registry of Acute Aortic Dissection. Journal of the American College of Cardiology. 2015;66(4):350-8.

19. Fukui T. Management of acute aortic dissection and thoracic aortic rupture. Journal of Intensive Care. 2018;6(1):1-8.

20. Sun Z, Al Moudi M, Cao Y. CT angiography in the diagnosis of cardiovascular disease: a transformation in cardiovascular CT practice. Quantitative Imaging in Medicine and Surgery. 2014;4(5):376-96.

21. Apfaltrer P, Hanna EL, Schoepf UJ, Spears JR, Schoenberg SO, Fink C, et al. Radiation dose and image quality at high-pitch CT angiography of the aorta: intraindividual and interindividual comparisons with conventional CT angiography. American Journal of Roentgenology. 2012;199(6):1402-9.

22. Schindera ST, Graca P, Patak MA, Abderhalden S, von Allmen G, Vock P, et al. Thoracoabdominal-Aortoiliac Multidetector-Row CT Angiography at 80 and 100 kVp: Assessment of Image Quality and Radiation Dose. Investigative Radiology. 2009;44(10):650-5.

23. Rampado O, Busso S, Garabello D, Marengo E, Valerio M, Capello S, et al. Aortic CT angiography dose reduction: investigation of optimal noise index and iterative algorithm strength in combination with low kV. La Radiologia Medica. 2016;121(4):291-300.

24. Liu Y, Xu J, Li J, Ren J, Liu H, Xu J, et al. The ascending aortic image quality and the whole

aortic radiation dose of high-pitch dual-source CT angiography. Journal of Cardiothoracic Surgery. 2013;8(1):1-5.

25. Zhang LJ, Zhao YE, Schoepf UJ, Mangold S, Felmly LM, Li X, et al. Seventy–peak kilovoltage high-pitch thoracic aortic CT angiography without ECG gating: evaluation of image quality and radiation dose. Academic Radiology. 2015;22(7):890-7.

26. Euler A, Taslimi T, Eberhard M, Kobe A, Reeve K, Zimmermann A, et al. Computed Tomography Angiography of the Aorta—Optimization of Automatic Tube Voltage Selection Settings to Reduce Radiation Dose or Contrast Medium in a Prospective Randomized Trial. Investigative Radiology. 2021;56(5):283-91.

27. Felmly LM, De Cecco CN, Schoepf UJ, Varga-Szemes A, Mangold S, McQuiston AD, et al. Low contrast medium-volume third-generation dual-source computed tomography angiography for transcatheter aortic valve replacement planning. European radiology. 2017;27(5):1944-53.

28. Shen Y, Sun Z, Xu L, Li Y, Zhang N, Yan Z, et al. High-pitch, low-voltage and low-iodine-concentration CT angiography of aorta: assessment of image quality and radiation dose with iterative reconstruction. PloS One. 2015;10(2):0117469.

29. Sun Z. Clinical Applications of Patient-Specific 3D Printed Models in Cardiovascular Disease: Current Status and Future Directions. Biomolecules. 2020;10(11):1577.

30. Nadagouda MN, Rastogi V, Ginn M. A review on 3D printing techniques for medical applications. Current Opinion in Chemical Engineering. 2020;28:152-7.

31. Sun Z. Insights into 3D printing in medical applications. Quantitaive Imaging in Medicine and Surgery. 2019;9(1):1-5.

32. Coles-Black J, Bolton D, Chuen J. Accessing 3D printed vascular phantoms for procedural simulation. Frontiers in Surgery. 2021;7:158.

33. Wu C-A, Squelch A, Sun Z. Optimal image segmentation protocol for 3D printing of aortic dissection through open-source software. Journal of 3D Printing in Medicine. 2021;5(1):37-49.

34. Wu C-A, Squelch A, Jansen S, Sun Z. Optimization of computed tomography angiography protocols for follow-up type B aortic dissection patients by using 3D printed model. Applied Sciences. 2021;11(15):6844.

35. McCollough CH, Primak AN, Braun N, Kofler J, Yu L, Christner J. Strategies for reducing radiation dose in CT. Radiologic Clinics. 2009;47(1):27-40.

36. Ippolito D, Talei Franzesi C, Fior D, Bonaffini P, Minutolo O, Sironi S. Low kV settings CT angiography (CTA) with low dose contrast medium volume protocol in the assessment of thoracic and abdominal aorta disease: a feasibility study. The British Journal of Radiology.

2015;88(1049):20140140.

37. Patel VK, Fruauff A, Esses D, Lipsitz EC, Levsky JM, Haramati LB. Implementation of an aortic dissection CT protocol with clinical decision support aimed at decreasing radiation exposure by reducing routine abdominopelvic imaging. Clinical Imaging. 2020;67:108-12.

38. Flors L, Leiva-Salinas C, Norton PT, Patrie JT, Hagspiel KD. Imaging follow-up of endovascular repair of type B aortic dissection with dual-source, dual-energy CT and late delayed-phase scans. Journal of Vascular and Interventional Radiology. 2014;25(3):435-42.

39. Böning G, Rotzinger RA, Kahn JF, Freyhardt P, Renz DM, Maurer M, et al. Tailored CT angiography in follow-up after endovascular aneurysm repair (EVAR): combined dose reduction techniques. Acta Radiologica. 2018;59(11):1316-25.

40. Freyhardt P, Solowjowa N, Böning G, Kahn J, Aufmesser B, Haage P, et al. CT-angiography of the aorta in patients with Marfan disease-High-pitch MDCT at different levels of tube voltage combined with Sinogram Affirmed Iterative Reconstruction. Clinical Imaging. 2018;51:123-32.

41. Sun Z. Use of three-dimensional printing in the development of optimal cardiac CT scanning protocols. Current Medical Imaging. 2020;16(8):967-77.

42. Aldosari S, Jansen S, Sun Z. Optimization of computed tomography pulmonary angiography protocols using 3D printed model with simulation of pulmonary embolism. Quantitative Imaging in Medicine and Surgery. 2019;9(1):53-62.

43. Abdullah KA, McEntee MF, Reed W, Kench PL. Development of an organ-specific insert phantom generated using a 3D printer for investigations of cardiac computed tomography protocols. Journal of Medical Radiation Sciences. 2018;65(3):175-83.

44. Georgios Koufopoulos M, Konstantinos Skarentzos M, Efstratios Georgakarakos M. 3D printing in vascular surgery. 3D Printing: Application in Medical Surgery E-Book. 2019:125.

45. Gomes EN, Dias RR, Rocha BA, Santiago JAD, Dinato FJdS, Saadi EK, et al. Use of 3D printing in preoperative planning and training for aortic endovascular repair and aortic valve disease. Brazilian Journal of Cardiovascular Surgery. 2018;33:490-5.

46. Tong Y-H, Yu T, Zhou M-J, Liu C, Zhou M, Jiang Q, et al. Use of 3D printing to guide creation of fenestrations in physician-modified stent-grafts for treatment of thoracoabdominal aortic disease. Journal of Endovascular Therapy. 2020;27(3):385-93.

47. Zhang M, Tong Y-H, Liu C, Li X-Q, Liu C-J, Liu Z. Treatment of Stanford type A aortic dissection with triple pre-fenestration, reduced diameter, and three-dimensional-printing techniques: A case report. World Journal of Clinical Cases. 2021;9(1):183.

48. CTisus BaltimoreMD. http://www.ctisus.com (Last access date: 05/07/2022)

CHAPTER 7

CONCLUSIONS AND FUTURE DIRECTIONS

7.1 Conclusions

Although the association between radiation dose and radiation-induced malignancy is still unclear, it is certain that the lower the radiation dose, the better for the patient. This study was performed to develop protocols which have lower dose than the traditional computed tomography (CT) scan radiation dose for post-thoracic endovascular aortic repair (TEVAR) follow-up Type B aortic dissection (TBAD) patients by using three dimensional (3D) printed models instead of real patients. Through one model manufacturing survey and three phantom experiments, expected outcomes are achieved with significant findings as reported below.

The study focuses on developing 3D printed models to simulate real patients to evaluate the low-dose CT protocols in association with radiation dose reduction. Therefore, high accuracy models were required to simulate the real situation. Due to complex anatomy structure of AD, the segmentation of TBAD in CT images can be quite challenging. Open-source software was used to develop and evaluate a series of workflows for the purpose of TBAD segmentation. The outcomes achieved are as follows:

- A workflow devised for the segmentation of TBAD. Application of this protocol to relevant CT image data can produce a high accuracy 3D model geometry suitable for three dimensional printing (3DP).
- The customised workflow can reduce the time for the image segmentation task and satisfactorily replicate the anatomy structure of TBAD patients, including small or thin parts such as intimal flap.
- The workflow only involves the basic software tools and functions, so it can be performed on different open-source software. Therefore, this method can be performed by someone who has general knowledge of performing

image post-processing and segmentation using software tools.

This research successfully identified appropriate commercially available materials for the replication of aorta of AD patients based on mechanical and radiological properties. Following this, a patient-specific 3D-printed AD model was developed using 3DP techniques and tissue mimicking materials. The results are summarized as follows:

- Based on AD aorta's mechanical properties, Both Visijet CE-NT and Agilus have tensile strength and elongation close to real patients' tissue. These materials have potential to make AD models for physical applications.
- Both materials had radiological properties close to real AD patients under CT scan without contrast. However, only Visijet CE-NT was considered as suitable material for AD models since it had no significant differences from real dissection aorta with contrast inside the model.
- A full size accurate patient-specific AD aorta model that had both mechanical and radiological properties similar to real patients was 3D printed with Visijet CE-NT.

Post TEVAR AD patients undergo routine CT follow-up scans at least every year for their rest of lifetime. To develop lower dose protocol while retaining the necessary image quality, a quantitative assessment of different scan parameters was performed on the patient-specific model. A commercial stent-graft was deployed into a full size patient-specific AD model to simulate the post TEVAR patient and CT scanned with different parameters for quantitative assessment. The key findings are as follows:

- Compared to adjusting tube voltage, adjusting the pitch value will greatly affect the image quality, especially when high pitch technique applied. Therefore, to retain the image quality needed it is better to reduce the tube voltage as the way of lowering radiation exposure.
- Through signal-to-noise ratio (SNR) measurements and comparison, high pitch value (such as 2.0, 2.5) with medium tube voltage (such as 80, 100 kVp) can effectively reduce the radiation dose while maintaining image quality.
- The contribution of 3DP to medical applications was explored. A patient-

specific model with proper material has potential to be used in surgery procedure simulation. This study also showed that 3D printed models can produce images close to the real patient under CT scan.

For follow-up patients, the aims of imaging tracking are clear due to prior understanding of their condition. Although the SNR significantly dropped when reducing pitch value, the image quality of the scans may still be suitable for diagnosis. To provide a qualitative assessment of the resulting images, radiologists and radiographers were invited to assess the CT image series scanned with different parameters and score them based on image quality and diagnostic value. The results are as follows:

- To reduce cumulative radiation exposure in the follow-up of patients after TEVAR, lowering tube voltage should be considered as an effective strategy for further dose reduction in combination with the high-pitch protocol.
- For follow up patients, low tube voltage with high pitch protocols can maintain adequate image quality for diagnosis while reducing radiation dose.
- 80 kVp with pitch value of 2.0 had highest score in this study which was able to reduce around 22% radiation dose compared to routine thoracic computed tomography angiography (CTA) protocol.
- Patient-specific 3D printed models with material which has radiological property close to human aorta are able to represent patients in CT scan experiments instead of scanning real human.

7.2 Future directions

This research investigated the reduction of radiation dose to patients and provides the possibility of image tracking dose for reducing postoperative patients. The study showed how 3DP techniques and tissue mimicking materials can be used to construct a customized AD model for the quantitative and qualitative assessment of radiation dose reduction.

Several questions and potential research directions have emerged as a result of this study, which would need to be investigated further as they fell outside of the scope of the study. Some suggestions for future research are as follows:

- Fully automatic segmentation AD workflow development. Despite the AD segmentation workflow has been arranged and simplified, semi-automatic method still takes longer time than full-automatic way. Design a software or segment through artificial intelligence may be a more efficient approach.
- With the development of 3DP technology, different materials are also becoming available. Although currently available commercial materials closest to the AD patients' aorta were identified for this study, their physical and radiological properties are not a perfect match. Therefore, it could be worthwhile testing new materials or mix of materials as they become available.
- In this study, a complete chest phantom did not used in most experiments. A suitable phantom can simulate organs and tissue surrounding aorta and make experimental results closer to clinical patients.
- In a real CTA scanning environment, blood flows in the aorta, the contrast mix and flows with the blood. A pump that simulates heartbeat and blood flow could help make the experimental environment more realistic.
- In this study, a single representative AD case was selected and used as the basis for the patient-specific model. In the future, a variety of AD cases can be used to create a range of different AD models that could be helpful for further validating this study and exploring greater possibilities of 3DP technology.
- The use of 3D printed AD models can be investigated for different applications. Currently in the medical field, 3DP can also be used in surgical simulation, education and training, etc. Patient-specific models with human tissue-like materials can be a powerful auxiliary tool.
- 3D printed models could be generated to represent different medical conditions other than AD. There are still many diseases that require postoperative follow-up using CT, and the use of 3D printed models can reduce patient dose in such studies. Also, 3DP still has a lot of undeveloped potential and exploring its varied applications could be helpful in the medical area.